EFFECTS OF S-ADENOSYL-L-METHIONINE ON COLLAGEN EXPRESSION IN ACTIVATED HEPATIC STELLATE CELLS

by

Kyle James Thompson

A dissertation submitted to the faculty of
The University of North Carolina at Charlotte
in partial fulfillment of the requirements for the
degree of Doctor of Philosophy in
Biology

Charlotte

2009

Approved by:

_____
Dr. Laura W. Schrum, Advisor

_____
Dr. Yvette M. Huet

_____
Dr. Iain H. McKillop

_____
Dr. Daniel A. Nelson

_____
Dr. Charles Y. Lee

ABSTRACT

KYLE JAMES THOMPSON. Effects of S-adenosyl-L-methionine on collagen expression in activated hepatic stellate cells. (Under the direction of DR. LAURA W. SCHRUM)

Liver fibrosis is defined as the excessive accumulation of extracellular matrix (ECM) components, which can disrupt the normal liver microcirculation and lead to injury. Unresolved, hepatic fibrosis can progress to cirrhosis, an end-state liver disease. Hepatic stellate cells (HSCs) are the chief mediator of fibrosis in the liver. Normal HSCs are quiescent, store vitamin A, and regulate sinusoidal blood flow. Upon a noxious stimulus, HSCs transdifferentiate into a myofibroblast-like cell, proliferate, migrate to the site of injury, and secrete ECM components, in particular type I collagen. The antioxidant S-adenosyl-L-methionine (SAMe) was evaluated as a therapeutic agent for the modulation of type I collagen in activated HSCs. Treatment with SAMe resulted in a 91% reduction in type I collagen secretion, however there was no significant change in intracellular collagen protein or mRNA expression. SAMe also increased NF-κB activity, a redox-sensitive transcription factor. Blocking NF-κB with a dominant-negative form of IκBα abolished SAMe-mediated type I collagen inhibition in Rat-1 fibroblasts. Examination of post-transcriptional fate of procollagen mRNAs revealed polyubiquitination of intracellular type I collagen following administration of SAMe. The endoplasmic reticulum (ER) proteins Grp78 and protein disulfide isomerase (PDI) were also significantly decreased by SAMe following 24 hours of treatment. These findings may represent a novel mechanism for modulating type I collagen expression in activated HSCs. We also report the development of a “two-hit” model of hepatic fibrosis,

utilizing the Lieber-DeCarli liquid ethanol diet with concomitant injections of 0.5 mg/kg LPS semi-weekly. After 8 weeks of ethanol and LPS, animals developed significant perivenular and perisinusoidal fibrosis. Treatment with 10 mg/kg of SAMe daily abolished ethanol and LPS-induced fibrosis with a decrease in oxidative stress, and expression of TGF-β and the downstream signaling molecule Smad3. SAMe also attenuated established hepatic fibrosis in a BDL model. These findings suggest SAMe is effective as both a preventative and curative treatment for hepatic fibrosis, and our "two-hit" model of ethanol feeding with LPS administration is appropriate for investigating liver fibrosis.

ACKNOWLEDGEMENTS

My dissertations studies at UNC Charlotte have tested the extent of my abilities both as a scientist and a person. With the support of the friendships developed over the years of my studies and the invaluable mentorship I have received from the faculty and staff at UNC Charlotte, I have been able to persevere through the many challenges of my project, as well as life outside the laboratory, have presented me. Without their assistance, it is doubtless I would not have succeeded. I have had the extreme fortune to do my studies under the direction of Dr. Laura Schrum. She has given me the freedom to develop myself as a scientist as well always being willing and able to help guide me in all matters, both personal and professional. I am deeply grateful for the opportunity she has given me to conduct research in her laboratory, and strongly feel that her dedication has helped shape me into a strong, independent scientist. I would also like to thank past and present members of the Schrum lab; Brian Cross, Ashley Lakner, Stephani Day, Alyssa Gulledge for their help and friendship, and especially Cathy Moore, who has been indispensible in assisting me with animal surgeries. Amel Karaa provided tremendous assistance in the preparation of data from alcohol studies. The Biology Department imaging technicians and the technicians at Carolinas Medical Center provided great help with histology. I would also like to acknowledge my Ph.D. committee members; Dr. Iain McKillop, Dr. Yvette Huet, Dr. Daniel Nelson, and Dr. Charles Lee. Through interactions in both the laboratory and the classroom I am fortunate to have had numerous opportunities to receive their guidance throughout my academic career. Lastly, I would like to express my profound gratitude to my family for their support over years, in particular my loving wife Sireesha, whose love and faith in me has never wavered.

TABLE OF CONTENTS

LIST OF TABLES

LIST OF FIGURES

LIST OF ABBREVIATIONS

4-HNE	4-hydroxy-2-nonenal
αSMA	smooth muscle α-actin
ADH	alcohol dehydrogenase
ALCAM	activated leukocyte cell adhesion molecule
ALD	alcoholic liver disease
ALDH	aldehyde dehydrogenase
ALT	alanine transferase
ATF6	activating transcription factor 6
BDL	bile duct ligation
BTEB	basic transcription element binding protein
CCl_4	carbon tetrachloride
Cre	cre recombinase
CYP2E1	cytochrome P450 2E1
ECM	extracellular matrix
DAPI	4',6-diamidino-2-phenylindole
DEPC	diethylpyrocarbonate
DMEM	Dulbecco's Modified Eagle's Medium
DTT	dithiothreitol
ER	endoplasmic reticulum
ERAD	ER-associated degredation
FCS	fetal calf serum
FITC	fluorescein isothiocyanate

G3	glyceraldehyde 3-phosphate dehydrogenase
GBSS	Gey's Balanced Salt Solution
GFP	green fluorescent protein
Grp78	78-kDa glucose-regulated protein
GSH	glutathione
GSSG	oxidized glutathione
HA	hemagglutinin
HCC	hepatocellular carcinoma
HSCs	hepatic stellate cells
Hsp47	47-kDa heat shock protein
i.p.	intraperitoneal
IFN-γ	interferon-gamma
IKK	IκB kinase
IL-6	interleukin-6
IRE1	type-I ER transmembrane protein kinase
JNK	*c-jun* N-terminal kinase
L-D	Lieber-DeCarli
LPS	lipopolysaccharide
MEOS	microsomal ethanol-oxidizing system
MesP1	mesoderm posterior 1
NASH	non-alcoholic steatohepatitis
NF-κB	nuclear factor-kappaB
NLS	nuclear localization signal

NO	nitric oxide
P4H	prolyl 4-hydroxylase
PDGF	platelet-derived growth factor
PDI	protein disulfide isomerase
PERK	PKR-like ER kinase
PMNs	polymorphonuclear leukocytes
ROS	reactive oxygen species
SAH	S-adenosylhomocysteine
SAMe	S-adenosyl-L-methionine
SEC	sinusoidal endothelial cell
SOCS1	supression of cytokine signaling-1
TFMELD	Tsukamoto-French Model of Ethanol Liver Injury
TGF-β	transforming growth factor-beta
TIMP	tissue inhibitor of metalloproteinase
TNF-α	tumor necrosis factor-alpha
UPR	unfolded protein response
UPS	ubiquitin-proteasome system
YFP	yellow fluorescent protein

CHAPTER 1: INTRODUCTION

Liver Fibrosis

Liver fibrosis is an exacerbation of the generic wound-healing process of the liver and is defined by excess synthesis and deposition of extracellular matrix (ECM) components [1]. The accumulation of ECM in the sub-endothelial space of Disse can disrupt the microcirculation of the liver leading to the damage and death of parenchymal cells (hepatocytes) [2]. Liver fibrosis is a major contributor of morbidity and mortality, as unresolved fibrosis may progress to cirrhosis and result in organ failure or progression to hepatocellular carcinoma (HCC) [3].

Cirrhosis is the end stage consequence of extended fibrosis, resulting in extensive scarring of the liver, dysfunction of the parenchyma, and ultimately death. Complications of cirrhosis include ascites, renal insufficiency, hepatic encephalopathy, and esophageal varicies [4]. Worldwide, cirrhosis is a significant cause of death with an estimated 786,483 fatalities attributed to the disease in 2002 according to the World Health Organization. This number is increased when factoring in deaths due to HCC, of which up to 80% of the cases have an underlying presence of cirrhosis worldwide [3]. In the United States, cirrhosis is the 12th leading cause of death, with 27,530 fatalities in 2005 according to the Centers for Disease Control.

Hepatic fibrosis is a common sequela for a variety of insults such as industrial solvent exposure, autoimmunity, cholestasis, in-born errors of metabolism, viral

infection, and ethanol abuse. Nonalcoholic steatohepatitis (NASH) has also been recently as a major cause of liver fibrosis [5]. Worldwide the primary cause of hepatic fibrosis is Hepatitis C infection. In the Western Hemisphere, however, chronic ethanol consumption is the principal cause of liver fibrosis; 44% of end-stage liver disease cases in the United States are associated with excessive ethanol consumption. Clinical intervention is limited by the presentation of disease; as many as 40% of patients with cirrhosis are asymptomatic [6]. However, deterioration of the liver progresses rapidly as complications such as encephalopathy and esophageal varicies arise with patients experiencing 50% mortality over 5 years.

The principal therapeutic resolution of cirrhosis is orthotopic liver transplantation. Unfortunately this course is limited by the availability of suitable organs for transplant. In 2006, there were 6,227 liver transplants performed in the United States. However, at year-end, 16,937 persons remained on the waiting list for transplantation according to the Organ Procurement and Treatment Network. Furthermore, not all individuals with end-stage hepatic disease are suitable candidates for transplantation. Thus, development of therapeutic strategies to prevent or reverse the progression of liver fibrosis to cirrhosis, in addition to prolonging the survival of patients with cirrhosis, remains of great interest. Additionally, accumulating findings suggest there may be reversibility of cirrhosis with resolution linked to removal of the underlying disease. Animal studies utilizing rodents treated with the hepatotoxin, carbon tetrachloride, followed by 4 weeks of recovery showed recovery of fibrosis. Similar studies using a bile duct ligation model of fibrosis and cirrhosis resolves following surgical biliojejunal anastomosis [7, 8]. In humans, evidence of regression of fibrosis or cirrhosis based on serial liver biopsies has been seen

in individuals with autoimmune hepatitis controlled by immunosuppression, viral hepatitis responsive to antiviral therapies, and biliary stasis caused by chronic pancreatitis or common bile duct stenosis corrected with adequate treatment [9-12].

The histological features of the scar tissue seen in cirrhosis are identical regardless of the etiology of the disease. However, the location of initial scarring often differs and its location can be attributed to both the underlying etiology and subsequent prognosis. Pericentral fibrosis (zone 3) (Fig. 1) is a common feature in alcoholic fibrosis, whereas in contrast, viral hepatitis typically results in periportal fibrosis (zone 1) [6]. These findings are not trivial as zone 3 fibrosis confers a higher likelihood to progress to severe fibrosis. The principle tool to diagnose liver fibrosis is liver biopsy. This is an invasive procedure that commonly results in pain and occasionally major complications for patients [13]. The heterogeneous distribution of fibrosis in the liver has also led to sampling error (a liver biopsy represents approximately $1/50000^{th}$ of human liver mass) of 15-25% of cases utilizing liver biopsies [14]. These pitfalls associated with liver biopsy as a diagnostic tool has led to efforts to develop novel identifiers of liver fibrosis. Many investigators have attempted to use a panel of biochemical and hematological markers to develop indices for the diagnosis of hepatic fibrosis, such as the proprietary algorithm derived from five biochemical variables and marketed as Fibrotest [15]. Other efforts have focused on noninvasive radiological techniques to diagnose liver fibrosis. One promising technique utilizes magnetic resonance elastography to calculate liver stiffness, a condition directly correlated with extent of hepatic fibrosis [16].

The fibrotic scar is comprised primarily of fibrillar collagens such as type I (a repeating heterotrimer of two α1(I) and one α2(I) polypeptide strands) and III, in contrast

to type IV collagen of the basement membrane. Accumulation occurs due to a net increase in deposition of ECM components; either through their synthesis or a decrease in degradation by matrix metalloproteinases (MMPs). Although the cirrhotic bands surrounding regenerative nodules are the most recognizable form of scarring, it is the deposition of ECM in the space of Disse leading to the disruption of hepatic microcirculation and diminished nutrient delivery to the parenchyma responsible for injury.

The liver is composed of four primary cell types: the hepatocytes, which are responsible for the majority of hepatic functions; endothelial cells which form the lumen of hepatic capillaries or sinusoids; Kupffer cells, which are the resident macrophages of the liver and reside within the sinusoid; and hepatic stellate cells (HSCs) located in the space of Disse between the parenchyma and the sinusoidal endothelium (Fig. 2). The cellular basis of hepatic fibrosis has long been debated with early focus on parenchymal cells of the liver. However, the development of procedures to isolate purified populations of nonparenchymal cells in the liver led to the identification of the HSCs as a principle source of collagens in fibrosis [17, 18]. This led to the realization that collagen production in previous isolates of hepatocytes were most probably due to contaminating HSCs [19]. Evidence has emerged supporting several distinct cell populations capable of producing collagens during hepatic fibrosis besides HSCs. Hepatic myofibroblasts capable of matrix production have been shown to emerge from fibroblasts residing within the portal connective tissue, perivascular fibroblasts associated with the portal and central veins, and periductular fibroblasts residing along bile duct epithelial cells [20-23].

Additional studies have suggested a substantial proportion of myofibroblasts in human hepatic fibrosis are of bone marrow origin [24].

Animal Models of Liver Fibrosis

Numerous animal models exist which permit the investigation of the underlying mechanism of hepatic fibrosis as well as examining the efficacy of potential treatments. Foremost are those most clinically relevant to the progression and presentation of liver fibrosis in humans. However, because of the varying success and ease of implementing these animal models, much attention is currently being paid to improving existing models and developing newer models of fibrosis.

Bile duct ligation (BDL) is a model often employed in rodents to establish cholestasis which can result in periportal fibrosis in 7 to 14 days. Through ligature of the common bile duct, stagnation of bile flow occurs resulting in jaundice due to the accumulation of conjugated bilirubin [25]. The blockage of free bile flow causes injury to hepatocyte membranes due to the strong detergent action of hydrophobic bile acids [25]. BDL also induces biliary epithelial and oval cell proliferation leading to the formation of new bile ductules [26]. Associated with hepatocyte death is inflammation often attributed to the accumulation of neutrophils, however it remains unclear the role played in the initiation and progression of fibrosis [27, 28].

The kinetics of events associated with BDL-mediated injury have been characterized in rats by Georgiev et al [29]. Following ligation of the common bile duct, there is an acute elevation of serum alanine transaminase (ALT), a serum marker often associated with liver damage, peaking at day 2, followed by a rapid decline at day 3 although remaining chronically elevated. This finding coincides with a peak in the

presence of biliary infarcts (areas of focal hepatocyte necrosis) at day 2, with few infarcts detectable in subsequent days. Concomitant with focal necrosis is a peak of transforming growth factor-alpha and hepatocyte growth factor, key cytokines in the initiation of hepatic regeneration. Following initiation of regeneration there is a peak at day 5 of Ki67+ hepatocytes, a marker of proliferation. An examination of key mediators of fibrosis revealed increase levels of tissue inhibitor of metalloproteinase (TIMP)-1, transforming growth factor-beta (TGF-β), and α1(I) collagen peaking at day 3, followed by a second peak for TIMP-1 at day 7 and day 14 for TGF- β and α1(I) collagen.

Although BDL is a well-characterized and reproducible method of introducing hepatic fibrosis, the model has several limitations. The technique requires an invasive survival surgery requiring well-trained staff and can lead to complications that may result in animal loss. BDL also represents a progression of fibrosis not commonly seen in the majority of human individuals with fibrosis as the fibrosis is periportal (zone 1) (Fig. 1) in nature.

Another frequently utilized animal model of fibrosis in rodents is treatment with the industrial solvent carbon tetrachloride (CCl_4). CCl_4 administration has the advantage of being a well-characterized and reproducible model that can be delivered by a variety of minimally-invasive routes such as intraperitoneal (i.p.) injection, oral gavage, and inhalation [30]. CCl_4 causes injury via its metabolism by hepatic oxidases to yield a trichloromethyl radical which in turn initiates lipid peroxidation and may also interact with proteins containing sulphydryl groups [31, 32].

CCl_4 administration induces zone 3 necrosis, apoptosis of hepatocytes, inflammation, and activation of HSCs. With repeated dosing, CCl_4 can be used to induce

bridging fibrosis (4 weeks), where fibrosis spreads to link the portal tract and central vein radicle, cirrhosis (8 weeks), and advanced cirrhosis with micronodule formation (12 weeks) [31].

Due to the high prevalence of alcoholic liver disease (ALD) in the Western Hemisphere there is an interest in developing animal models of ethanol-induced liver fibrosis or cirrhosis. To date a number of models have been developed with varying degrees of success in reproducing the features of ALD. There remains, however, a need to develop a clinically-relevant model of ethanol-induced liver fibrosis that produces the classic pattern of alcoholic hepatitis in humans and is readily accessible to investigators.

The most widely-used method of feeding ethanol to rodents is the Lieber-DeCarli (LD) liquid ethanol diet. Ethanol is delivered by a calorically- and nutritionally-complete diet with 36% of the calories provided by ethanol [33]. L-D liquid ethanol diet administration causes pronounced steatosis and apoptosis within 4 weeks; however, there is an absence of inflammation and fibrosis [34]. Thus, it was postulated that in rodents on liquid ethanol diets that a secondary stress was needed to induce fibrosis. Studies using the L-D diet with a substitution of calorie source (high fat, low carbohydrates) resulted in mild fibrosis and extensive steatosis [35]. More dramatic fibrosis was induced with the addition of high levels of Vitamin A to the L-D, diet whereas simple Vitamin A administration alone did not cause injury [36, 37].

Although the L-D diet alone does not result in hepatic fibrosis in rodents, it remains a valuable tool for ethanol feeding in rodents. It is a non-invasive method to deliver ethanol that overcomes the natural aversion to ethanol that rodents possess [38]. The model also allows for the easy manipulation of the dietary conditions in the addition

of secondary stresses to better establish a reproducible model of fibrosis that is relevant to human pathology.

Another model of delivering ethanol to rodents is the Tsukamoto-French Model of Alcoholic Liver Injury (TFMELD). Using an intragastric tube, ethanol can be constantly infused into the stomachs of rodents, allowing for the maintenance of consistent levels of ethanol. TFMELD alone does not induce cirrhosis; however, a rapid fibrosis, and subsequent cirrhosis, occurs when ethanol is supplemented with a carbonyl iron source [39, 40]. Use of TFMELD by investigators is limited as the model requires the long-term placement of a gastric feeding tube into the stomachs of rodents, requiring skilled staff to place and maintain the feeding tube. The model is also limited as it does not represent the normal route of ethanol consumption in humans.

Hepatic Stellate Cells

The response to injury in hepatic fibrosis involves several cell types in the liver, as well as the involvement of infiltrating cells such as neutrophils and macrophages. However, HSCs are directly responsible for the majority of the synthesis and accumulation of ECM components, particularly type I collagen [18]. Despite this active role in liver fibrosis, HSCs have several important functions including retinoid storage and metabolism, secretion of growth factors and cytokines, maintenance of the ECM via production of its components (in the normal liver, typically type IV collagen) and MMPs, and regulation of sinusoidal perfusion by virtue of the contraction and relaxation of HSCs in response to vasoactive substances [41].

The embryonic origin of HSCs has been the focus of much controversy as extensive efforts have yet to yield a definitive answer. Several hypotheses have been

suggested as to the origin of HSCs: septum transversum mesenchyme, mesothelial cells lining Glisson's capsule on the liver's surface, neural crest, and endoderm [42, 43]. HSCs are known to express a number of neural markers such as reelin, nestin, neural cell adhesion molecule, glial-fibrillary acidic protein, and receptors for neurotransmitters [44-47]. However, the likelihood of a neural crest origin of HSCs was diminished by a study utilizing double transgenic mice possessing a transgene encoding Wnt-1-Cre (Cre recombinase) and a second transgene, encoding yellow fluorescent protein (YFP) floxed (flanked by *loxP*) by a stop cassette. In this system, cells expressing Wnt-1 would also produce Cre. Cre catalyzes site-specific recombination of DNA between *loxP* sites. Because all known cells derived from neural crest express Wnt-1, utilizing these transgenic mice, the stop cassette preventing transcription of the YFP gene would be removed in neural crest-derived cells allowing expression (Fig. 3) [48, 49]. All known neural crest-derived cell populations expressed YFP in the transgenic mice; however, no YFP was detected in the developing liver during the period desmin, a known marker for HSCs, was shown to be concomitantly expressed [50].

A more recent study has suggested HSCs may be derived from mesenchymal cells derived from mesoderm. Cell lineage mapping was again conducted utilizing double transgenic mice; one transgene being MesP1 (mesoderm posterior 1), a transcription factor expressed in mesoderm, driven Cre and the second being *lacZ* floxed by a stop cassette [51]. The study indentified three populations of mesoderm-derived mesenchyme in the liver, with a sub-population of activated leukocyte cell adhesion molecule (ALCAM) positive cells being the precursors to HSCs in the developing liver [52]. The

mesodermal-derived hypothesis of HSC origin is further strengthened by the observation that Foxf1 transcription factor is expressed in the developing and regenerating liver [53].

Evidence suggesting HSCs may be derived from endoderm exists in the form of findings that stellate cells and hepatoblasts both exhibit transient expression of cytokeratins. Specifically, a population of cluster of differentiation (CD) 34+/cytokeratin 7/8+ cells were found in humans expressing markers for HSCs , including desmin and smooth muscle α-actin (αSMA) and possessed a morphology similar to stellate cells [54].

HSCs represent 15% of the total number of resident liver cells and exist in two distinct phenotypes, with one being described as quiescent found in the normal liver [55]. Quiescent HSCs possess many retinyl ester-containing lipid droplets in the cytoplasm which fluoresce under ultraviolet light, a key distinguishing characteristic [18]. Additionally, quiescent HSCs have finely-branched cytoplasmic processes that wrap around the hepatic sinusoid [56]. HSCs in normal liver are distributed homogenously throughout the liver lobule, the functional unit of the liver. However, there appears to be phenotypic variation among intralobular HSCs as those located near zone 3 store less retinyl esters as zone 1 HSCs [57]. Upon fibrogenic stimuli, HSCs transdifferentiate to an activated, myofibroblast-like phenotype. Activated HSCs lose their cytoplasmic lipid droplets, undergo proliferation, possess the ability to migrate, express stress fibers, and secrete an abundance of fibrillar ECM components, specifically type I collagen [6]. Additionally, the homogenous distribution of HSCs is lost, either through local proliferation and/or migration of activated HSCs in response to chemoattractive agents.

The specific mechanisms underlying the activation of HSCs remain unclear; however, a variety of factors that contribute to the activation of HSCs have been

identified. Factors released from damaged liver cells, such as lipid peroxides, drug metabolites, such as acetaldehyde from the metabolism of ethanol, and reactive oxygen species (ROS) can activate the resident macrophage of the liver, the Kupffer cell. Activation of Kupffer cells can result in the release of cytokines that play a significant role in the activation process of HSCs. Kupffer cells may also be activated by distal events, such as the increased permeability of the gut to the endotoxin lipopolysaccharide (LPS) following ethanol consumption. LPS is a potent stimulator of Kupffer cells and may play a major role in ethanol-induced liver fibrosis [58]. Activated HSCs also express toll-like receptor 4 and stimulation with LPS increases inflammatory cytokine production through the transcription factor nuclear factor-kappaB (NF-κB) [59].

Activation of HSCs can be categorized into two stages: the initiation phase and the perpetuation phase (Fig. 4). In the initiation phase, quiescent HSCs undergo marked changes in gene expression and phenotype that renders it responsive to cytokines and other stimuli. Factors leading to initiation of HSCs include infiltrating inflammatory cells (particularly neutrophils), injury to the hepatic parenchyma and neighboring sinusoidal endothelial cells (SEC), proliferation and paracrine stimulation from Kupffer cells, and changes in the surrounding ECM [60]. During the perpetuation stage, the activated phenotype of HSCs is maintained and even amplified by the increased expression of growth factors, as well as the enhanced response of HSCs to these factors. Whereas the events that mediate the initiation of activation are largely paracrine, the perpetuation of activation is comprised of both paracrine and autocrine stimuli.

In normal liver, quiescent HSCs store retinyl esters, play a role in hemodynamics by modulating sinusoidal diameter, and maintain the normal basement membrane. These

HSCs secrete predominantly small amounts of type IV collagen and negligible amounts of fibrillar collagens such as types I and III. The basement provides the proper orientation of cells of the hepatic sinusoid as well as signals that maintain the differentiated state of surrounding cells. This facilitates the proper delivery of oxygen and nutrients across the fenestrated SECs, perisinusoidal space of Disse, and subsequently to the parenchymal cells of the liver. In response to chronic liver injury, activated HSCs are the principal cell type responsible for the substantial increase in the synthesis and secretion of type I collagen. In activated HSCs there is a 60- to 70-fold increase in steady-state mRNA levels of α1(I) procollagen compared to quiescent HSCs [61]. The dramatic increase in α1(I) procollagen levels is thought to be largely due to an increase in mRNA half-life. Although the transcription rate of α1(I) procollagen mRNA is two-fold higher in activated HSCs, the mRNA half-life is increased from 1.5 h in quiescent HSCs to > 24 h in activated cells. The increase in mRNA half-life is thought to be caused by increased binding of proteins in the 3' untranslated region of the α1(I) procollagen mRNA [61].

The most potent pro-fibrotic cytokine identified is TGF-β. TGF-β stimulates the production and deposition of fibrillar ECM components such as type I and III collagen [62]. HSCs are a major source of TGF-β production in the liver, but Kupffer cells, hepatocytes, and platelets can also secrete this cytokine. Furthermore, TGF-β sequestered in the ECM can be liberated following injury. Thus in activated HSCs TGF-β can stimulate in both autocrine and paracrine manners. TGF-β signals through the constitutively active type II TGF-β receptor which in turn recruits and phosphorylates the type I receptor. This recruits Smad2 and Smad3 proteins which are both phosphorylated.

Smad2 and Smad3 then form a heterotrimeric complex with Smad4, resulting in the translocation of the complex to the nucleus where it interacts with specific DNA sequences to regulate transcription [63]. TGF-β has been reported as a potent inducer of both α1(I) and α2(I) collagen genes although a TGF-β response element has only been clearly identified in the promoter of the α2(I) collagen gene [64, 65].

Activated HSCs potentiate fibrosis not just through an increase in the rate of ECM component production, but also by increasing the pool of fibrogenic cells through proliferation. Although HSCs can respond to a variety of mitogens, platelet-derived growth factor (PDGF) is considered the most proliferative stimulus. Expression of PDGF and its receptor (PDGF-R) are up-regulated during activation of HSCs [66]. PDGF stimulation is associated with chemotaxis, loss of retinoids, and growth. Expression of PDGF and its receptor are further modulated by other cells such as SECs and Kupffer cells. PDGF is a heterodimeric protein composed of either of its two polypeptide A and B chains. HSCs have been shown to be most responsive to PDGF-BB, which is upregulated by TGF-β via increasing PDGF-BB mRNA levels [67]. Thus common mechanisms exist that upregulate both the proliferative and ECM-depositing capacities of HSCs upon their activation.

Another clinical manifestation of hepatic fibrosis is the hypercontractile nature of activated HSCs. HSCs can contract and relax to regulate sinusoidal diameter dependant on a balance of vasodilators such as nitric oxide (NO) and vasconstrictors such as ET-1. Upon activation, HSCs initially upregulate production of both ET-1 and NO. However, as disease progresses, the balance is shifted towards ET-1 [68]. Coupled with an increase in stress fibers in the cytoplasm, such as αSMA, activation of HSCs renders them

hypercontractile. Hypercontractile HSCs inappropriately constrict the sinusoid diameter, further depleting the parenchyma of oxygen and nutrients and giving rise to portal hypertension. This causes systemic consequences as the extra blood must be shunted away from the liver and often gives rise to esophageal varicies.

Resolution of underlying liver disease has been experimentally shown to result in spontaneous recovery with a reduction in the number of activated HSCs [7-12]. The decrease in HSCs may be attributed to one of two mechanisms: reversion of phenotype back to the quiescent state and apoptosis of activated HSCs. Reversion of phenotype has been experimentally shown *in vitro;* however, it remains unclear whether this phenomenon can occur *in vivo* [69]. Activated HSCs express the cell surface death receptor Fas, and apoptosis can be induced with Fas ligands, such as Fas-activating antibodies [70]. TNF-α-mediated apoptosis, however, is inhibited by NF-κB activity, thus apoptosis of activated HSCs may require the downregulation of key survival signals.

Type I collagen

Collagens are the main connective tissue protein in animals and are the most abundant protein found in mammals [71]. Secreted into the ECM along with glycoproteins, proteoglycans, and elastins, collagens help maintain the integrity of many tissues by interacting with cell surfaces, other ECM components, and growth and differentiation factors [72]. Collagens are synthesized as a triple helix from three polypeptide α chains composed of continuous Glycine- (Gly) X-Y peptide repeats [73]. Glycine is essential in the first position as its side chain is the only one small enough to fit within the center of the coiled-coil triple helix [74]. Proline is frequently found in the X position and Hydroxyproline typically occupies the Y position [75]. These two amino

acids limit rotation of the triple helical structure and their placement on the surface of the triple helix facilitates self-assembly and polymerization of collagen molecules through charge-charge and hydrophobic interactions [73].

Type I collagen is a fibrillar collagen and is the most abundant protein in mammals, comprising much of the ECM scaffold in the tendons, skin, lungs and many other tissues such as bone where it provides the majority of its tensile strength [76]. Type I collagen is an important component in the wound-healing process and is found in large quantities in scar tissue associated with a variety of pathological conditions [77, 78]. In the liver, chronic damage stimulates activation of HSCs resulting in a phenotype change towards excessive production and secretion of ECM products, particularly type I collagen [18].

Synthesis of type I collagen is initiated by the expression of the *col1a1* and *col1a2* genes [79]. Levels of these gene products can be regulated at both the transcriptional and post-transcriptional level [80]. Despite being located on different chromosomes, expression of these two genes are coordinately regulated in a tissue-specific manner giving rise to α1(I) and α2(I) procollagen mRNA products in a 2:1 ratio respectively [81, 82]. Regulation of *col1a1* and *col1a2* gene transcription is regulated by the promoter and first intron [83-85]. The *col1a1* and *col1a2* genes can also be regulated through chemical modifications such as methylation [86]. Several CpG islands have been identified upstream of the promoter, and methylation of these sites causes a reduction in collagen gene transcription [87].

A variety of cytokines and protein factors can modulate collagen expression. Several inflammatory cytokines such as TGF-β, interleukin-6 (IL-6), tumor necrosis

factor-alpha (TNF-α), and interleukin-1β have been shown to upregulate type I collagen production [88-91]. Nuclear factor-1 has been shown to be the required transcription factor for TGF-β-mediated upregulation of *col1a2* transcription [92]. The basic transcription element binding protein (BTEB) and Sp1 [93] are zinc-finger family transcription factors that also enhance type I collagen production. BTEB specifically is linked to *c-jun* N-terminal kinase- (JNK) dependent increases in type I collagen synthesis following UV irradiation [94]. Other cytokines have been implicated in the inhibition of type I collagen transcription, such as interleukin-10 (IL-10) [95], interferon gamma (IFN-γ) [96], and fibroblast growth factor [97]. Modulation of collagen synthesis can also be regulated post-transcriptionally as demonstrated by increased mRNA stability [61].

Translation of these mRNAs results in procollagen polypeptides of approximately 1000 amino acids. The polypeptide is flanked by globular C- and N-terminal propeptide domains and contains approximately 338 repeats of the Gly-X-Y motif [98]. Most proteins begin folding at the N-terminal prior to completion of translation and translocation. For type I collagen, however, folding is initiated at the C-terminal following cotranslational translocation into the endoplasmic reticulum (ER) [99]. Several proteins play an important role in facilitating the proper folding and trafficking of α chains into triple helix procollagen molecules. The 78-kDa glucose-regulated protein (Grp78) recognizes hydrophobic residues on polypeptide chains to help maintain solubility and may also bind the C-propeptide [100]. Protein disulfide isomerase (PDI) also plays a role in triple helix formation by catalyzing disulfide bonds between C-propeptide domains of the three α chains [101, 102]. PDI also acts as a subunit for prolyl 4-hydroxylase (P4H) by keeping the catalytic α-subunits in a soluble state [103]. Further

stabilization of the triple helix is accomplished through hydroxylation of select proline residues (typically in the Y position) by the P4H enzyme which in turn facilitates hydrogen bonding and the formation of water bridges within and between collagen chains [104, 105]. The 47-kDa heat shock protein (Hsp47) is a collagen-specific chaperone which also plays an important role in collagen trafficking [106]. Although the exact role of Hsp47 has not been clearly defined, studies utilizing Hsp47$^{-/-}$ mice showed they are embryonically lethal at day 11.5 [107]. After procollagens traverse the Golgi apparatus and are secreted into the extracellular space, the C- and N-prodomains are cleaved by C- and N-peptidases respectively [108]. This process drops the concentration required for fibril formation and results in the self-assembly of collagens into fibrils [109] (Fig. 5).

Nuclear Factor-kappaB

HSCs upon activation also undergo gene expression changes that further exacerbate injury through the recruitment of inflammatory molecules. NF-κB is a redox-sensitive transcription factor which has been implicated in stimulating an increase in inflammation in the injured liver [110]. NF-κB is composed of members of the Rel family (p65, p50, p52, c-Rel, and RelB). Each member contains a consensus DNA binding domain, a dimerization domain that allows both the formation of homo or heterodimers, and a nuclear localization signal (NLS) [111]. Although all members contain a DNA binding domain, only the p65, c-Rel, and RelB are considered transcriptional activators wherase p50 and p52 are generally associated with transcriptional repression [112, 113]. In the cytoplasm the repressor IκBα is bound to the NLS of NF-κB, sequestering the complex in the cytoplasm. In response to the appropriate stimulus, IκBα is phosphorylated by the IκB kinase (IKK) complex and is

polyubiquinated and subsequently degraded by the 28S proteosome [114]. Degradation of IκBα liberates NF-κB by unmasking the NLS, allowing translocation to the nucleus to bind specific sequences and alter gene expression [115].

There are two major pathways that lead to the activation of NF-κB. In the canonical activation of NF-κB a variety of upstream stimuli such as IL-1, TNF-α, and Toll-like receptor signaling leading to the phosphorylation and activation of the IKKβ subunit of the IKK complex [110]. In non-canonical activation of NF-κB, a limited number of stimuli such as CD40 activates the IKKα subunit, typically leading to activation of p52/RelB heterodimers as opposed to p65/p50 heterodimers with subsequent activation of a different group of gene targets [110].

In quiescent HSCs the p50/50 homodimer dominates and is mainly sequestered in the cytoplasm. Upon activation, there is an increase in the p65/50 complex [116]. Activators of p65/50 in HSCs include acetaldehyde and TNFα leading to the transcription of inflammatory gene products such as intracellular adhesion molecule-1, macrophage inflammatory protein-2, and IL-6 [117, 118]. NF-κB activation, however, does not appear to affect the activation of HSCs [119]. Paradoxically, p65/50 appears to inhibit the *col1a1* and *col1a2* genes in activated HSCs, suggesting NF-κB has a complex role in activated HSCs [120, 121].

Matrix Metalloproteinases

The ECM is a complex network of protein and macromolecules that provides a variety of functions to the surrounding cells and tissues. Constituents of the ECM are typically divided into three categories: collagens, glycoproteins, and proteoglycans. The most widely appreciated role of the ECM is the ability of collagens to provide a basement

membrane and support to a variety of tissue types. The ECM also is involved in regulation of biological functions through the expression of integrins on cells interacting with the ECM. Type I collagen can stimulate cell division by interacting with integrin β_1 to induce focal adhesion kinase phosphorylation and activation of phosphoinositide-3 kinase.

The composition of the ECM must be tightly regulated to ensure normal biological function of the surrounding tissues. A net accumulation of ECM components (either through excessive production or a decrease in degradation) results in fibrotic conditions, regardless of the site. However the ECM is a dynamic environment undergoing constant turnover. Thus, a means of tightly regulating the accumulation and destruction of ECM components must exist.

Regulation of the ECM is accomplished in part by a diverse family of calcium- and zinc-dependant endopeptidases called MMPs. There are 25 identified unique members of the MMPs, of which 24 are found in mammals, and they are capable of degrading a variety of matrix components. MMPs can be divided into five categories: interstitial collagenases, gelatinases, stromelysins, membrane-type collagenases, and a metalloelastase (MMP-12) although there is some overlap in function between these groups. MMP-1, MMP-8, MMP-13 are the interstitial collagenases; however, MMP-2 (a gelatinase) and MT1-MMP (a membrane-type collagenase) can work together to cleave interstitial collagens [122, 123]. Although the main function of the MMPs has long been considered to be the degradation of ECM components from tissues, increasing evidence suggests cleavage of ECM and cell-surface molecules by MMPs can alter cell-matrix and

cell-cell interactions, affecting biological function and releasing growth factors sequestered within the ECM [124].

Structurally, typical MMPs consist of a propeptide of approximately 80 amino acids containing a 'cysteine switch' with the PRCGXPD consensus sequence, a catalytic domain of approximately 170 amino acids, a linker peptide commonly referred to as the 'hinge region', and a hemopexin domain of approximately 200 amino acids which is considered important in substrate recognition [125]. The propeptide maintains the zymogen in the inactivated state by coordinating a Cys residue with a Zn^{2+} ion bound to the HEXXHXXGXXH motif within the catalytic domain, resulting in the exclusion of a water molecule necessary for catalysis [125].

MMPs have evolved multiple levels of regulation due to their important role regulating the ECM. In the normal steady-state tissue, the activity of most MMPs is low with transcription upregulated by inflammatory cytokines, growth factors, hormones, and cell-cell and cell-matrix interactions [126]. MMPs are translated as pre-proenzymes with a signal peptide, which is cleaved during translation, targeting them for secretion (or insertion into the membrane as with the MT-MMPs). Following secretion, the zymogen can be activated by cleavage of the propeptide domain. This often occurs in a 'stepwise process' requiring the presence of two or more proteinases [127]. Transient MMP activation can also occur in the presences of oxidants in inflammatory settings through reactions with the cysteine switch of the propeptide [128, 129].

MMPs are also regulated through protein-protein interactions via two types of inhibitors: α_2-macroglobulin and TIMPs. α_2-macroglobulin inhibits MMPs by entrapping the proteases within a complex with α_2-macroglobulin and subsequent clearance through

the low density lipoprotein receptor-related protein-1 [130]. Four TIMPs have been identified (TIMP-1, TIMP-2, TIMP-3, and TIMP-4) each consisting of 184-194 amino acids. TIMPs inhibit MMPs by directly binding to the catalytic domain of MMPs in a 1:1 stoichiometric ratio. TIMPs have been shown to inhibit the activity of each MMP, though with varying efficiency [131]. In particular TIMP-1 is a poor inhibitor of MT1-MMP [132].

The expression profiles of MMPs and their inhibitors play an important role in the progression and resolution of hepatic fibrosis as there is a ten-fold increase in the deposition of ECM components, particularly interstitial collagens, during fibrosis [133]. In particular, MMP-1 (MMP-13 in rodents), MMP-2, MMP-9, MT1-MMP, TIMP-1, and TIMP-2 show significant changes in their expression and activity profiles during the initiation, progression, and resolution of hepatic fibrosis (Fig. 6).

In the liver the main interstitial collagenase is MMP-1 in humans and MMP-13 in rodents. MMP-3 (stromelysin-1) is another interstitial collagenase expressed in liver, however, it exhibits weak proteolytic activity towards ECM components [134]. MMP-13 expression in the liver is expressed by HSCs, fibroblasts , Kupffer cells, and sinusoidal endothelial cells [26]. Expression of MMP-13 mRNA can be stimulated by a variety of inflammatory cytokines and growth factors including IL-1α, IL-1β, TNF-α, and EGF [135-138]. TGF-β does not influence the expression of MMP-13; however, it has been shown to abrogate the expression of MMP-1 [136, 139].

In animal models of fibrosis, MMP-13 levels rise shortly after initial injury and decline to baseline levels as fibrosis develops [140]. This initial peak of expression may actually be deleterious, as MMP-13 may destroy surrounding tissue permitting the

deposition of newly synthesized ECM components and the liberation of inflammatory cytokines sequestered in the ECM. Disruption of MMP-13 expression during fibrogenesis attenuates injury, supporting a role in initiating injury [141]. Following withdrawal of the noxious stimulus, hepatic fibrosis undergoes spontaneous resolution. Associated with the resolution is a rise in the expression of MMP-13. The source of MMP-13 during resolution of hepatic fibrosis may be scar-associated macrophages, as HSCs undergoing apoptosis would no longer be an adequate source of MMP-13 secretion [142]. The role of MMP-13 in hepatic fibrosis appears to be dual: in the initiation of injury, MMP-13 can disrupt the normal ECM permitting the deposition of newly synthesized ECM products by HSCs. Disruption of the ECM can also release sequestered pro-fibrotic cytokines such as TGF-β, further perpetuating injury. In the resolution of injury, MMP-13 can cleave interstitial collagens such as type I collagen allowing restoration of the normal liver architecture. Increasing MMP-13 activity is an attractive therapeutic, but attention should be paid to the stage of injury.

The gelatinase MMP-2 and the membrane-type collagenase MT1-MMP appear to be involved together in hepatic fibrosis as both collagenases are expressed in HSCs following liver injury [135]. Studies have suggested that the transcription of MMP-2 and MT1-MMP in HSCs may be co-regulated [143]. MMP-2 appears to be activated by MT1-MMP at the cell surface when a ternary complex is formed between proMMP-2, MT1-MMP, and TIMP-2 [144].

In normal liver, levels of both MMP-2 and MT1-MMP mRNA are low [145]. However, following injury in both $CC1_4$ and BDL models of experimental fibrosis, there is sustained increase in the expression of both proteins during initiation, fibrogenesis, and

resolution [146, 147]. Despite sustained elevation during hepatic injury, MMP-2 appears to have a diverse role. MMP-2 is a stimulator of proliferation and migration of activated HSCs and is upregulated by ROS and TGF-β in cultured human HSCs [148]. In the resolution of hepatic fibrosis there is a decline of TIMP-1 levels despite sustained levels of MMP-2 and MT1-MMP which may be at least partially responsible for fibrolysis in resolution of hepatic fibrosis [149].

MMP-9 is another gelatinase expressed in liver during hepatic fibrosis. It is expressed under inflammatory conditions by several cell types in the liver. MMP-9 is produced *in vitro* by TNF-α- or IL-1β-stimulated hepatocytes, IL-1α-stimulated HSCs, and activated Kupffer cells [135, 136, 150]. MMP-9 is activated by MMP-3 and can cleave latent TGF-β into the active form, possibly influencing hepatic fibrosis [151]. In experimental models of fibrosis, MMP-9 is elevated and likely sources included HSCs and inflammatory cells such as neutrophils [136, 152].

Important modulators of hepatic fibrosis may be TIMP-1 and TIMP-2. TIMP-1 expression is mediated by a number of inflammatory cytokines such as IL-1β, IL-6, TNF-α, and TGF- β [139, 153, 154]. In the fibrotic liver, TIMP-1 appears to be principally produced by HSCs in both CCl_4 and BDL models of injury [155, 156]. To illustrate the importance of TIMP-1 in hepatic fibrogenesis, studies utilizing TIMP-1 overexpressing mice showed severe injury in a CCl_4 model of liver fibrosis as compared to control mice. However, TIMP-1 alone does not induce fibrosis [157, 158]. Additionally TIMP-1 antisense therapy and neutralizing antibodies were shown to lessen hepatic fibrosis [159, 160]. Besides the well-established direct role of TIMPs as inhibitors of MMPs, TIMP-1 is capable of indirect inhibition of HSC apoptosis [157, 161]. Furthermore, reduction of

TIMP-1 levels is associated with increased hepatocyte proliferation via degradation of fibrotic ECM to permit hepatocyte expansion and liberation of ECM-bound hepatocyte growth factor [162].

TIMP-2 expression in liver cells was detected in activated HSCs, Kupffer cells, and myofibroblasts [135]. In models of liver fibrosis, TIMP-2 expression was elevated in a BDL model but not a CCl_4 model of disease [147, 149]. TIMP-2 may be most relevant in the earlier stages of hepatic fibrosis, as it is responsible for activation of MMP-2 along with the presence of MT1-MMP.

MMPs and their inhibitors clearly play an important role in the development, progression, and resolution of hepatic fibrosis. However, the context of MMP and TIMP expression must be considered when developing therapeutic strategies to target their activity. In early stages of hepatic fibrosis, MMPs appear to play a deleterious role, whereas in the resolution of fibrosis, MMP activity is critical to reduce the scar and achieve restoration of the normal liver architecture.

Endoplasmic Reticulum Stress

In cells there is a constant synthesis and degradation, or “turnover”, of proteins. When eukaryotic cells are subjected to stress, two mechanisms are employed to maintain protein stability: the heat-shock response which occurs in the cytosol and the unfolded protein response (UPR) which occurs in the endoplasmic reticulum (ER) [163, 164]. Unlike the heat-shock response, the UPR is a normal physiological process that allows cells to expand their production of proteins for secretion through the upregulation of molecular chaperones responsible for transporting and facilitating proper protein structure.

Nascent polypeptides enter the ER in the unfolded state where they then encounter specific chaperones which fold and modify the proteins for subsequent secretion [165]. In the ER proteins undergo quality control which differentiate between properly folded and misfolded or improperly assembled proteins. Misfolded proteins are eliminated from the ER through retro-translocation through the Sec61 complex [166] into the cytoplasm and subsequent polyubiquitination and ultimately degradation by the 26S proteasome in a process called ER-associated degradation (ERAD) [165, 167]. Perturbations that signal the ERAD process include an increase in secretory protein synthesis, accumulation of mutant or misfolded proteins, deprivation of glucose, Ca^{++} depletion within the ER, and a shift in redox status within the cell [168].

The UPR is typically mediated by three intracellular sensors: type-I ER transmembrane protein kinase (IRE1), activating transcription factor 6 (ATF6) and the PKR-like ER kinase (PERK) [169-172]. In each instance the ER luminal domains of these proteins bind to the Grp78 under normal physiological conditions. Upon conditions resulting in an increase in the unfolded protein burden within the ER, Grp78 dissociates with these ER-resident sensors and binds to the unfolded proteins. This in turns generates signal transduction events among the sensor proteins: IRE1 dimerizes and is autophosphorylated and ATF6 is cleaved to generated nATF6 with both translocating to the nucleus to stimulate the production of new chaperone proteins. PERK autophosphorylates and in turn phosphorylates eIF-2a which attenuates transcription [168]. Thus by increasing the production of chaperone proteins and decreasing the amount of nascent polypeptides being delivered to the ER, while retro-translocating

misfolded proteins for proteasomal destruction, the cell can clear the accumulation of misfolded proteins.

While the UPR is a normal response, prolonged UPR and ERAD can be deleterious to the cell. Retrotranslocation of unfolded proteins for degradation is an energy-dependent process, which is a contributing factor in apoptosis [173, 174]. Prolonged ER stress is also linked to a release of ER stores of Ca^{++} into the cytosol, potentially damaging the mitochondria and generating oxidative stress, which can in turn lead to inflammation through activation of NF-κB [175, 176]. Chronic ethanol consumption can also lead to prolonged ER stress through hyperhomocysteinemia [177, 178].

Ethanol and Oxidative Stress

Worldwide, the principal cause of hepatic fibrosis is viral hepatitis. However, excess consumption of ethanol is the leading cause of liver fibrosis in the United States and Europe. Strongly associated with the onset of fibrosis is the development of oxidative stress. Oxidative stress following chronic ethanol abuse is consequence not only of its metabolism, but of the serious alterations in critical dietary nutrients involved in maintaining overall antioxidant status. Chronic ethanol consumption through its intake and metabolism likely causes damage not only through pro-oxidant production but also via a decrease in anti-oxidant defense.

Three metabolic pathways for ethanol have been identified in the liver: cytoplasmic alcohol dehydrogenase (ADH), the inducible microsomal ethanol-oxidizing system (MEOS) found in endoplasmic reticulum, and catalase located within peroxisomes [179-181]. Each pathway generates a specific toxic metabolite,

acetaldehyde being a common metabolite. The hepatocyte is the main site for ethanol metabolism and utilizes all three pathways. It is through the metabolism of ethanol that the majority of reactive oxygen species (ROS) and reactive nitrogen species are generated.

ADH is a constitutively-expressed zinc metalloenzyme with eight different types of subunits (α, β1, β2, β3, γ1, γ2, π, and χ) that arise from 5 gene loci [181]. A recently identified new subunit (σ) has also been discovered from human stomach. ADH converts ethanol to acetaldehyde with the loss of H^+, which in turn reduces NAD to NADH. With chronic ethanol consumption, the large burden of reducing equivalents prevents the hepatocyte from maintaining redox homeostasis [182]. Perturbations in hepatocyte homeostasis result in a variety of metabolic disorders, such as hypoglycemia and hyperlacticacidemia [183]. The increased accumulation of NADH also promotes fatty acid synthesis and opposes β-oxidation of lipids, resulting in fat accumulation; a finding described as steatohepatitis [183]. Disruption of the redox state of cells can also stimulate redox-sensitive transcription factors such as NF-κB leading to an increase in inflammation in the liver.

The key enzyme of the MEOS is the ethanol-inducible cytochrome P450 2E1 (CYP2E1). CYP2E1 catalyzes the conversion of ethanol to acetaldehyde utilizing NADP as a proton acceptor. This reaction has been shown to be loosely coupled to cytochrome reductase, providing a source of electrons to oxygen to form superoxide anion or cause lipid peroxidation [184]. The induction of CYP2E1 is transcriptionally regulated and its expression stimulated by ethanol consumption; samples from liver biopsies of recently-drinking individuals showed a 4- to 10-fold increase in CYP2E1 levels [185]. The

induction of CYP2E1 results in a metabolic tolerance to ethanol that exists in addition to CNS tolerance [186]. This is significant as rapid metabolism of xenobiotics (including ethanol, acetaminophen, and social drugs of abuse commonly linked to ethanol consumption) can overwhelm the main intracellular antioxidant, glutathione. Animals fed ethanol chronically show increased glutathione (GSH) turnover, and an increased in oxidized glutathione (GSSG) [187].

Ethanol may also lead to oxidative stress in nonparenchymal cells in addition to hepatocytes. Kupffer cells have been shown to produce ROS via NADPH oxidase following chronic infusion of ethanol in mice via a gastric feeding tube as evidenced by electron spin resonance. However $p47^{phox}$ knockout mice which lack a critical subunit of the NADPH oxidase showed no liver pathology [188]. The metabolism of ethanol in HSCs is controversial, however. HSCs have been shown to express ADH but conflicting data exists in the literature regarding CYP2E1 [189, 190]. However, given the ratio of HSCs to parenchymal cells in the liver, it is expected the majority of ethanol metabolism via ADH would occur in hepatocytes [191].

HSCs, given their proximity to both hepatocytes and Kupffer cells, are subject to paracrine and systemic effects of ethanol metabolism. Although the primary product of ethanol metabolism, acetaldehyde, is metabolized to acetate via aldehyde dehydrogenase, the activity of this enzyme is sufficiently slow to allow accumulation of acetaldehyde systemically; many of the physical effects of hangovers have been ascribed to acetaldehyde. Acetaldehyde is known to potentiate collagen transcription though the precise action remains unclear [192]. However, it is known that acetaldehyde can form adducts with proteins via Schiff bases, most commonly with the α-amino group of lysines

[193, 194]. These acetaldehyde-protein adducts can be detected in the livers of ethanol-fed rats and the majority of alcoholic individuals have antibodies against these adducts in their serum. This may compound disease progression by promoting auto-immunity in the liver [195].

Acetaldehyde-dependant increases in collagen transcription appear to be dependent on *de novo* protein synthesis. Treatment of HSCs with acetaldehyde stimulates the binding of the transcription factor BTEB to a region of the α_1(I) collagen promoter originally described as the UV response element [94]. The production of BTEB following acetaldehyde stimulation appeared to be mediated by JNK [94].

Ethanol consumption also leads to nutritional deficiencies that can deplete antioxidants in the body. Ethanol is a very energetic compound, and chronic alcoholics can receive as much as 50% of their calories from ethanol consumption [196]. Thus the reduction in the diet of protein, nutrients, and vitamins can perturb metabolic pathways and deplete key intermediates in antioxidant pathways. Ethanol consumption has been shown to deplete methionine and decrease absorption of folate from the gut [197]. Both compounds are important intermediates in the regeneration of the intracellular antioxidant glutathione.

Prolonged ethanol consumption can cause significant liver injury. Through both the metabolism of ethanol and the actions of its metabolites, there is a tremendous generation of oxidative stress and alteration of the redox state, particularly in the liver. Antioxidant stores are further depleted by ethanol consumption via the decrease of upstream intermediates such as folate and methionine. Thus the identification of

therapies that can correct the altered nutritional and antioxidant state of the body remain attractive.

S-adenosyl-L-methionine

S-adenosyl-L-methionine (SAMe) is a pleiotropic molecule found in all living organisms. The importance of SAMe is due to its ability to participate in a diverse number of biological reactions, likely second only to ATP. SAMe is the principal biological methyl donor, the precursor of aminopropyl groups used in polyamine biosynthesis, and in the liver is also a precursor to glutathione by conversion to cysteine via the trans-sulfuration pathway (Fig. 7) [198]. Therefore, deficiency in SAMe can be expected to have major detrimental effects on cellular function, given the importance of methylation in processes such as gene expression and membrane fluidity. Accumulating evidence has shown that SAMe administration can attenuate liver disease, and studies have shown SAMe as a treatment for depression [199].

Though SAMe is synthesized in the cytoplasm of all cells, the liver is the primary site of SAMe homeostasis [200]. Generation of SAMe is catalyzed by methionine adenosyltransferase (also called s-adenosylmethionine synthetase) by the introduction of an adenosyl group from ATP to form a high-energy sulfonium ion, generating a molecule that readily loses its methyl group to a variety of substrates such as proteins, nucleic acids, phospholipids, and amines [201]. Half of the dietary intake of methionine is used to synthesize SAMe, with approximately 95% of the 6-8 g produced each day used in transmethylation reactions [202]. Less than 5% of SAMe metabolism is attributed to polyamine synthesis, although this amount can increase during liver regeneration [202]. Demethylation of SAMe generates S-adenosylhomocysteine (SAH). SAH is a potent

inhibitor of transmethylation reactions, necessitating its rapid removal. In the liver, SAH is cleared by its conversion to cysteine, demonstrating a role for SAMe as a precursor to glutathione [203].

With oxidative stress a prominent feature of ethanol-induced liver fibrosis, a role for antioxidants has long been pursued as a treatment for liver disease. However, exogenous administration of antioxidants such as vitamin E, carotenoids, and glutathione have failed to show any significant benefit in human patients with liver disease [36, 37, 204]. In contrast, a variety of animal studies have shown a benefit when attempting to modulate liver disease with antioxidant therapies. In particular, SAMe has shown beneficial effects in several fibrotic animal models [205-208]. Additionally, a clinical trial of patients with alcoholic liver cirrhosis, SAMe treatment resulted in delayed transplantation and increased survival [209].

While the beneficial effects of SAMe in experimental models of injury have been well accepted, little is known about its mechanism of action. In rodent models of fibrosis, SAMe decreased several markers of liver injury such as liver transaminases and bilirubin levels. Furthermore, SAMe was shown to decrease hepatic collagen content by hydroxyproline assay [210]. However, no studies have been performed to determine the molecular mechanisms of SAMe in activated HSCs. Given its property as the principal biological methyl donor, SAMe may be acting to decrease type I collagen by methylating DNA. The α_1(I) and α_2(I) collagen promoters are both rich in CpG islands, the main sites of DNA methylation. With methylation often associated with gene silencing, SAMe may be methylating the promoters to repress their transcriptional activation.

Another potential mechanism for SAMe-mediated decreases in hepatic collagen is its role as an antioxidant. SAMe as mentioned is a precursor to the main intracellular antioxidant glutathione. By restoring antioxidant levels in the liver and reestablishing proper redox balance, SAMe may decrease the activation of redox-sensitive transcription factors such as AP-1 and NF-κB.

Hypothesis

We hypothesize that SAMe can inhibit type I collagen production in culture-activated hepatic stellate cells. Furthermore, we hypothesize that SAMe functions to decreases oxidative stress mediated by the redox-sensitive transcription factor NF-κB. In order to address these hypotheses, we also developed an animal model of ethanol-induced hepatic fibrosis utilizing the Lieber-DeCarli liquid ethanol diet with concurrent injections of LPS in a “two-hit” model of liver fibrosis.

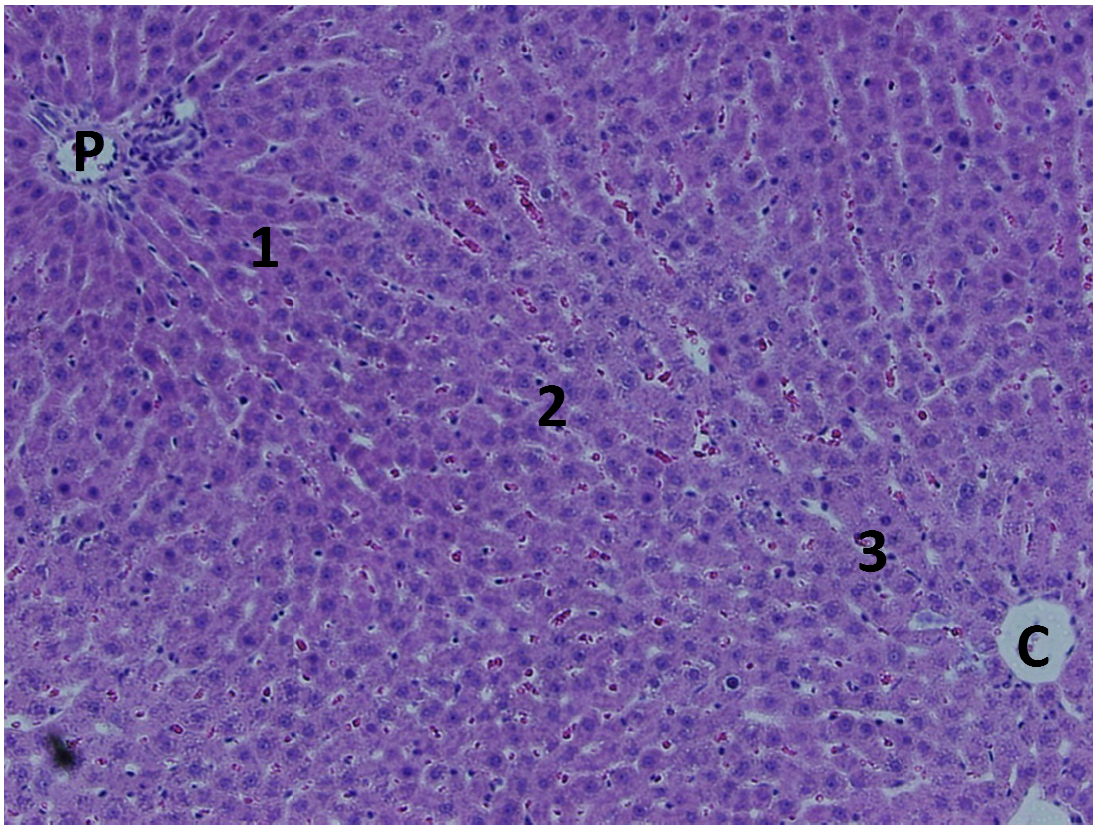

Figure 1. Pericentral and periportal zones of the liver. Fibrosis begins in zone 1 when hepatitis or cholestasis causes liver injury, whereas zone 3 is initially damaged during ethanol-induced fibrosis and carbon tetrachloride exposure. **P**- portal vein, **C**- central vein.

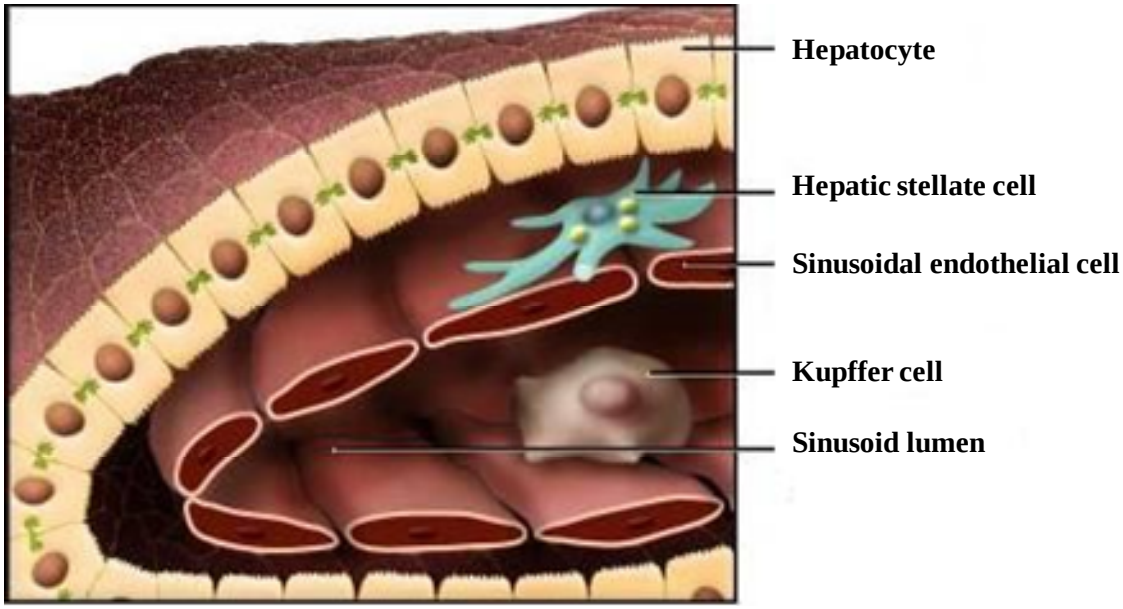

Figure 2. Architecture of hepatic sinusoid and localization of hepatic stellate cells. The hepatocyte is the primary cell type of the liver and is separated from blood flow by sinusoidal endothelial cells by the space of Disse. HSCs reside in the space of Disse and Kupffer cells are the resident macrophages found in the sinusoidal lumen. (Adapted from Bataller et al. 2005)

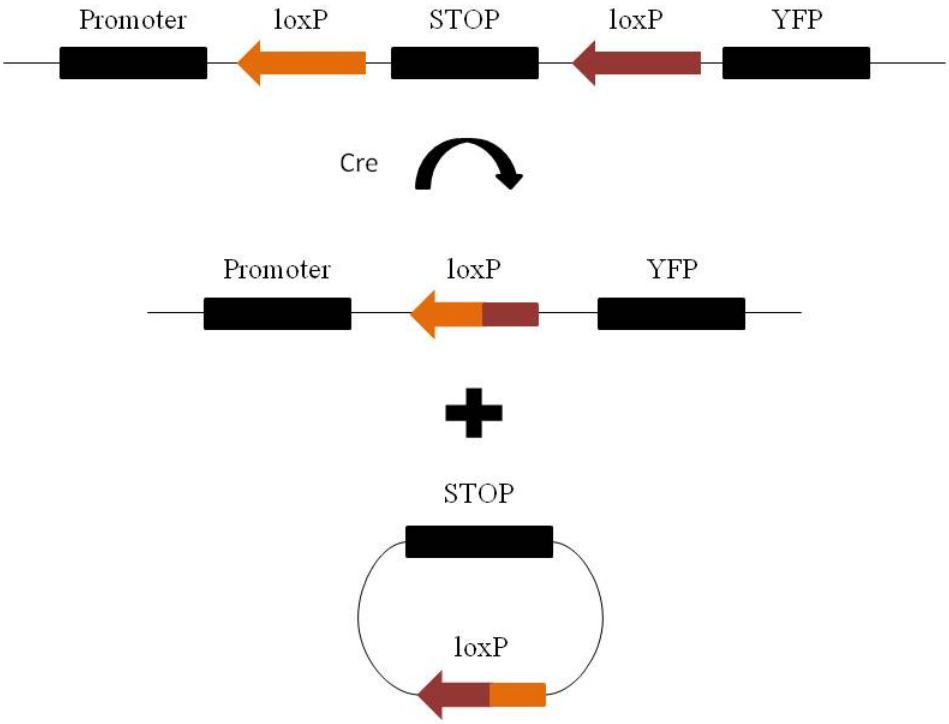

Figure 3. Cre-mediated DNA recombination allowing conditional expression of transgenes flanked by loxP.

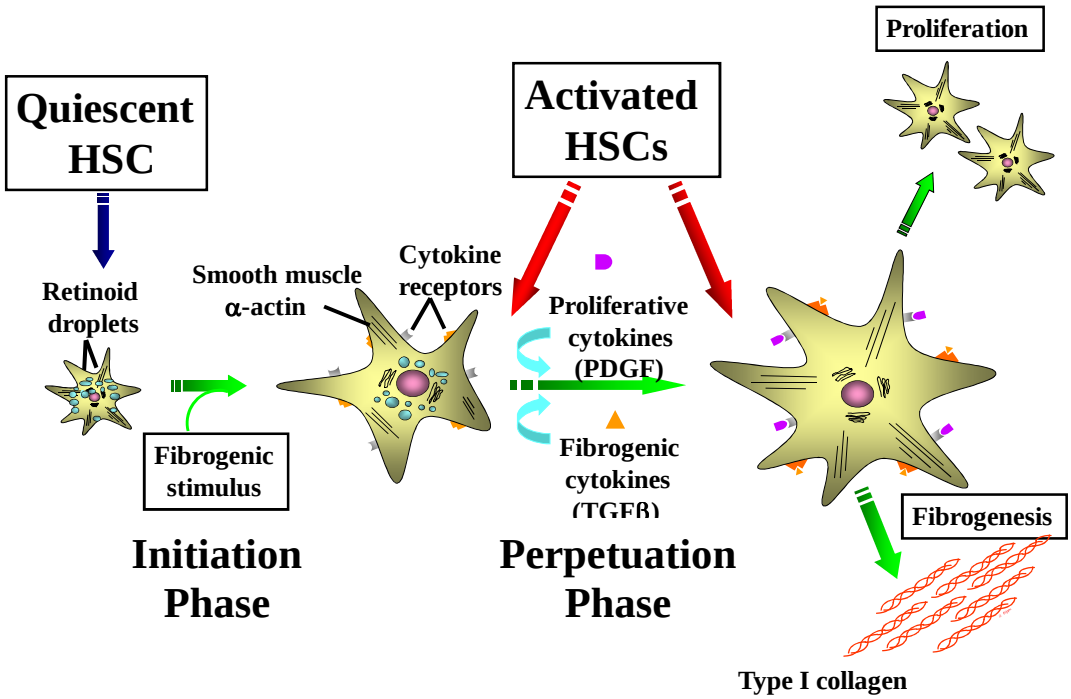

Figure 4. Activation of hepatic stellate cells. Quiescent HSCs are vitamin A-storing cells that reside in the space of Disse. Upon exposure to a noxious stimulus, HSCs undergo a phenotypic change to an activated, myofibroblast-like state characterized by loss of vitamin A and expressin of stress fibers. Activated HSCs migrate to the site of injury, proliferate, and secrete collagen and cytokines to facilitate wound healing. (Adapted with permission from Rippe, RA)

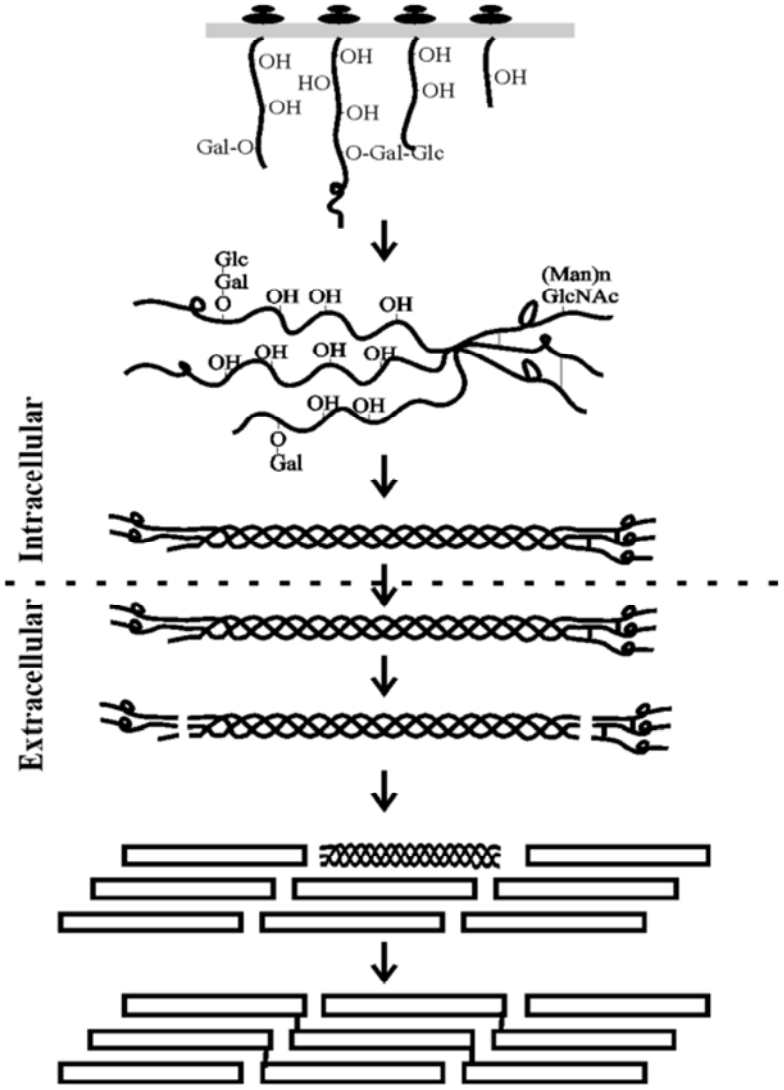

Figure 5. Processing of type I collagen. Following translation, nascent procollagens enter the ER where they undergo extensive modification and folding into a triple helix by ER resident proteins. Upon secretion into the extracellular space, N- and C-terminal prodomains are cleaved by peptidases, resulting in the mature type I collagen molecule. Type I collagens molecules sponatenously arrange and assemble into fibrillar supramolecules.

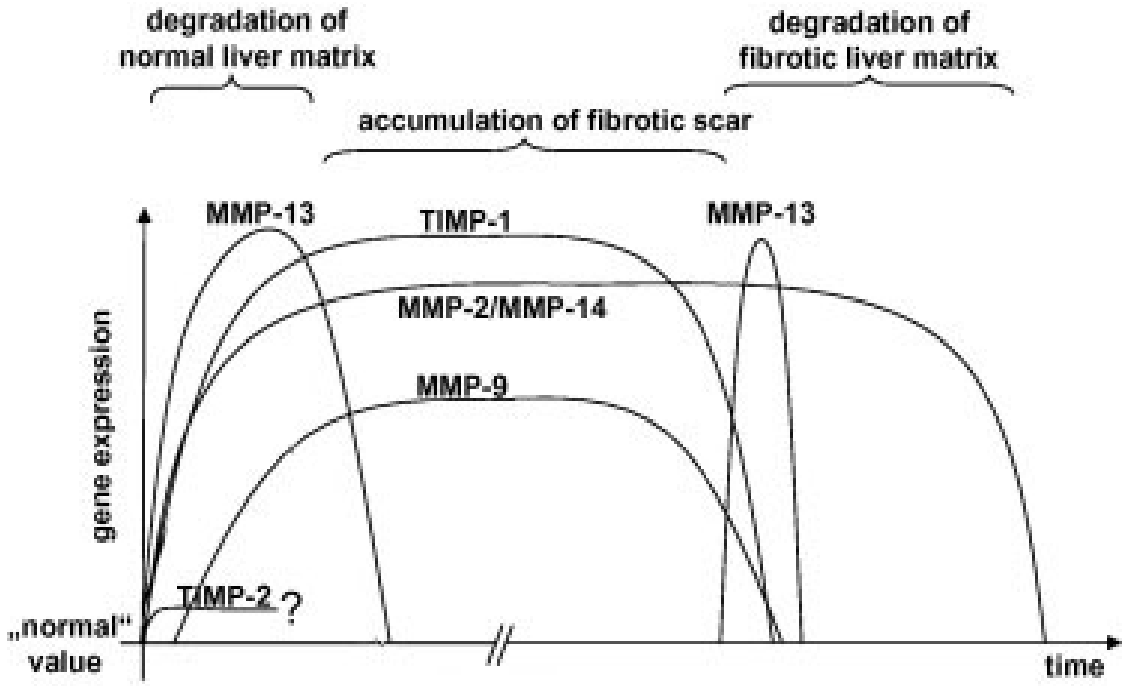

Figure 6. Expression profile of MMPs and their inhibitors. Graphic representation of the expressin of MMPs and TIMPs during the initiation, progression, and resolution of hepatic fibrosis. (Adapted from Hemmann et al. 2007)

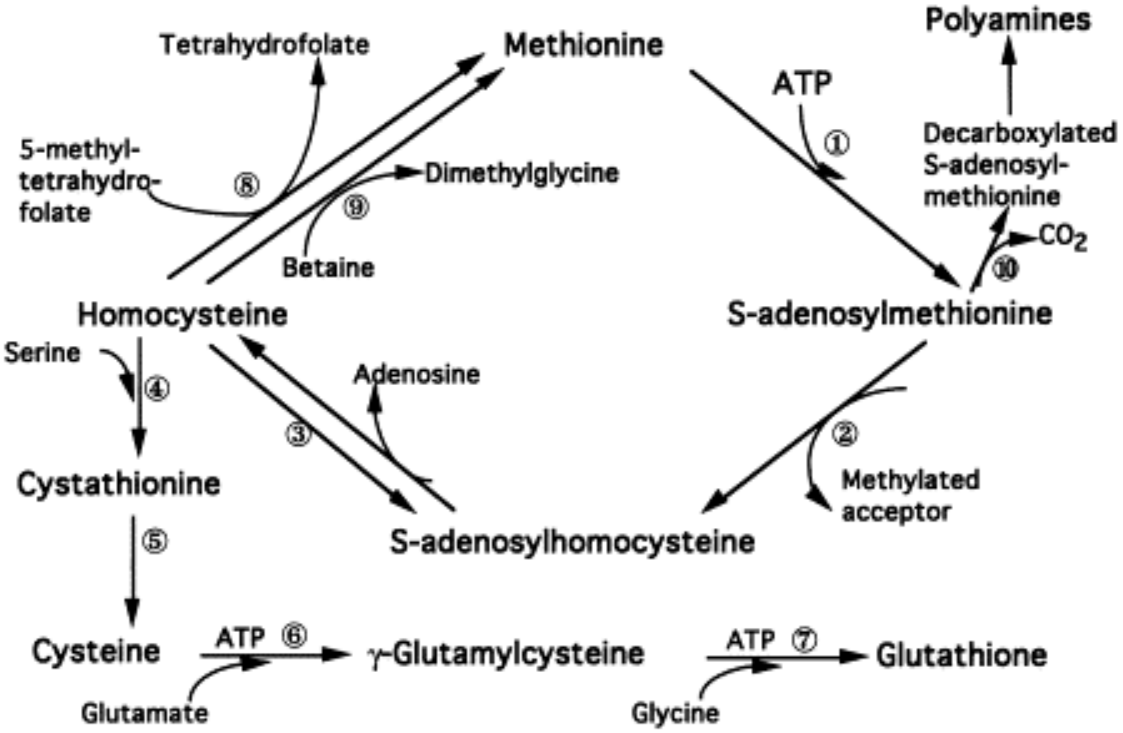

Figure 7. Synthesis and metabolic pathways for SAMe. SAMe is a precursor for the intracellular antioxidant glutathione via the trans-sulfuration pathway. (Adapted from Lu 2000)

CHAPTER 2: MATERIALS AND METHODS

Isolation and culture of Hepatic Stellate Cells

Primary hepatic stellate cells (HSCs) were isolated from male Sprague-Dawley retired breeder rats (>400g) [211, 212]. Rats where anesthetized with isofluorane. The hepatic portal vein was canulated, and rats were exsanguinated by cutting the inferior vena cava. The liver was first perfused with approximately 200 mL of Minimum Essential Medium (S-MEM, without calcium) (Invitrogen, Carlsbad, CA) supplemented with 1X Antibiotic-Antimycotic suspension (Sigma-Aldrich, St. Louis, MO). The liver was then digested with Gey's Balanced Salt Solution (GBSS) (137 mM NaCl, 2.7 mM $NaHCO_3$, 5.0 mM KCl, 1.5 mM $CaCl_2 \cdot 2H_2O$, 1.0 mM $MgCl_2 \cdot 6H_2O$, 0.7 mM Na_2HPO_4, 0.2 mM KH_2PO_4, 0.3 mM $MgSO_4 \cdot 7H_2O$, 5.5 mM glucose, 25 mM HEPES) containing 0.045% (w/v) pronase (Roche, Indianapolis, IN) and 0.05% (w/v) type IV collagenase (Sigma-Aldrich) supplemented with 1X Antibiotic-Antimycotic suspension. Following digestion, the liver was mechanically agitated at 37ºC for 10 min in GBSS containing 1X Antibiotic-Antimycotic suspension and 20 μg/mL DNase1 (Sigma-Aldrich). Hepatocytes were removed by centrifugation at 50 x g for 2 min in an Eppendorf (Hamburg, Germany) 5810 R centrifuge with an A-4-62 swing-bucket rotor and the nonparenchymal cell-containing supernants were transferred to fresh 50 mL conical tubes after each spin. Nonparenchymal cells were isolated by centrifugation at 700 x g for 7 min. The nonparenchymal cell suspension was layered on an arabinogalactan (Sigma-Aldrich)

gradient using 1.035 and 1.045 g/mL densities. The cells were centrifuged at 61,120 x g for 35 min at 20ºC in a SW40 Beckman swinging-bucket rotor (Beckman Instruments, Inc., Fullerton, CA). Pure HSCs were recovered from the interface between the GBSS and 1.035 g/mL layers. HSCs were cultured on plastic using Dulbecco's Modified Eagle's Medium (DMEM) (Gibco, Grand Island, NY) supplemented with 10% fetal calf serum (FCS) (Atlanta Biologicals, Lawrenceville, GA), 2 mM L-glutamine (Gibco), and 1X Antibiotic-Antimycotic suspension (Sigma-Aldrich) in a 95% air-5% CO_2-humidified atmosphere at 37ºC. HSCs were spontaneously activated by culturing on plastic for 13-15 days. Media was changed every 48 h, with the exception of one media change 24 h after initial plating of HSCs. All experimental procedures were approved by the Institutional Animal Care and Use Committee and performed in accordance with the National Institutes of Health criteria for care and use of laboratory animals.

Treatment of HSCs

S-adenosyl-L-methionine (SAMe) and acetaldehyde were purchased from Sigma-Aldrich. To inhibit p38 MAPK activity, cells were pretreated with 5 μM SB203580 (CalBiochem, San Diego, CA) for 30 min prior to treatment with SAMe. Where acetaldehyde was used, cells were pretreated with SAMe for 30 min prior to the addition of acetaldehyde. Cells were serum-starved in 0.2% (v/v) (HSCs) or 0.5% (v/v) FCS (Rat-1 fibroblasts and NIH 3T3 fibroblasts) for 24 h prior to the addition of SAMe. Viability of cells was assessed by Trypan Blue exclusion.

Isolation of RNA and cDNA generation

Total RNA was isolated from HSCs (6-well plate) or liver tissue (approximately 50 mg) using 1 mL of TRIzol reagent (Gibco-BRL, Gaithersburg, MD). Homogenates

were placed in 1.5 mL microcentrifuge tubes and incubated in TRIzol for 5 min at room temperature to permit the complete dissociation of nucleoprotein complexes. Following incubation, 0.2 mL of chloroform was added to each tube and shaken vigorously. Tubes were then centrifuged at 12,000 x g for 15 min at 4ºC. Following centrifugation, the aqueous phase was transferred to fresh 1.5 mL microcentrifuge tubes, and RNA was precipitated by addition of 900 µL of isopropanol for 10 min at room temperature. Samples were then centrifuged for 10 min at 12,000 x g at 4ºC. Supernants were then decanted, and RNA pellets washed in 1 mL of 75% ethanol and immediately centrifuged at 12,000 x g for 5 min at 4ºC. Supernants were again decanted; samples were pulse-centrifuged, and remaining ethanol aspirated using a 200 µL pipet tip. Pellets were then suspended in 12 (RNA from HSCs) or 50 (liver tissue) µL of diethylpyrocarbonate (DEPC)-treated H_2O. RNA quantification was performed using a GeneSpec spectrophotometer (MiraiBio, South San Francisco, CA).

Ribonuclease Protection Assay

Radiolabeled riboprobes for the RNase protection assay were derived from the 375-nucleotide *Pst*I-*Ava*I fragment of rat α1(I) procollagen cDNA. The riboprobe for the rat GAPDH gene was generated from the plasmid pTRI-GAPDH-Rat (Ambion, Austin, TX), which was linearized with *Hin*dIII. Radiolabeled probes were mixed with 5 µg of total RNA, and the dried pellets were suspended in 30 µL of hybridization buffer (100 mM PIPES, pH 6.7, 400 mM NaCl, 2 mM EDTA, and 80% formamide). Samples were heated at 85°C for 10 min and then incubated at 45°C overnight. The hybridization reaction was then performed at 37°C for 1 h in RNase buffer (300 mM NaCl, 10 mM Tris·HCl, pH 7.6, 40 µg/mL RNase A, and 2 mg/mLRNase T1). Subsequently, 20% SDS

and proteinase K (10 µg/mL) were added, and the reaction mixture was incubated at 37°C for an additional 15 min. The reaction mixture was extracted with phenol and precipitated with the addition of yeast tRNA and 100% ethanol. The samples were suspended in formamide dye (95% formamide, 20 mM EDTA, 0.05% bromophenol blue, and 0.05% xylene cyanol FF) and loaded onto a standard 6% sequencing gel. After electrophoresis, bands were visualized by autoradiography and quantitated with a PhosphorImager (Molecular Dynamics, Sunnyvale, CA).

Reverse Transcription of RNA

To eliminate contaminating genomic cDNA, 1 µL RQ1 RNAse-free DNase Reaction Buffer (Promega) and 1 µL RQ1 RNAse-free DNase (Promega) was added to 8 µL of HSC total RNA or 2 µg of liver tissue total RNA (*quantum sufficit* to 8 µL with DEPC-treated H_2O) and incubated at 37ºC for 30 min in 0.5 mL microcentrifuge tubes. Following incubation, 1 µL of RQ1 RNAse-free DNase Stop Solution and 1 µL of DEPC-treated H_2O were added to each tube. Following DNase treatment, total RNA was reverse-transcribed in a 20 µL reaction containing 1 µL of 0.5 µg/µL random hexamers (Invitrogen, Carlsbad, CA), 1 µL of 0.1 M dithiothreitol (DTT), 1 µL of 20 mM dNTP, and 1 µL of 200 U/µL RNase H- Superscript II reverse transcriptase (Promega, Madison, WI) buffered by 4 µL 5X First Strand Buffer (Promega). Reaction samples were incubated at room temperature for 15 min to allow random priming. Samples were then incubated for 1.5 h at 37ºC, followed by a 95ºC incubation for 3 min to inactivate the reverse transcriptase enzyme. cDNA was precipitated overnight at -20ºC in 300 µL of 100% ethanol and 2 µL of 3M sodium acetate, pH 5.2. Samples were then centrifuged at 16,000 x g for 10 min at 4ºC, supernants aspirated, and the cDNA pellets washed with

300 μL of 75% ethanol. Samples were again centrifuged at 16,000 x g for 10 min at 4ºC. Following centrifugation, supernants were aspirated, samples pulsed, and the remaining ethanol aspirated using a 200 μL pipet tip. cDNA were then dried in a tissue-culture hood and suspended in 50 μL of DEPC-treated H_2O.

Semi-quantitative Reverse Transcription – PCR

Polymerase chain reaction (PCR) was performed on 2% of the reverse-transcribed cDNA product to quantify expression of the steady-state mRNAs. The reaction mixture consisted of 1.0 μL cDNA, 20 μL DEPC-treated H_2O, 1.0 μL of each primer (0.5 ug/μL), and 25 μL of GoTaqGreen (Promega). Samples were denatured for 5 min at 94ºC. PCR was performed using 92ºC denaturation for 30 sec; annealing at 51ºC – 56ºC (α_1(I) procollagen, 51ºC; α_2(I) procollagen, 52ºC; G3PDH, 51ºC; αSMA, 55ºC; MMP-2, 56ºC; MMP-13, 56ºC; TIMP-1, 56ºC; TIMP-2, 52ºC; Smad3, 52ºC; Smad7, 50ºC; TGF-β, 52ºC); and extension at 72ºC for 30 sec with the final extension extended to 5 min using a Techne TC-512 Thermal Cycler (Techne Incorporated, Burlington, NJ). The total number of cycles varied (20-30) to ensure PCR products were in the linear range. Primers used in reactions are listed in Table 1. PCR products were subjected to electrophoresis in a 2% agarose (Fisher Scientific, Hampton, NH) buffered with 0.5X TAE pH 8.0 (0.04M Tris – acetate, 0.001M EDTA). Bands were visualized by UV transillumination using a Biospectrum AC Imaging System (UVP, Upland, CA). Relative expression,determined by band densitometry, was performed using Quantity One software (Bio-Rad, Hercules, CA).

Quantitative Reverse Transcription – PCR

Quantitative (Real-Time) Polymerase chain reaction was performed on 2% of the reverse-transcribed cDNA product to more accurately quantify expression of the steady-state mRNAs encoding α_1(I) procollagen, α_2(I) procollagen, matrix metalloproteinase-2 (MMP-2), tissue inhibitor of matrix metalloproteinase-2 (TIMP-2), and glyceraldehyde 3-phosphate dehydrogenase (G3). The reaction mixture consisted of 1.0 μL cDNA, 5 μL DEPC-treated H_2O, 1.0 μL of each primer (5 μM), and 5 μL SYBR Mix (Qiagen, Hilden, Germany). Reactions were also prepped in the absence of template cDNA to detect any contamination for each primer pair. Samples were loaded into reaction capillaries and centrifuged in a LC Carousel Centrifuge 2.0 (Roche, Basel, Switzerland).

For each primer pair, a cDNA sample positive for the target product was serially diluted and subjected to amplification using a LightCycler 1.5 (Roche) for 50 cycles along with the experimental samples to permit calculation of the efficiencies (E) of the amplifications. Relative message levels of each target gene product was determined by normalizing the target gene crossing point (Cp) to the Cp of the housekeeping gene G3PDH using the formula: relative expression ratio = $(E_{target}{}^{\Delta CPtarget\ (control - sample)}$ / $(E_{reference}{}^{\Delta CPreference\ (control - sample)}$ [213].

Immunoblot analysis

Cultured HSCs were washed with PBS and whole-cell extracts (WCEs) were prepared with radioimmunoprecipitation assay (RIPA) buffer (1% NP-40, 0.5% deoxycholate, 0.1% SDS, 0.5 mM phenylmethylsulfonyl fluoride (PMSF), 0.05 mM Na_3VO_4, 2 μg/mL aprotinin, in phosphate-buffered saline (PBS)). Nuclear proteins were prepared using the NE-PER kit (Pierce Biotechnology, Rockford, IL) according to the

manufacturer's protocol. Protein concentrations were determined using the Bradford method (BioRad Laboratories, Hercules, CA [214]. Protein samples (10-25 μg per lane) were boiled in an equal quantity of 2X Sample Buffer (0.125 M Tris base, 20% glycerol, 0.2% (w/v) sodium dodecyl sulfate, 0.2% (v/v) 2-mercaptoethanol, 0.02% (w/v) bromphenol blue, pH 6.8) and applied to standard 10% SDS polyacrylamide gels. After electrophoresis, proteins were transferred to nitrocellulose membranes (Schleicher and Schuell, Keene, NH) using a transblot apparatus. The membranes were stained with 0.5% Ponceau S solution to assure equal protein loading and transfer. The membranes were blocked using 5% non-fat milk in Tris-buffered saline (TBS, 25 mM Tris pH 8.0, 144 mM NaCl) containing 0.05% (v/v) Tween-20 (TBS-Tween) at 25^{o}C for > 1 h. Afterwards, the membranes were incubated at 4^{o}C with primary antibodies for > 12 h. Primary antibodies utilized are listed in Table 2. Primary antibodies were diluted 1:1000 in 5% non-fat milk in TBS-Tween. Membranes were then washed three times for 10 min with TBS-Tween. After washing, the membranes were incubated with either goat anti-rabbit IgG-HRP (Santa Cruz Biotechnology), donkey anti-goat IgG-HRP, or goat anti-mouse IgG-HRP (Santa Cruz Biotechnology) at a dilution of 1:5000 in 5% non-fat milk at 4^{o}C for 1 h. The membranes were then washed three times for 10 min in TBS-Tween and developed using the SuperSignal West Pico Chemiluminescent Substrate kit (Pierce). To visualize bands, membranes were then exposed to x-ray CL-Xposure Film (Thermo Scientific, Rockland, IL) and developed using a Mini Medical film developer (AFP Imaging, Elmsford, NY). Relative protein expression was determined by band densitometery utilizing Quantity One software.

Transient Transfections and Reporter Assays

NIH 3T3 fibroblasts were cultured in DMEM supplemented with 10% FCS, 2mM L-glutamine, 100 units penicillin/mL, 0.1 mg/mL streptomycin, and 0.25 μg/mL amphotericin B in a 95% air-5% CO_2-humidified atmosphere. NIH 3T3 cells were seeded into 6-well dishes at a density of 4.5 x 10^5 cells per well. The day after seeding 0.5 μg of pRSV-β-gal (Promega) and 0.5 μg of pNF-κB 3XLUC [215] were co-transfected using 11 μg of LipofectAMINE (Invitrogen) per well for 8 h in serum-free media. Follwing transfection, media was aspirated and replaced with growth media overnight to allow cells to recover. Cells were then serum-starved for 24 h and subsequently treated in the presence or absence of 250 - 1000 μM SAMe for 24 h. In experiments to block p38-MAPK activity, cells were pretreated with either DMSO or 5 μM SB203580 for 30 min prior to treatment with SAMe. Following incubation, cells were washed gently with 1X PBS and lysed by adding 80 μL of 1X Reporter Lysis Buffer (Promega) to each well. Cells were scraped, transferred to a 1.5 mL microcentrifuge tube, and subjected to freeze/thaw at -70ºC. Lysates were then centrifuged at 16,000 x g and supernants transferred to fresh tubes. Samples were diluted 1:10 in Reporter Lysis Buffer and luciferase activity was determined by incubating 1 μL of sample in 100 μL of Luciferase Reporter System solution (Promega). Luciferase activity was then immediately determined using a TD-20/20 Luminometer (Turner BioSystems, Sunnyvale, CA). Values were recorded as the average of two readings.

To normalize for transfection efficiency, β-galactosidase activity was determined. Extracts were prepared as with the Luciferase assay and 30 μL of extract was added to 790 μL of sodium phosphate buffer (87.5 mM sodium phosphates, 1 mM $MgCl_2$, and

0.8% β-mercaptoethanol) and 200 μL 4 mg/mL ortho-nitrophenyl-β-galactosidase. Samples were incubated at 37ºC for 2 h in semi-microcuvettes. Following incubation β-galactosidase activity was determined by reading A_{410} using a DU 650 Spectrophotometer (Beckman).

Adenoviral Infection of HSCs

The recombinant replication-deficient adenoviruses Ad5IκB and Ad5GFP were generously supplied as a gift from Dr. David Brenner and have been described [216]. Rat-1 fibroblasts were cultured in DMEM supplemented with 10% FCS, 2mM L-glutamine, 100 units penicillin/mL, 0.1 mg/mL streptomycin, 0.25 μg/mL amphotericin B in a 95% air-5% CO_2-humidified atmosphere. Cells were seeded into 6-well dishes at a density of 5.0 x 10^5 cells per well. The following day cells were infected with either Ad5IκB or Ad5GFP at an MOI of 300 for 6 h in 2.0% FCS media. Cells were allowed to recover > 12 h in 10% FBS media following infection. The cells were then serum-starved for 24 h in media with serum reduced to 0.5% FBS. Cells were then treated in the presence or absence of 1 mM SAMe for 12, 24, and 48 h. After each time point WCEs were prepared using RIPA buffer. To ensure sufficient adenovirus infection efficacy, cells were viewed under an IX71 fluorescent microscope (Olympus, Central Valley, PA) using the fluorescein isothiocyanate (FITC) filter to determine the population of green fluorescent protein- (GFP) expressing cells.

Co-Immunoprecipitation

Cultured HSCs were washed with PBS and WCEs were prepared with RIPA buffer. Protein samples (200-250 μg) were incubated overnight at 4°C with 2 μg rabbit anti-type I collagen (Rockland, Gilbertsville, PA). This antibody has been previously

shown to bind to pro-α1(I) chain, the mature α(I) chain, and the heterotrimer of type I collagen, but does not recognize α2(I) chain. Immune complexes were precipitated by incubation with Protein A/G agarose beads for 6 h. Precipitated complexes were washed 3 times with RIPA buffer and stored in 2X Sample Buffer. Immunocomplexes were analyzed by 10% acrylamide gel followed by transfer to nitrocellulose. Immunoblot analysis and detection was performed using mouse anti-polyubiquitin IgM (Biomol, Plymouth Meeting, PA) diluted 1:1000 and goat anti-mouse IgM (Santa Cruz Biotechnology) diluted 1:2000.

p38 MAPK Assay

All reagents and instructions were provided by the p38 MAPK Assay Kit (Cell Signaling). Culture-activated HSCs plated on p100 dishes were pretreated with 0, 500, 1000, or 2000 µM SAMe for 30 min. Cells were then treated for 30 min in the presence or absence of 200 µM acetaldehyde (Sigma-Aldrich) at 37ºC in a CO_2 incubator. Plates were wrapped with parafilm to prevent loss of acetaldehyde. Cell lysates were then collected using 0.5 mL of cold 1X Cell Lysis Buffer. Cells were scraped and transferred to a 1.5 mL microcentrifuge tube. Cells were subjected to 3 cycles of freeze-thaw for 5 min each utilizing the -70ºC freezer. Samples were then microcentrifuged for 10 min at 4ºC and the supernants transferred to new 1.5 mL microcentrifuge tubes. phospho-p38 MAPK was then precipitated by incubation with 20 µL of immobilized antibody Bead Slurry overnight at 4ºC. Immune complexes were then centrifuged for 30 seconds at 14,000 x g at 4ºC. Pellets were washed two times with 500 µL of cold 1X Cell Lysis Buffer followed by repeated centrifugation. Pellets were then suspended in 50 µL of 1X Kinase Buffer supplemented with 200 µM ATP and 1 µL of ATF-2 Fusion Protein.

Samples were incubated for 30 min at 30ºC. Following incubation, reactions were stopped with the addition of 2X Sample Buffer and immunoblot analysis using an antibody recognizing phospho-ATF-2 (Thr71) was performed.

Fluorescent Immunohistochemistry

Slides with paraffin-embedded sections were heated at 60ºC for 1 h. Paraffin was removed by incubation in D-limonene three times for 5 min. Sections were then re-hydrated by successive incubation in 100% ethanol, 95% ethanol, 80% ethanol, and distilled H_2O each twice for 5 min. Following rehydration, sections were subjected to antigen capture. Slides were placed in a rice cooker and steamed for 30 min in the presence of 10mM sodium citrate and 0.05% Tween 20. Following incubation, slides were allowed to cool to room temperature for 20 min. Sections were then incubated on ice with 1% $NaBH_4$ diluted in PBS 3 times for 15 min. Sections were then rinsed twice in PBS for 2 min followed by 5 min incubation in TBS-Tween.

Slides were then blocked at room temperature for 30 min with 5% goat serum and 1% BSA diluted in TBS-Tween. Sections were then incubated with primary antibody; rabbit anti-rat type I collagen (Rockland), rabbit anti-4-hydroxy-2-nonenal (Alpha Diagnostics, San Antonio, TX), rabbit anti-polymorphonuclear leukocytes (PMNs) (Cederlane, Ontario, Canada), and mouse anti-polyubiquitin IgM (Biomol) diluted at 1:100 overnight at 4ºC in a humidified environment. Slides were then rinsed twice for two min with TBS-Tween and then incubated in secondary antibody; goat anti-rabbit IgG conjugated to AlexaFluor488 (Invitrogen) and goat anti-mouse IgM conjugated to AlexaFluor 594 (Invitrogen) diluted 1:100 for 1 h at room temperature in a humidified environment protected from light. Sections were then washed three times for 10 min

with TBS-Tween. Slides were then incubated with 4',6-diamidino-2-phenylindole (DAPI) at a concentration of 21 µg/mL for 5 min in the dark. Subsequently, slides were washed 3 times 5 min in PBS and mounted with ProLong Antifade Gold (Invitrogen) before covered with glass coverslips. Slides were allowed to cure at room temperature for 24 h prior to image capture. Images were captured with an Olympus fluorescent microscope using DAPI, FITC, and Texas Red filters. Five fields per section were captured using each filter at both 10X and 20X magnifications. For co-localization studies, captured images were merged utilizing Image Master (Photon Technology International, Birmingham, NJ) and the total amount of overlap and the ratio of overlap to FITC-positive areas was calculated.

Ethanol Assay

Reagents were obtained from the QuantiChrom Ethanol Assay Kit (BioAssay Systems, Hayward, CA). Serum was deproteinated with 2 volumes of 10% tricholoracetic acid. Samples were centrifuged for 5 min at 14,000 x g at 4ºC and supernants were transferred to fresh tubes. Ethanol standards were prepared in duplicate from a 2 mL stock solution of 10% ethanol (v/v) ranging from 0% to 2% with a total volume of 150 µL per standard. For each experimental sample, 150 uL of deproteinated serums was used in triplicate. To each standard and experimental sample, 100 uL of Reagent A was added using a multi-channel pipettor in a 96-well plate. Samples were incubated at room temperature for 30 min. Following incubation, 100 uL of Reagent B was added to each sample using a multi-channel pipettor. OD_{580} was then determined using a Bio-Rad 550 Microplate Reader.

Alanine Aminotransferase Assay

Alanine Aminotransferase (ALT) was determined using standards and reagents from Pointe Scientific (Lincoln Park, IL). ALT reagents were warmed to 37ºC prior to use. To each well of a 96-well microplate, 10 uL of standard or experimental sample were added. 100 uL of ALT reagent was then added to each well using a multi-channel pipettor. OD_{340} was determined every 1 min for 6 min at 37ºC using a Bio-Rad 550 Microplate Reader. Concentration change per minute was then determined by using minutes 2-4. ALT was calculated by multiplying the concentration change per minute by 6183.527.

Glutathione Assay

Reagents were provided from the Glutathione Assay Kit (Cayman Chemical Company, Ann Arbor, MI). 50 mg liver tissue was sonicated in 2 mL ice-cold 1X MES buffer (0.2M 2-(N-morpholino)ethanesulphonic acid, 0.05 M phosphate, 1 mM EDTA, pH 6.0). Samples were centrifuged for 15 minutes at 10,000 x g at 4ºC. Supernants were transferred to new tubes and deproteinated with an equal volume of 10 % metaphosphoric acid. Samples were then vortexed and incubated for 5 min at room temperature followed by centrifugation at 2,000 x g for 2 min at room temperature. Supernants were collected and transferred to new tubes. Assay Cocktail was prepared using 11.25 mL 1X MES Buffer, 0.45 mL Cofactor Mixture, 2.1 mL Enzyme Mixture, 2.3 mL H_2O, and 0.45 mL of DTNB. Immediately prior to assaying, 50 µL of 4M triethanolamine was added per 1 mL of sample. 50 µL of standard or 50 µL of experimental sample were added to each well of a 96-well plate. All standards and experimental samples were assayed in duplicate. 150 µL of Assay Cocktail were then added to each well and OD_{405} was

measured following 25 min incubation at room temperature in a dark environment. For determination of GSSG, the same procedure was followed; however, 10 uL of 2-vinylpyridine was added to each standard and experimental sample 60 minutes prior to the addition of Assay Cocktail. GSH and GSSG levels were normalized for amount of tissued initially used and expressed as µM/g. GSSG/GSH was calculated by dividing the concentration of GSSG by the concentration of GSH for a particular sample.

Statistical Analysis

In vitro experiments were performed at least in triplicate. Data are presented as mean ± SEM. Student's t-test (parametric) or the Mann-Whitney Rank Sum Test (non-parametric) was performed for paired data. One or two-way ANOVA (parametric) or ANOVA on the Ranks was performed on unpaired data. Post-hoc analysis depended on the comparisons being made. SigmaStat version 2.0 was utilized for all statistical analysis with a P value of less than 0.05 considered significant.

Table 1. PCR forward and reverse primers.

Target	Product size	Primers
α_1(I) procollagen	269 b.p.	5'-CACTGCAAGAACAGCGTAGC-3' 5'-ATGTCCATTCCGAATTCCTG-3'
α_2(I) procollagen	286 b.p.	5'-AAGGCATTCGAGGACACAAC-3' 5'- TTACCAACAGGCCCAAGTTC-3'
G3PDH	292 b.p.	5'-ATCCCGCTAACATCAAATGG-3' 5'- ACTGTGGTCATGAGCCCTTC-3'
αSMA	446 b.p.	5'-GCTGGACTCTGGAGATGGCGTGAC-3' 5'- CCCGAGAGGACGTTGTTAGCATAG-3'
MMP-2	290 b.p.	5'-ACACTGGGACCTGTCACTCC-3' 5'-AGTGGCTTGGGGTATCCTCT-3'
MMP-13	290 b.p.	5'-GCATACGAGCATCCATCCCGAGAC-3' 5'- GCATCTACTTTGTCGCCAATTCC-3'
TIMP-1	309 b.p.	5'-GCCATGGAGAGCCTCTGTGG-3' 5'-GCAGGCAGGCAAAGTGATCG-3'
TIMP-2	250 b.p.	5'-GCATCACCCAGAAGAAGAGC-3' 5'-GGGTCCTCGATGTCAAGAAA-3'
TGF-β	282 b.p.	5'-GCAACAACGCAATCTATGACA-3' 5'-TGATTTCCACGTGGAGTACAT-3'
Smad3	297 b.p.	5'-GTGACACTCCTGAAGGCCATAC-3' 5'-GGCCAACAAAGAGGGTTCTAGT-3'
Smad7	276 b.p.	5'-TCCTTACTCCCAGATACCGATG-3' 5'-TGACTCTTGTTGTCCGAATTGA-3'

Table 2. Antibodies used for immunoblot analysis.

Antibody	Host	Specificity	Manufacturer
anti-type I collagen	Rabbit	Rat	Biodesign
anti-αSMA	Mouse	Human	DAKO
anti-IκBα	Rabbit	Human	Cell Signaling
anti-p65	Rabbit	Human	Chemicon
anti-PDI	Goat	Human	Santa Cruz
anti-grp78	Goat	Human	Santa Cruz
anti-β-actin	Goat	Human	Santa Cruz
anti-HA	Mouse	Human	Sigma
anti-CYP2E1	Rabbit	Human	Chemicon
anti-ADH	Rabbit	Mouse	Santa Cruz
anti-ALDH	Goat	Human	Santa Cruz

CHAPTER 3: EFFECTS OF S-ADENOSYL-L-METHIONINE ON TYPE I COLLAGEN

Introduction

Hepatic fibrosis remains a significant health problem throughout the world. In Africa and Asia, viruses and parasites are the principal cause of fibrosis, whereas in Europe and the United States chronic excessive ethanol consumption is the underlying cause for the majority of cases. Because liver fibrosis is defined by the accumulation of excess extracellular matrix components, principally type I collagen, therapies that decrease the production, or stimulate the breakdown, of type I collagen are of interest.

To date a number of therapeutic agents have been evaluated in both animal models and human clinical trials as treatments for hepatic fibrosis. Colchicine, an alkaloid derived from *Colchicum autumnale*, is a compound best known for its effects as an antimitotic agent. It has also been shown to possess anti-inflammatory and hepatoprotective properties [217-219]. In humans, colchicine was shown to prolong survival in patients with alcoholic cirrhosis. However, a follow up study examining the results of 14 randomized clinical trials demonstrated no significant improvement [220]. The use of colchicines is further compounded by the toxicity associated with its administration and thus must be given at low doses to prevent adverse effects.

Another class of drugs that has received interest as a therapy for hepatic fibrosis is the corticosteroids. These compounds have been shown to decrease inflammation in alcoholic hepatitis, reduce production of cytokines, mitigate formation of acetaldehyde

adducts, and diminish type I collagen production [221]. Short term survival was also increased in patients with severe alcoholic hepatitis [222]. However, a systematic review of trials utilizing corticosteroids was unable to identify any significant benefit on liver histology, frequency of liver complications, or liver-related mortality [223].

Because hepatic fibrosis is often associated with oxidative stress, therapies utilizing antioxidants as treatments have received much attention. Silymarin, a mixture of four flavonoids isolated from the milk thistle plant (*Silybum marianum*), has been noted for centuries as a treatment for liver diseases [224]. Silymarin has been shown to possess antioxidant, anti-lipid peroxidative, and anti-fibrotic properties and could prevent injury in a CCl_4 intoxication model of fibrosis [225, 226]. However, when silymarin was used as a treatment for established CCl_4-induced fibrosis, no positive effect was seen, suggesting silymarin may be more effective as a preventative therapy for hepatic fibrosis than a reversing agent [227]. This pattern was also present in human clinical trials where silymarin was beneficial in several studies examining management of early liver injury but no positive pathological benefit was seen when silymarin was used in patients with alcoholic cirrhosis [228-230]. Thus, it is important to determine the clinical settings in which a particular treatment may be beneficial; prevention of hepatic fibrosis vs. resolution of hepatic fibrosis.

Another antioxidant that has received attention as a potential therapy for hepatic fibrosis is resveratrol, a phytoalexin (a class of antibiotics produced in plants) naturally found in grapes and commercially in red wine. Resveratrol exhibits anti-inflammatory properties, anti-oxidant effects, and modulates metabolism of lipids [231]. In a CCl_4-mediated model of fibrosis, resveratrol prevented fibrosis with concomitant inhibition of

NF-κB translocation and attenuation of TGF-β production [232]. Inhibition of NF-κB by resveratrol was also reported *in vitro* along with a decrease in proinflammatory cytokine production [233, 234]. There is however a lack of human studies examining the efficacy of resveratrol as a treatment for liver disease.

S-adenosyl-L-methionine (SAMe) is an endogenous molecule that participates in a large number of reactions in the liver and is important in maintaining liver health. SAMe levels are reported to decrease in a number of liver injury models, and supplementation with exogenous SAMe prevents depletion of GSH, the principal intracellular antioxidant, suggesting a role for SAMe as an antioxidant therapy [235, 236]. In numerous animal models, SAMe has been shown to attenuate fibrosis and also decrease neoplastic nodules in models of liver cancer [200, 210, 237, 238]. An analysis of clinical studies utilizing SAMe in human patients suggested SAMe does not have an effect on alcoholic liver disease compared to placebo [239]. The authors commented; however, that the quality of the studies reviewed varied and further clinical studies are necessary before concluding whether SAMe is an effective treatment for ALD. Studies in patients with non-alcoholic liver disease did receive benefit from SAMe administration. A well-conducted study utilizing SAMe in cirrhotic patients resulted in a significant decrease in mortality [209]. Additionally, SAMe appears to attenuate cholestatic liver disease [239]. *In vitro* studies utilizing SAMe have focused on HSCs that have been culture-activated for less than 7 days. These studies revealed SAMe decreases type I collagen production in HSCs with attenuation of TGF-β signaling [240, 241].

The most widely-accepted model for mimicking activated HSCs during hepatic fibrosis is culture-activation on plastic for 14 days. Because previous studies have focused on experiments with early-activated HSCs, there is a need to examine the effects of SAMe on later stages of culture-activated HSCs. Based on data generated from previous studies utilizing SAMe and other antioxidants in HSCs, we hypothesized that SAMe inhibits type I collagen production in culture-activated HSCs by ameliorating the effects of oxidative stress through attenuation of NF-κB activity.

Results

SAMe attenuates type I collagen protein expression in activated HSCs.

Recent findings [240] have demonstrated SAMe decreases type I collagen expression in early cultures of primary HSCs. However, HSCs do not fully trans-differentiate into their activated myofibroblast-like phenotype until 14 days of culture. This results in an 80-fold increase in type I collagen expression and is considered a suitable *in vitro* model for hepatic fibrosis. To determine the effect of SAMe on type I collagen in culture-activated HSCs, cells were treated with 250, 500, or 1000 μM SAMe for 6, 12, and 24 h. Cell viability was >95% following all treatments as determined by Trypan Blue exclusion. SAMe treatment attenuated intracellular type I collagen protein expression in a time and dose-dependent manner with the maximum effect being 24 h of treatment with 1000 μM SAMe (Fig. 8). One-way ANOVA analysis revealed, however, that the decrease in intracellular type I collagen expression was not statistically significant compared to untreated cells.

SAMe significantly decreases type I collagen protein secretion in activated HSCs.

Since hepatic fibrosis is the result of excessive deposition of extracellular matrix products, principally by the HSCs, the effects of SAMe treatment on the secretion of type I collagen into culture media was evaluated. Following treatment for 12 and 24 h with 1000 µM SAMe, media was collected, concentrated, and analyzed for type I collagen content by Western blot analysis. SAMe treatment resulted in a highly significant ($p<0.001$) decrease in type I collagen secretion into culture at 24 h as determined by Student's t-test (Fig. 9).

αSMA mRNA expression is decreased by SAMe in activated HSCs.

The most widely used histological marker for hepatic fibrosis in humans is αSMA expression, a marker for HSC activation. To determine if SAMe can inhibit acetaldehyde-mediated increases in αSMA expression in culture-activated HSCs, cells were pretreated for 30 min with 0, 250, 500, 1000, or 2000 µM SAMe. Cells were then treated for 12, 24, and 48 h with 200 µM acetaldehyde, a metabolic by-product of ethanol metabolism. Screw-top T25 tissue culture flasks were used to prevent evaporation of acetaldehyde. RT-PCR for αSMA showed addition of acetaldehyde increased αSMA expression compared to control, most notably at 12 h. Treatment with SAMe showed a slight decrease in acetaldehyde-mediated increases in αSMA expression at only 12 h. There was also a dose-dependent decrease in αSMA expression at 24 and 48 h (Fig. 10).

NF-κB activity is upregulated by SAMe in HSCs.

Many antioxidants have been shown to downregulate the redox-sensitive transcription factor NF-κB in activated HSCs. It was hypothesized that SAMe would decrease NF-κB activity in SAMe-treated HSCs. However, increasing doses of SAMe

resulted in significantly-increased translocation of the p65 subunit of NF-κB to the nucleus following 1 h of treatment of culture-activated of HSCs (Fig. 11). Treatment with 100 ng/mL of LPS was used as a positive control for the translocation of p65. To determine if SAMe treatment also increased binding of NF-κB, EMSA was performed. SAMe treatment increased retention of labeled probe containing the NF-κB consensus sequence (Fig. 12). Utilization of antibodies to the p50 and p65 subunits of NF-κB resulted in further retention of the complex, suggesting increased binding of the p65/p50 complex in activated HSCs. To determine if the increases in NF-κB were associated with degradation of IκBα, immunoblot analysis was performed on Rat-1 fibroblasts, a type I collagen-producing cell-line, and culture-activated HSCs treated with either 0, 500, or 1000 μM SAMe for 15, 30, and 60 min. Treatment with SAMe resulted in a decrease in IκBα (Fig. 13) expression with degradation appearing greater in Rat-1 fibroblasts than HSCs. To evaluate NF-κB transcriptional activity, transient transfections of an NF-κB-responsive luciferase plasmid were performed utilizing NIH 3T3 fibroblasts, a readily-transfectable, collagen-producing mouse cell-line. Following 24 h of treatment with 250, 500, or 1000 μM SAMe there was a significant increase in luciferase activity with the 500 and 1000 μM doses of SAMe, suggesting an increase in transcriptional activation by SAMe (Fig. 14). To evaluate if SAMe-dependent stimulation of NF-κB transcriptional activation was dependent on p38 MAPK, a known phosphorylator and activator of NF-κB, the specific p38 MAPK inhibitor SB203580 was used. SB 203580 inhibits p38 MAPK activity by competitively inhibiting binding of ATP, preventing kinase activity. The increase in SAMe-dependent NF-κB transcriptional activation was abolished at the 1000 μM dose when pre-treating for 30 min with 5 μM SB203580 (Fig. 14).

p38 MAPK activity is increased by SAMe in activated HSCs.

Because the SAMe-mediated increase in NF-κB-dependent transcriptional activation in NIH 3T3 fibroblasts appeared to be blocked with the addition of the specific p38 MAPK inhibitor SB203580, we examined the effects of SAMe on p38 MAPK activity in activated HSCs. Cultured activated HSCs were pretreated with 0, 500, or 1000 μM SAMe for 30 min followed by treatment with 200 μM acetaldehyde for 30 min. phospho-p38 MAPK was immunoprecipitated from lysates and kinase activity was determined by measuring phosphorylation of the p38 MAPK target, ATF-2. No activity was seen in untreated cells and cells treated with acetaldehyde alone; however, there was a small amount of activity following 2000 μM SAMe treatment alone (Fig. 15). Activity was enhanced by co-treatment of SAMe and acetaldehyde in a dose-dependent manner.

NF-κB activity is required for SAMe-mediated type I collagen inhibition.

Previous studies demonstrated that overexpression of the p65 subunit of NF-κB can inhibit transcriptional activation of α1(I) procollagen expression [109]. To investigate whether the observed increases in NF-κB activity had an influence on type I collagen protein levels, NF-κB activity was blocked utilizing an adenovirus that expresses a dominant-negative form of the IκBα regulatory protein. Rat-1 fibroblasts were infected with either Ad5IκB, which was HA-tagged, or Ad5GFP (to serve as a control vector) at an MOI of 300. HSCs were unable to be used for these experiments due to the observation that Ad5IκB-infected HSCs appeared to "round up" and detach from the tissue culture plates following SAMe treatment. Following overnight recovery cells were serum-starved for 24 h. SAMe was then added at 0, 250, 500, or 1000 μM concentrations for 24 h. Whole-cell extracts were generated and immunoblot analysis for

type I collagen was performed. In Ad5GFP (control) infected cells, SAMe significantly decreased type I collagen protein expression. However, Ad5IκB-infected cells did not show a significant decrease in type I (Fig. 16), suggesting intact NF-κB signaling is necessary for SAMe to decrease type I collagen. To verify infection and expression of Ad5IκB, immunoblot analysis was performed for HA. Ad5IκB, but not Ad5GFP-infected cells expressed HA (Fig. 16).

SAMe does not affect α1(I) procollagen steady-state mRNA levels in activated HSCs.

Previous findings have suggested SAMe decreases type I collagen expression in early cultures of HSCs by decreasing levels of α1(I) and α2(I) procollagen mRNA levels [240, 241]. Additionally, Rippe et al. reported overexpression of p65 decreased α1(I) procollagen gene expression in activated HSCs [120]. We hypothesized SAMe decreases type I collagen protein expression via transcriptional-inhibition of the α1(I) procollagen gene by increasing p65 nuclear translocation. To examine this hypothesis steady-state mRNA levels of α1(I) procollagen message were measured by RPA and RT-PCR. Culture-activated HSCs were incubated in 1000 μM SAMe for 6, 12, and 24 h, and total RNA were isolated. Ribonuclease protection assay analysis revealed no significant change in steady-state mRNA levels of the α1(I) procollagen gene by SAMe (Fig. 17). Additionally, RT-PCR revealed no significant change in α1(I) and α2(I) procollagen gene steady-state mRNA levels (Fig. 18).

SAMe stimulates polyubiquitination of type I collagen in activated HSCs.

Because SAMe did not decrease α1(I) and α2(I) procollagen gene steady-state mRNA levels, we examined the post-translation status of type I collagen. We hypothesized SAMe targets type I collagen for degradation by the ubiquitin-proteasome

system (UPS), potentially by disrupting the normal folding and assembly of type I collagen or transiently stimulating an ER stress response. To examine the post-translational fate of type I collagen, cultured HSCs were treated in the presence or absence of 1000 µM SAMe for 3, 6, 12, or 24 h and whole cell extracts were prepared following each time point. Proteins complexed with type I collagen were immunoprecipitated and immunoblot analysis was performed against polyubiquitin. SAMe resulted in a slight increase in polyubiquitination of type I collagen at 3 h followed by a substantial increase at 6 and 12 h (Fig. 19). By 24 h there was a dramatic decrease in polyubiquitination, potentially due to proteasomal degradation of polyubiquitinated procollagens. Quantitation of results and densitometric analysis was limited by the high level of background on developed films.

ER resident proteins are decreased by SAMe in activated HSCs.

To determine a potential mechanism responsible for SAMe-mediated polyubiquitination of type I collagen, we examined the effects of SAMe on ER resident proteins involved in the folding, assembly, and processing of type I collagen. Culture-activated HSCs were treated in the presence of absence of 1000 uM SAMe for 3, 6, 12, and 24 h. Whole cell lysates were collected and Western blot analysis was performed for Grp78, PDI, and Hsp47. SAMe treatment resulted in no significant change in Hsp47 levels. Grp78 levels were slightly decreased by SAMe at 6 and 12 h and significantly decreased ($P < 0.05$) at 24 h as determined by Mann-Whitney Rank Sum Test. Protein expression of PDI was unchanged by SAMe at 3, 6, and 12 h; however, there was a significant decrease in PDI expression at 24 h ($P < 0.05$) as determined by student's t-test (Fig. 20).

SAMe does not increase polyubiquitination of type I collagen in a BDL model of hepatic fibrosis.

To determine if the stimulation of type I collagen polyubiquitination by SAMe is observed *in vivo*, a BDL model of experimental fibrosis was utilized. Male Sprague-Dawley rats were subjected to BDL or sham surgery. One week post-surgery animals were treated with either 10 mg/kg of SAMe i.p. or an equal volume of saline as a vehicle. Treatments were given daily for 7 days. At the end of two weeks, animals were sacrificed and tissues were harvested. Immunofluorescence was performed on sections from paraffin-embedded slides. Antibodies against type I collagen and polyubiquitin were detected using secondary antibodies conjugated to fluorescent probes. Image capture and processing to generate merged images of staining against type I collagen and polyubiquitin revealed no co-localization, suggesting that in this model of experimental fibrosis SAMe does not stimulate polyubiquitination of type I collagen (Fig. 21).

Discussion

SAMe is a candidate treatment for hepatic fibrosis as well other liver diseases. Animal studies have shown SAMe can decrease fibrosis through a decrease in type I collagen accumulation [200, 210]. Clinical trials have also shown a benefit when using SAMe to treat ALD and cirrhosis; however, there is a lack of quality human studies to conclusively determine if SAMe is beneficial [209, 239]. Because *in vitro* studies detailing the effects of SAMe on HSCs focused on early-activated cells, we investigated the role of SAMe in type I collagen production by culture-activated (day 14) HSCs. Evaluating the efficacy of putative treatments for hepatic fibrosis, especially when targeting HSCs, is important due to the dramatic phenotype change that occurs during

transdifferentiation of HSCs. Unpublished data by our laboratory demonstrated a marked change in the gene expression profiles of HSCs when comparing different days in culture. Thus, a treatment that inhibits collagen expression or prevents the onset of hepatic fibrosis may not necessarily be an appropriate agent for targeting established fibrosis or modulating activated HSCs.

Treatment with increasing doses of SAMe did not have a significant effect on intracellular type I collagen expression in HSCs, although there was a trend showing decreased levels in a dose-dependent manner at the 6 and 24 h time-points. There was however, a significant decrease in type I collagen secretion at 24 h following treatment with 1000 µM SAMe. This finding suggests SAMe may be an appropriate agent for targeting activated HSCs in hepatic fibrosis, since the main causative agent in liver fibrosis is excessive secretion of matrix components; specifically type I collagen. In comparison to other studies utilizing SAMe in HSCs, there is a wide range of conditions and dosages used. Nieto and Cederbaum treated early-cultures (up to day 7) of primary HSCs with 10 or 30 µM SAMe added daily in the absence of serum and observed a decrease in both type I collagen protein and α1(I) procollagen mRNA expression [240]. Matsui and Kawada, however, used doses ranging from 100 µM to 10 mM in their experiments. Primary HSCs were cultured for 24 h with 10% serum, and then cultured for 3 days with daily SAMe supplementation in the absence of serum, again seeing a decrease in α1(I) procollagen mRNA expression [241]. The normal intracellular concentration of SAMe is 60 µM, however, dosages up to 1.5 g/day are well tolerated in humans and this dosage would be approximately 500 µM upon absorption into the blood stream, thus we feel the concentrations used in the study are pharmacologically

appropriate [209, 242]. It is also important to note that the two studies were conducted largely in the absence of serum. HSCs are typically culture-activated for 14 days in media supplemented with 10% serum prior to experimentation to model the *in vivo* phenotype during hepatic fibrosis, as serum provides growth factors necessary to drive the transdifferentiation process (Schrum lab, unpublished data). The studies by Kawada and Nieto were conducted on HSCs cultured 7 days or less with daily SAMe supplementation in the absence of serum. Thus, these studies are more appropriate for evaluating SAMe as a preventative treatment for hepatic fibrosis by inhibiting the activation of HSCs, as opposed to utilizing SAMe as a curative agent in activated HSCs by reducing type I collagen expression. The differences in experimental designs may also explain why Nieto et al. demonstrated a decrease in type I collagen expression with lower doses of SAMe, as they may have been working with cells that were less transdifferentiated than cells that have been culture-activated for 14 days in the presence of serum.

To examine whether treatment of SAMe could prevent acetaldehyde from increasing αSMA expression in culture-activated HSCs, cells were pretreated with SAMe followed by treatment with acetaldehyde for 12, 24, and 48 h. Acetaldehyde was chosen instead of ethanol based on findings that suggest HSCs do not express relevant amounts of CYP2E1. SAMe did not have a significant effect on αSMA expression at 12 h; however, there was a substantial decrease in steady-state mRNA levels following SAMe treatment at 24 and 48 h, dropping expression below the basal level of expression in the untreated groups. These data suggest that SAMe may function to revert activated HSCs

back to the quiescent phenotype, as αSMA expression results in stress fiber formation and is considered a marker for HSC activation.

To investigate a potential mechanism for type I collagen inhibition in HSCs by SAMe, we examined the transcription factor NF-κB. This transcription factor is increased in activated HSCs, and switches from predominantly p50/50 to p65/50 with this change typically associated with an increase in transcription. Stimulation of NF-κB is linked to oxidative stress [243, 244], a key factor implicated in the progression of hepatic fibrosis. SAMe administration has been shown to decrease NF-κB activity in other cell types [245] along with increasing levels of GSH, suggesting a decrease in oxidative stress [246]. These findings, along with the report of SAMe-mediated decreases in TGF-β in HSCs, a target of NF-κB, led us to hypothesize SAMe decreases NF-κB activity in culture-activated HSCs. Surprisingly, treatment with SAMe for 60 min revealed a statistically significant dose-dependent increase in p65 translocation. To examine NF-κB binding activity, EMSA was performed utilizing a radiolabelled probe of the NF-κB consensus sequence. SAMe treatment resulted in a dose-dependent increase in p65/50 binding in extracts isolated from activated HSCs. Concomitant with p65 translocation and binding was an increase in IκBα degradation following treatment with SAMe.

Because NF-κB translocation and binding alone does not result in transcriptional activation, we utilized an NF-κB responsive luciferase plasmid transfected in NIH 3T3 fibroblasts. This cell line was chosen for its ease of transfection, as primary HSCs and Rat-1 fibroblasts are difficult to transfect. Treatment with SAMe caused a dose-dependent increase in luciferase activity, suggesting that SAMe significantly increases NF-κB transcriptional activation. Because p38 MAPK has been shown to phosphorylate

p65 [247-249], we examined the effect of blocking p38 MAPK on SAMe-mediated NF-κB transcriptional activation using the specific inhibitor SB203580. This resulted in a decrease in NF-κB transcriptional activation down to control levels. Further analysis revealed SAMe stimulates phosphorylation of p38 MAPK in culture-activated HSCs. This suggests that p38 MAPK cross-talk with NF-κB is important for modulating p65/50 transcriptional activation in SAMe-treated HSCs.

The role of NF-κB in HSCs is somewhat ambiguous. Treatments that decrease NF-κB have been shown to improve hepatic fibrosis [232, 250, 251]; however, p65 is protective against fibrosis in hepatitis C infection [252], does not stimulate transdifferentiation of HSCs [118], and overexpression in HSCs can inhibit both α1(I) and α2(I) procollagen mRNA expression [120, 121]. This led us to revise our hypothesis that SAMe inhibited type I collagen expression through NF-κB-mediated transcriptional inhibition.

Utilizing an adenovirus that expresses a dominant-negative form of the NF-κB inhibitory protein, IκBα, NF-κB activity was blocked in Rat-1 fibroblasts. Treatment with SAMe resulted in a significant decrease in type I collagen expression in control cells infected with Ad5GFP, however cells infected with Ad5IκBα showed no significant decrease in collagen expression when treated with SAMe. This suggests SAMe is indeed inhibiting type I collagen production through an NF-κB-mediated pathway. These experiments could not be conducted in primary HSCs due to the observation that that inhibition of NF-κB followed by treatment with SAMe resulted in cell death. Because NF-κB enhances survival by resisting apoptosis in activated HSCs [118], it is possible

that treatment with SAMe stimulates pro-apoptotic pathways that are normally blocked by high p65 expression.

To determine if SAMe-mediated type I collagen expression is also inhibited at the mRNA levels, cultured-activated HSCs were treated with SAMe for 24 hours and steady-state mRNA levels of α1(I) procollagen mRNA were assessed by RPA. RT-PCR was also performed for both α1(I) and α2(I) procollagen mRNA levels. Despite inhibition of collagen by SAMe at the protein expression level, there was no significant change in the steady-state mRNA levels of either α1(I) or α2(I) procollagen.

Post-transcriptional regulation of procollagens were investigated next as a possible mechanism for SAMe-mediated type I collagen inhibition. After transcription, SAMe may be disrupting normal translation of procollagen mRNAs or perturbing the normal processing and folding of procollagen polypeptides, resulting in a decrease in secretion. This later hypothesis would potentially account for why there was no significant decrease in intracellular type I collagen following SAMe treatment, but a highly significant decrease in secreted type I collagen. To examine this possibility, culture-activated HSCs were treated in the presence or absence of 1000 μM SAMe for 3, 6, 12, and 24 hours. Immunoprecipitation of type I collagen complexes was performed and polyubiquitin was analyzed by immunoblot analysis. SAMe treatment resulted in a substantial amount of polyubiquitination of type I collagen compared to untreated cells at 6 h and peaking at 12 h before a marked decrease at 24 h. This drop may be associated with type I collagen degradation by the 26S proteasome. Unfortunately experiments to rescue the observed phenotype through inhibition of the 26S proteasome were

unsuccessful, as proteasomal inhibition results in apoptosis of activated HSCs as seen by other laboratories [253].

The processing and folding of procollagen polypeptides involves several ER resident proteins. A decrease in any of these proteins by SAMe may perturb the normal processing of procollagen polypeptides and lead to unfolded or misfolded molecules. This would in turn trigger the UPS and lead to the degradation of improperly processed proteins by the 26S proteasome. The ER resident proteins Hsp47, PDI, and Grp78 were assessed by Western blot analysis following treatment in the presence or absence of 1000 µM SAMe for 3, 6, 12, and 24 h. There was no decrease in the collagen-specific chaperone Hsp47; however, there was a decrease in PDI at 24 h following SAMe treatment. The kinetics of type I collagen polyubiquitination, however, may rule out involvement of PDI. Grp78 levels following treatment with SAMe dropped immediately and reached their peak at 24 h. This suggests Grp78 may be important in preventing the misfolding or misprocessing of procollagen polypeptides. Decreases in Grp78 can lead to activation of PERK and Ire1, and transport of phosphor-ATF6, signaling the UPS. SAMe has also been shown in an animal model to correlate inversely with levels of Grp78 in the liver [254].

The redox status of the cell, and particularly the ER, plays an important role in ER stress and proper folding of nascent polypeptides. Treatment of yeast with reducing agents such as DTT resulted in protein misfolding and a reduction in the amount of disulfide bonds [255]. The study also illustrated that under reducing conditions other secretory proteins that did not require disulfide bond formation were normally secreted, suggesting that selective retention of proteins requiring disulfide bond formation may

occur during ER stress generated by changes in the redox state. Although the mammalian ER is less oxidizing than the ER of yeast, the environment is still more oxidizing than the cytosol with a GSH:GSSG ratio of 3:1 in the ER as opposed to 100:1 in the cytosol [256]. SAMe-mediated type I collagen inhibition may be occurring under the same mechanism, as SAMe has been shown *in vitro* and *in vivo* to increase levels of reduced glutathione. This may result in an increase in the pool of reduced PDI in the ER, limiting its capacity to oxidize thiol groups to form disulfide bonds. Reduction in PDI disulfide bond formation has been demonstrated in a reducing ER environment utilizing a model of alpha1-antitrypsin transgenic mice [257]. Thus, the identification of PDI inhibitors and mediators of a more reduced ER environment may represent a novel strategy for stimulating type I collagen degradation by the UPS without affecting the protein secretory pathway as a whole. Future experimentation should focus on resolving the role of SAMe as either a direct antioxidant or antioxidant precursor. Utilizing the methyltransferase inhibitor, ethionine, the conversion of SAMe to glutathione can be blocked, allowing for distinction between SAMe-specific effects and effects that arise as SAMe is converted to other compounds, such as glutathione. These studies are complicated by the variety of reactions in which SAMe participates. Inhibition of SAMe demethylation may drive the conversion of SAMe to MTA, which has also been shown to attenuate liver injury. Thus, care must be taken when considering the contribution of SAMe and its many metabolites in determining mechanism of action.

To investigate if polyubiquitination of type I collagen occurred an animal model of hepatic fibrosis, a BDL model was utilized. Following 1 week of either sham or BDL surgery, animals were treated with either 10 mg/kg SAMe or an equal volume of saline

by intraperitoneal injection daily for an additional 7 days. Immunofluoresence was then performed to determine if there was any colocalization of polyubiquitin and type I collagen in SAMe-treated animals. Fluorescent microscopy revealed no colocalization of polyubiquitin and type I collagen. Possibilities that may account for this observation include the BDL period prior to treatment was not long enough to fully activate HSCs or lack of sensitivity, since polyubiquitinated type I collagen would be found in HSCs, and the majority of collagen staining occurred in acellular areas. Additionally, earlier time points should be examined prior to the degradation or downregulation of type I collagen.

These studies have helped elucidate the mechanisms of SAMe on culture-activated HSCs. Whereas previous studies have focused on SAMe as a preventative therapy by utilizing early-cultured HSCs, we focused on examining the role of SAMe as a reversing agent for fibrosis through the use of culture-activated HSCs. These distinctions are important, as much of the morbidity associated with ALD is the refusal to cease consumption of ethanol. Therapies that can successfully treat hepatic fibrosis in an environment where removal of the underlying etiology is not possible are desirable for this reason. Further experimentation to understand the precise molecular mechanisms of SAMe-mediated effects on culture-activated HSCs will help in our ability to determine the efficacy of SAMe in humans, as well as potentially lead to new therapeutic strategies to augment mechanisms of action by SAMe to inhibit type I collagen production. One particular approach may be the specific targeting of ER proteins to modulate collagen expression in HSCs.

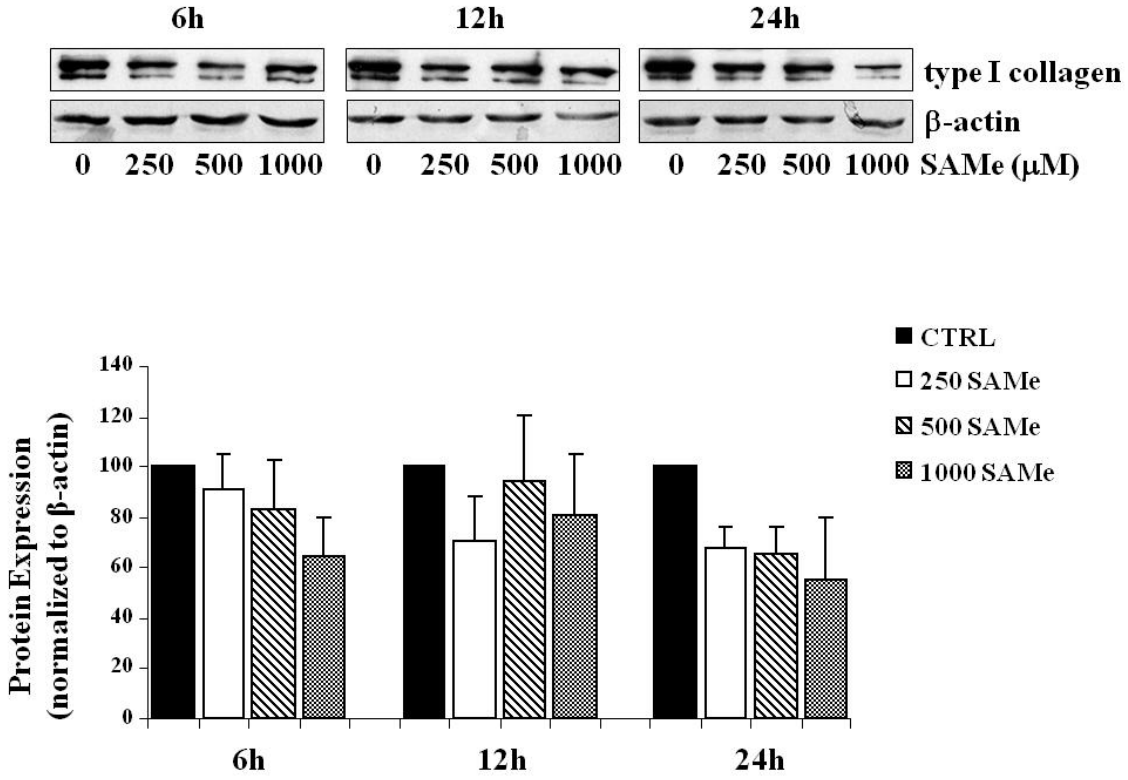

Figure 8. SAMe attenuates type I collagen expression in activated HSCs. Culture-activated (day 14) HSCs were treated with 0, 250, 500, or 1000 μM SAMe for 6, 12, and 24 h. Whole-cell extracts were isolated and immunoblot analysis was performed to analyze type I collagen expression. Expression was normalized to β-actin (n=3).

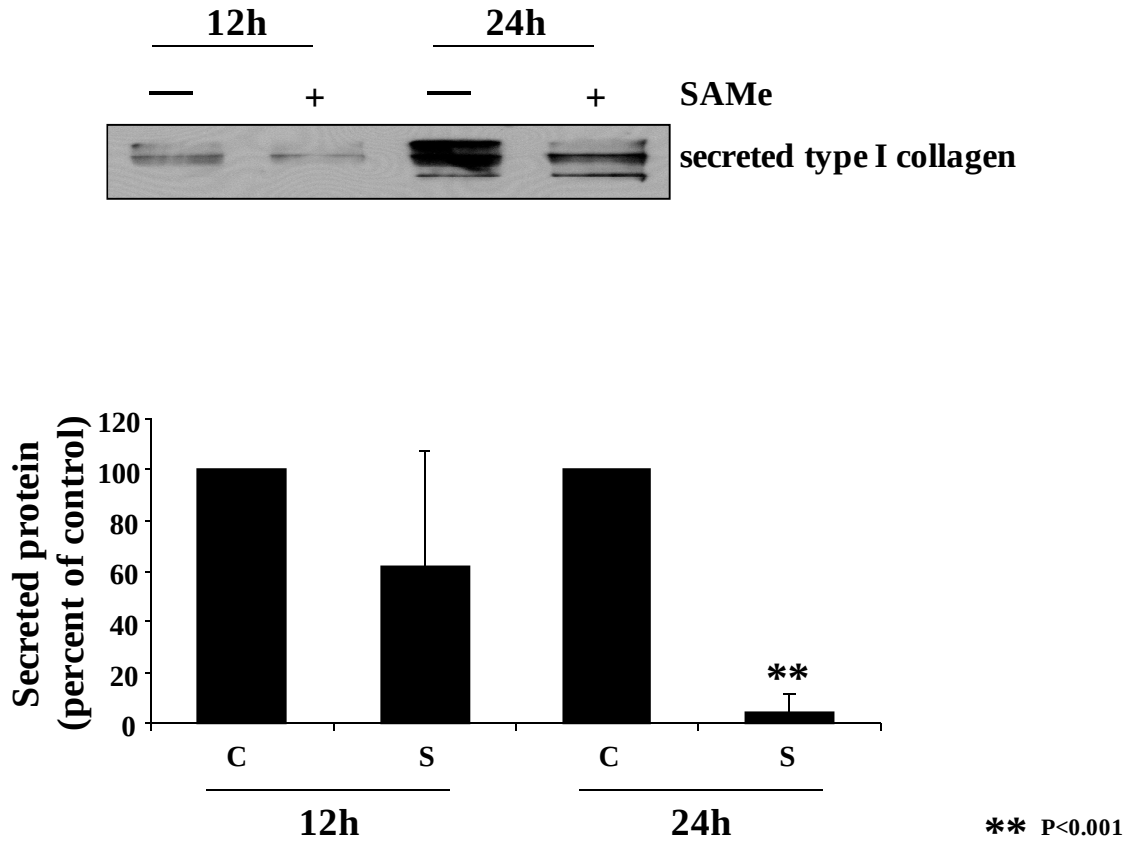

Figure 9. SAMe significantly decreases type I collagen secretion in activated HSCs. Culture-activated (day 14) HSCs were treated with 0 (C) or 1000 μM SAMe (S) for 12 and 24 h. Conditioned media was concentrated and immunoblot analysis was performed to analyze type I collagen secretion (n=4).

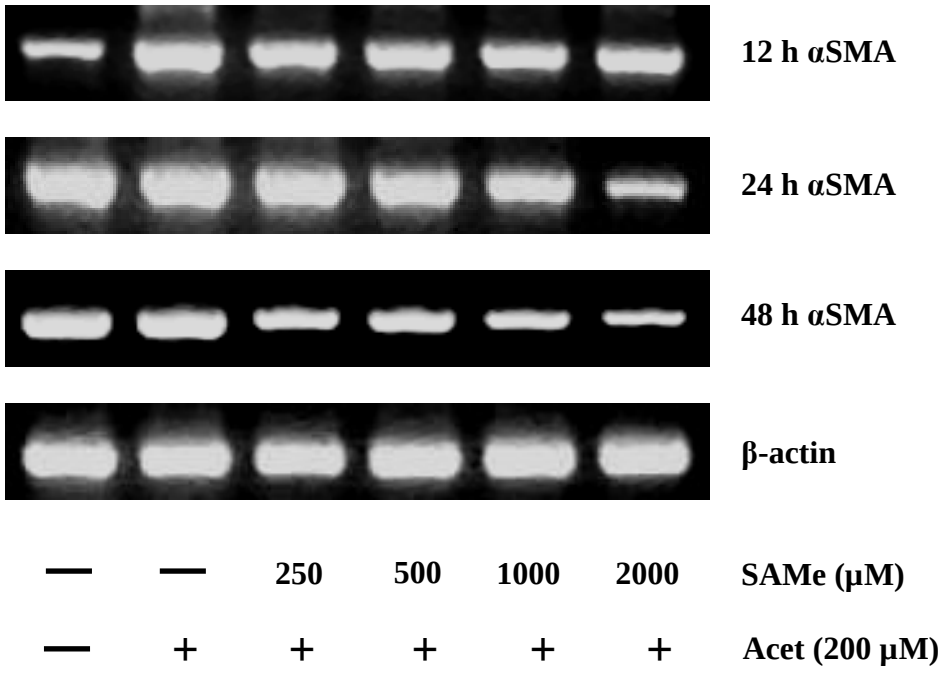

Figure 10. αSMA steady-state mRNA levels are decreased by SAMe in activated HSCs. Culture-activated HSCs were pre-treated with 0, 250, 500, 1000, or 2000 μM SAMe for 30 min. Cells were then treated in the presence or absence of 200 μM acetaldehyde (Acet) for 12, 24, and 48 h. Total RNA was isolated following each time point and reverse-transcribed to cDNA. RT-PCR was then performed for cDNAs encoding αSMA and β-actin.

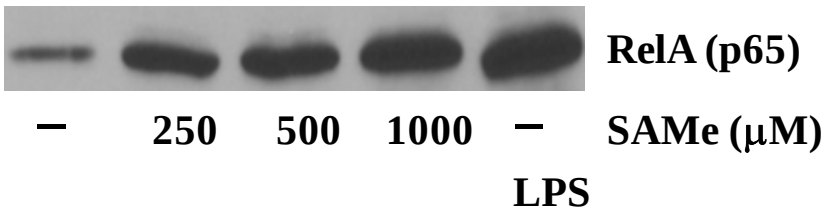

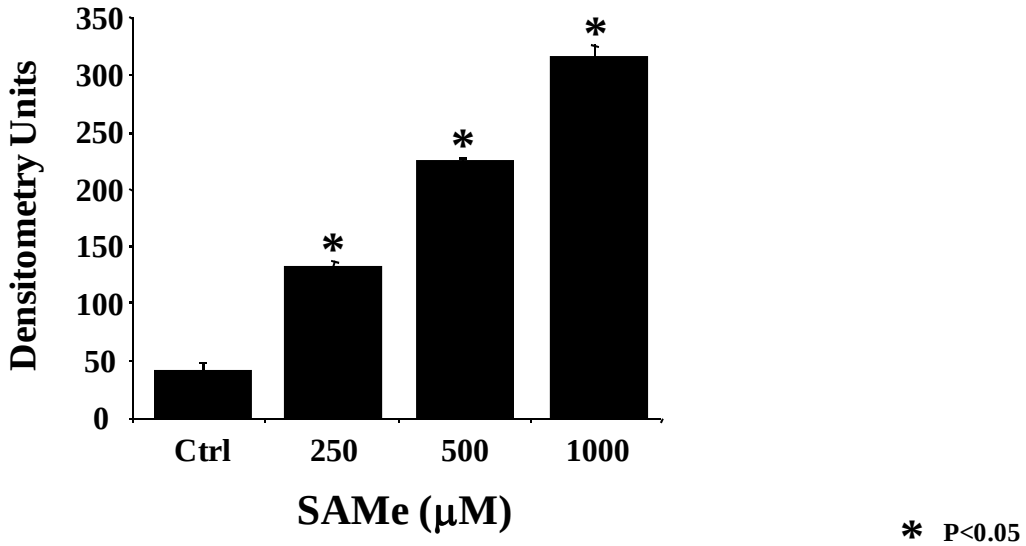

Figure 11. SAMe increases p65 nuclear translocation in activated HSCs. Culture-activated (day 14) HSCs were treated with 0 (□ ,Ctrl), 250, 500, or 1000 μM SAMe for 1 h. Nuclear extracts were isolated and immunoblot analysis was performed. LPS (100 ng/mL) was used as a positive-control for p65 translocation (n=3).

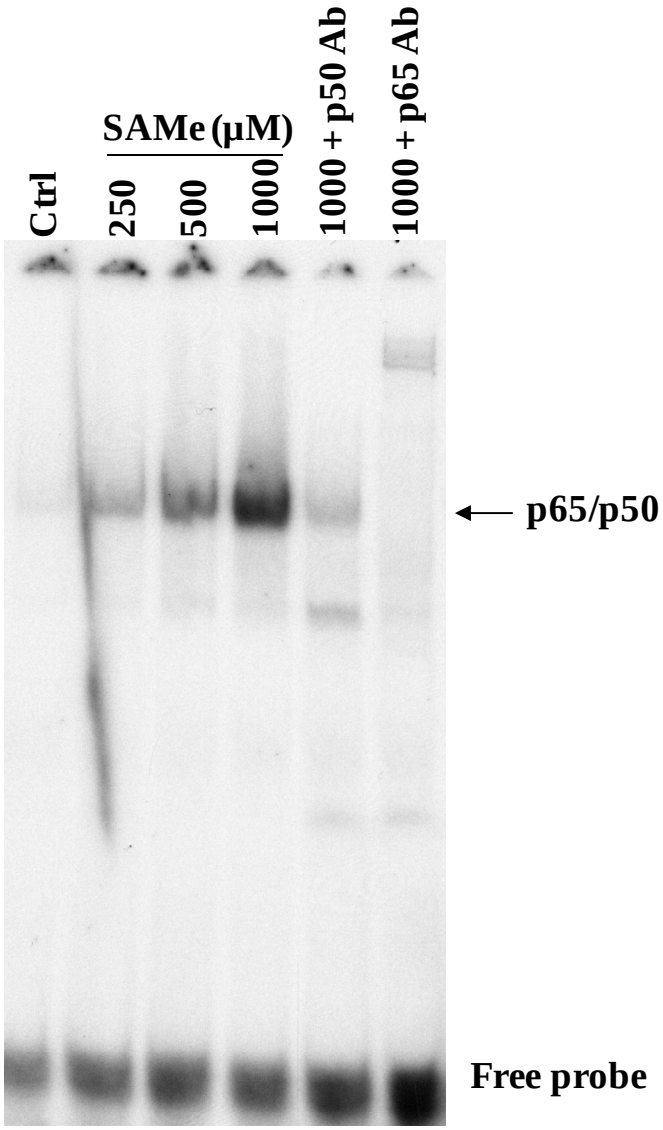

Figure 12. SAMe enhances NF-κB binding in activated HSCs. Culture-activated (day 14) HSCs were treated with 0, 250, 500, or 1000 μM SAMe for 1 hour. Nuclear extracts were isolated and EMSA was performed. To identify specific complexes, antibodies were utilized that recognize the p65 and p50 subunits of NF-κB (n=3).

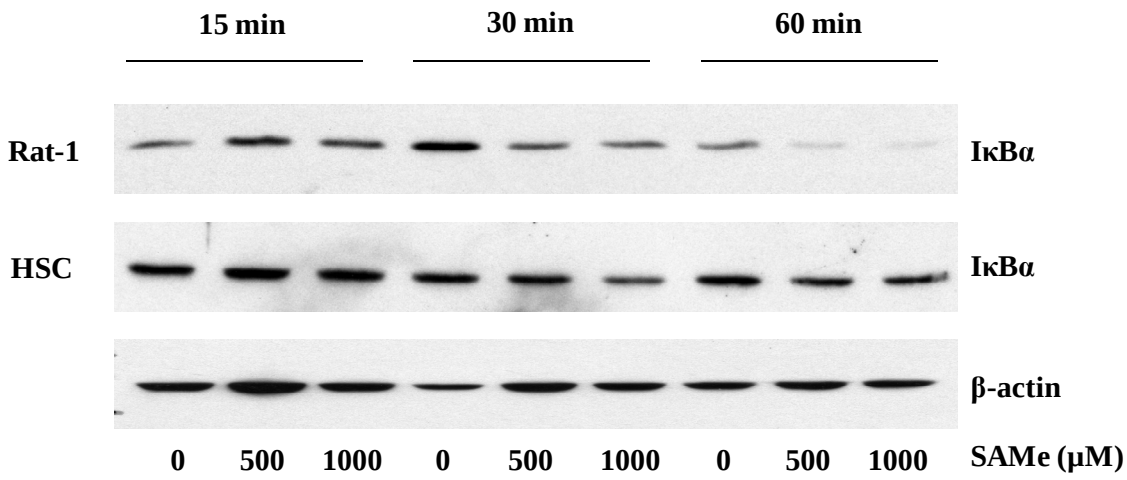

Figure 13. SAMe increases IκBα degradation. Culture-activated (day 14) HSCs or Rat-1 fibroblasts were treated with 0, 500, or 1000 μM SAMe for 15, 30, and 60 min. Whole cell extracts were isolated and immunoblot analysis was performed using an antibody against IκBα. β-actin was utilized as a control for protein sample loading (n=3).

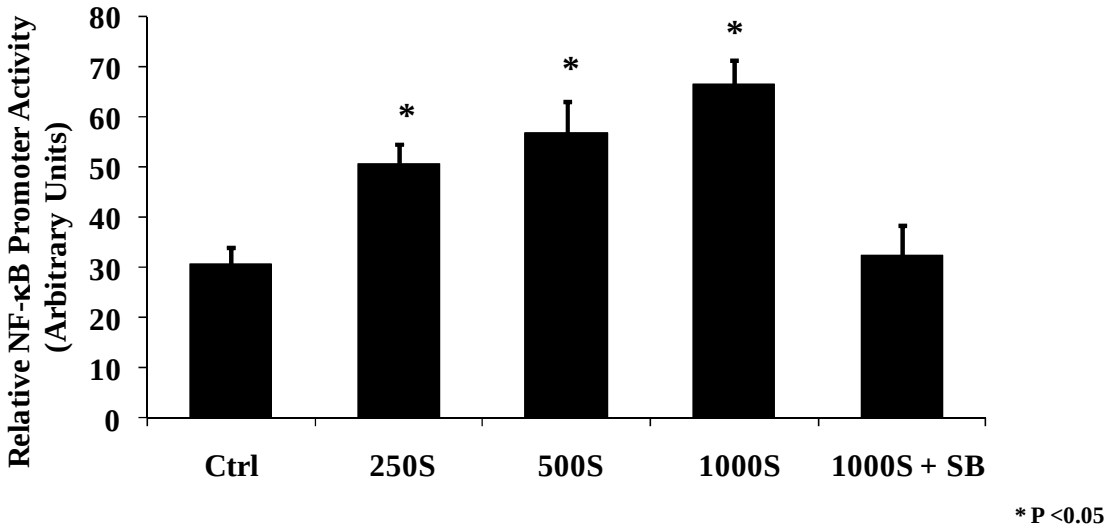

Figure 14. NF-κB transcriptional activation is enhanced by SAMe. NIH 3T3 fibroblasts were transfected with pNF-κB 3XLUC. Cells were then treated for 24 h with 0 (Ctrl), 250, 500, or 1000 μM SAMe (S). To inhibit p38 MAPK activity, cells were pretreated for 30 min with 5 μM SB203580 (SB). Lysates were used to determine luciferase activity (n=3).

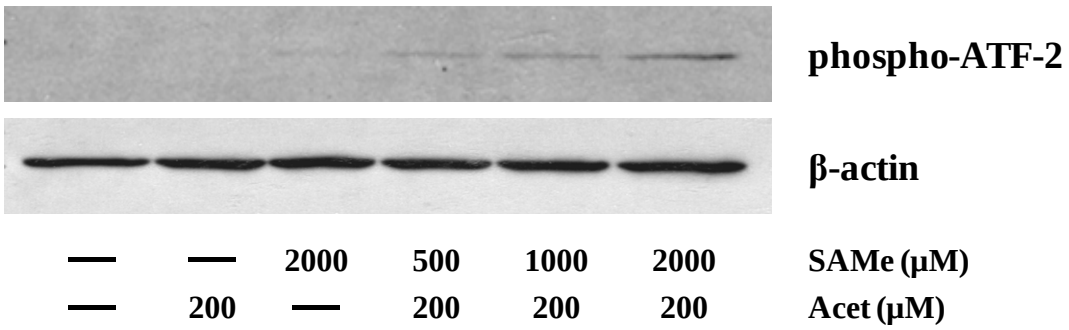

Figure 15. SAMe stimulates p38 MAPK activity. Culture-activated HSCs were pretreated for 30 min with 0, 500, 1000, or 2000 μM SAMe. Cells were then treated for 30 min in the presence or absence of 200 μM acetaldehyde (Acet). Immunoprecipitation of phospho-p38 MAPK (Thr180/Tyr182) was performed followed by incubation with a ATF-2 Fusion protein to evaluate kinase activity. Western blot analysis was then performed using an antibody that recognized phosphorylated ATF-2 (n=3).

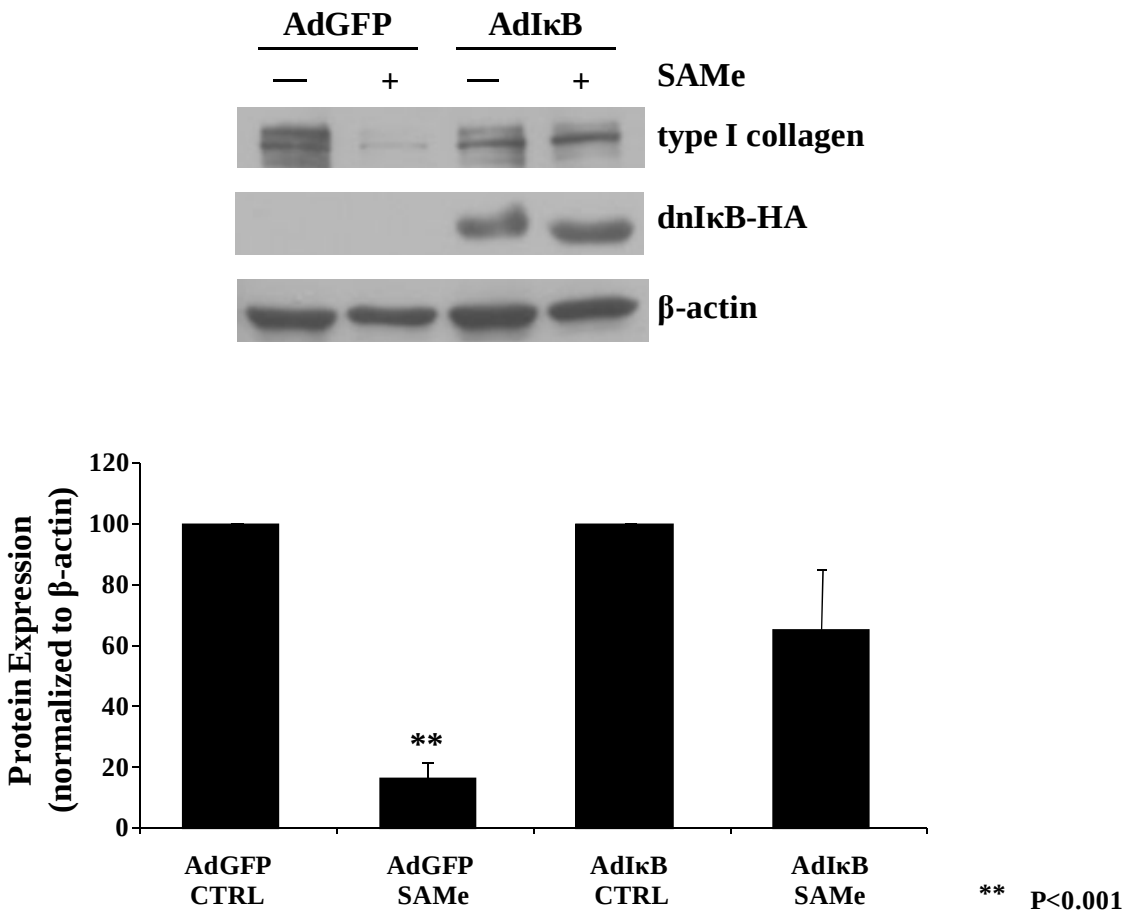

Figure 16. NF-κB activity is required for SAMe-mediated type I collagen inhibition. Rat-1 fibroblasts were infected with either Ad5GFP (AdGFP) or HA-tagged Ad5IκBα (AdIκB) and treated in the presence (SAMe) or absence (CTRL) of 1000 μM SAMe for 24 h. Whole cell extracts were analyzed for type I collagen expression and normalized to β-actin expression. To evaluate expression of dnIκBα, immunoblot analysis was performed for HA (n=3).

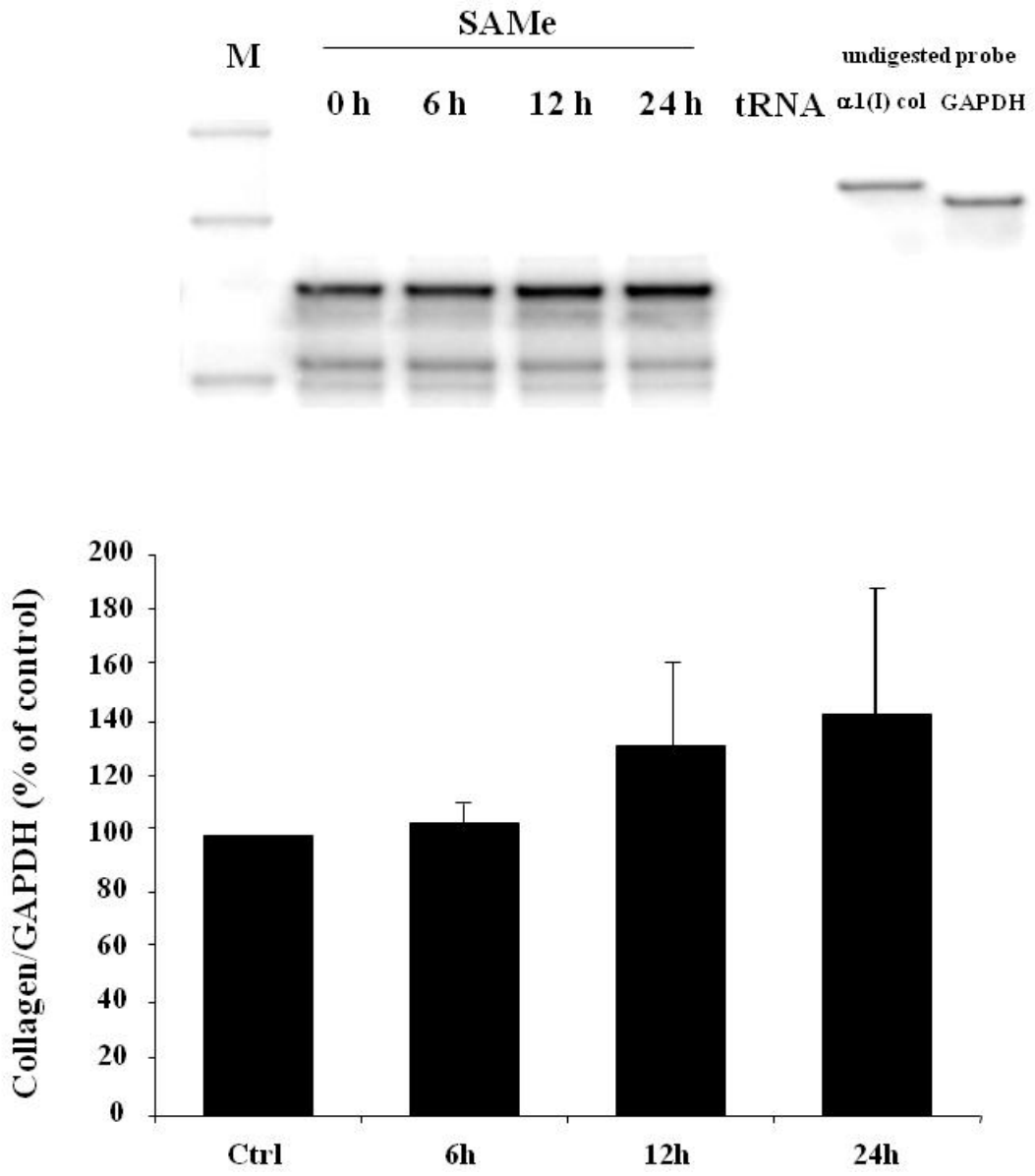

Figure 17. α1(I) procollagen mRNA levels are not significantly affected by SAMe in activated HSCs. Culture-activated HSCs were treated in the presence of 1000 µM SAMe for 0 (Ctrl), 6, 12, or 24 h. Ribonuclease protection assay was performed utilizing riboprobes for α1(I) procollagen, and GAPDH as a control. Although SAMe increased steady-state mRNA levels of α1(I) procollagen mRNA this increase was not statistically significant. (M) Molecular weight standards (n=3).

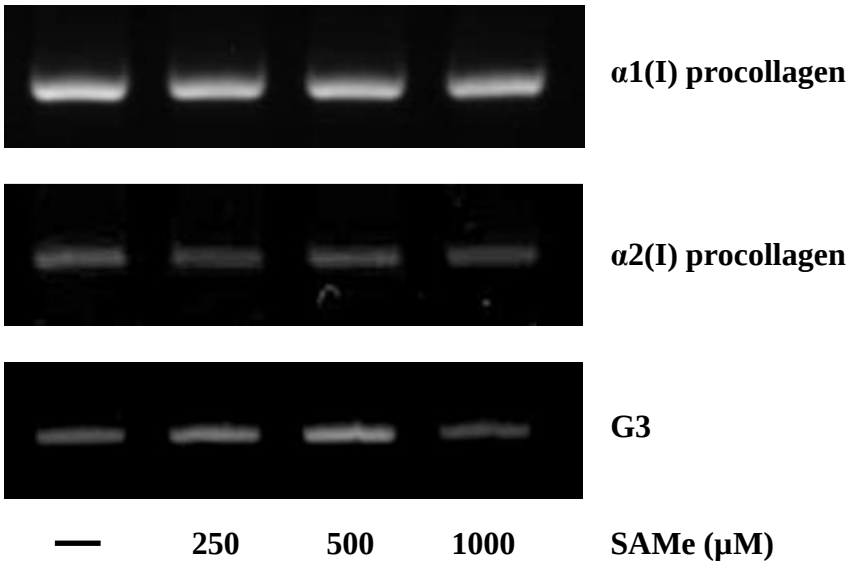

Figure 18. SAMe does not affect procollagen mRNAs in culture-activated HSCs. Culture-activated HSCs were treated with 0, 250, 500, or 1000 uM SAMe for 24 h. RT-PCR was performed utilizing primers for α1(I) procollagen, α2(I) procollagen, and GAPDH as a control. SAMe treatment had no effect on the levels of either procollagen (n=3).

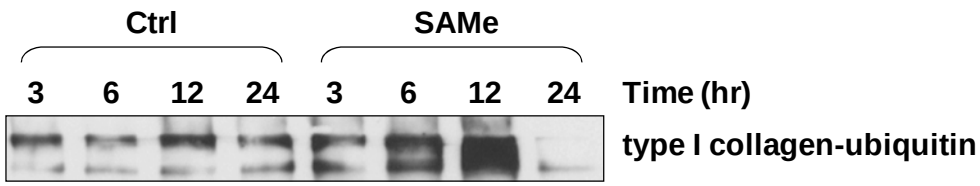

IP: type I collagen

IB: polyubiquitin

Figure 19. SAMe stimulates polyubiquitination of type I collagen in culture-activated HSCs. Culture-activated HSCs were treated in the presence or absence of 1000 µM SAMe for 3, 6, 12, and 24 h. Coimmunoprecipitation of complexes recognized by an antibody to type I collagen was performed on lysates, and immunoblot analysis was conducted utilizing an antibody that recognizes polyubiquitin (n=3).

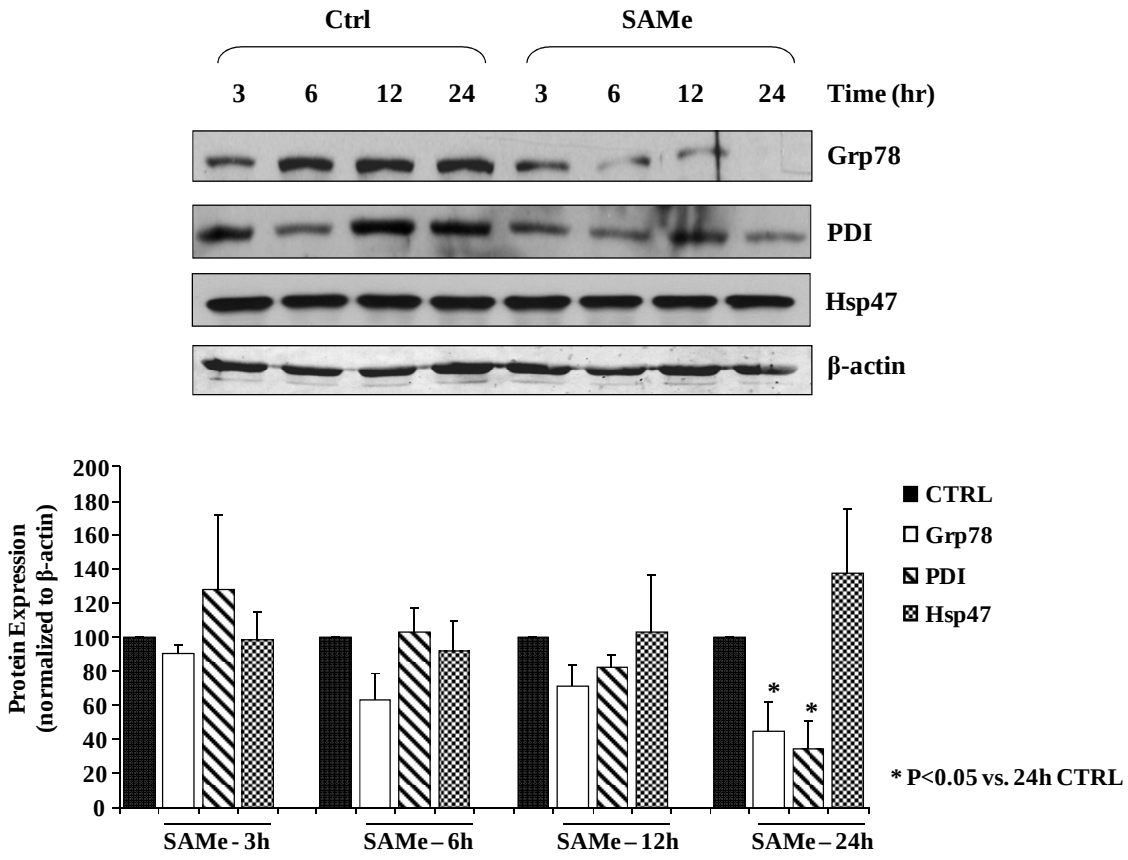

Figure 20. ER resident proteins Grp78 and PDI are decreased by SAMe. Culture-activated HSCs were treated in the presence or absence of 1000 μM SAMe for 3, 6, 12, and 24 h. Whole cell lysates were prepared and analyzed by immunoblot analysis utilizing antibodies recognizing Grp78, PDI, and Hsp47. Western blot analysis was also performed utilizing an antibody recognizing β-actin as a loading control (n=4).

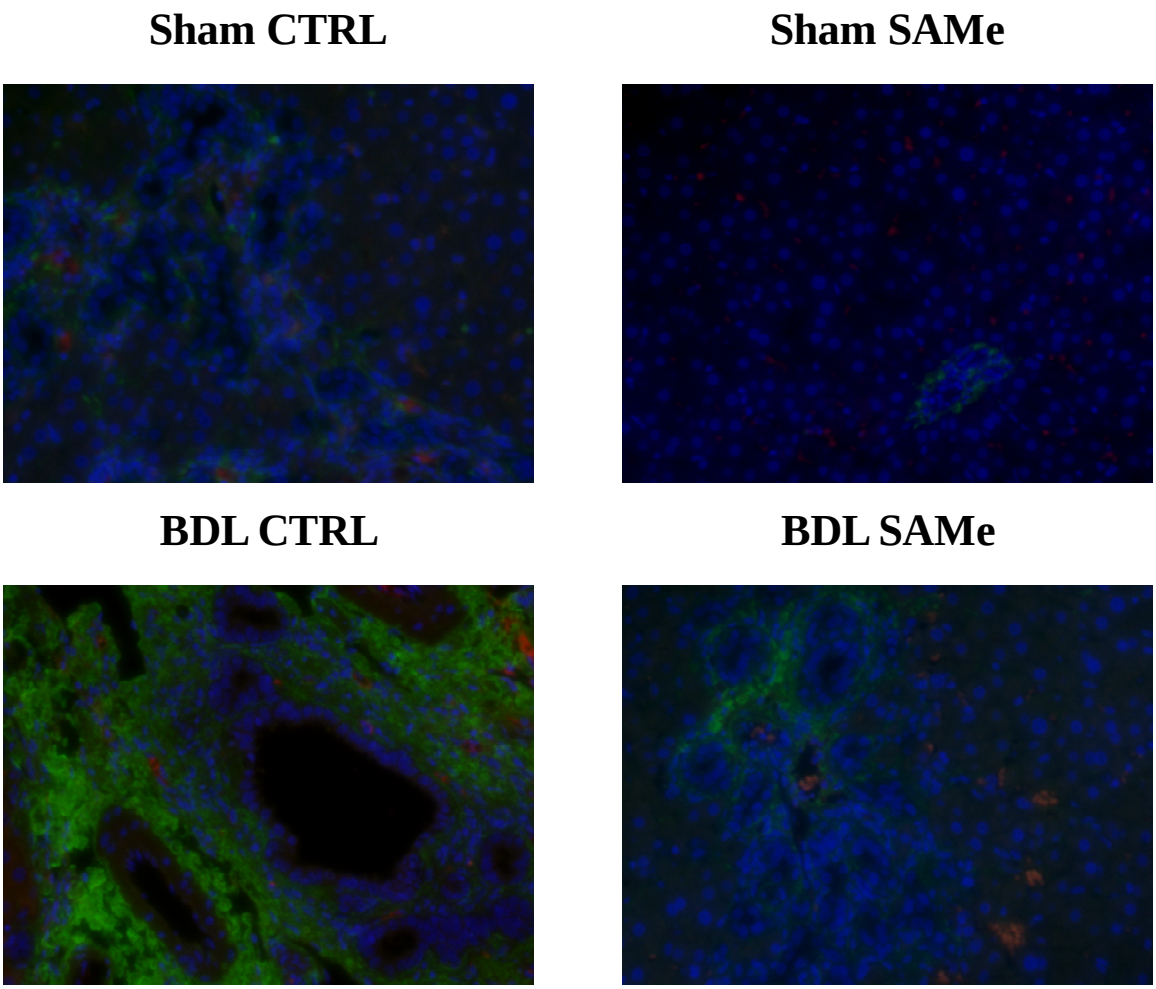

Figure 21. SAMe does not increase polyubiquitination of type I collagen in a BDL model of hepatic fibrosis. Sprague-Dawley rat were subjected to either Sham or BDL surgery. Beginning on post-operative day 7 animals were treated with either 50 mg/kg SAMe or vehicle by i.p. injection daily for an additional 7 days. Liver cross sections were co-stained with antibodies recognizing type I collagen and polyubiquitin followed by detection with fluorescent-labelled secondary antibodies. DAPI (blue) was used to indicate cell nuclei. Type I collagen (green) was visualized with the FITC filter and polyubiquitin (red) was visualized with the TR filter (n=8).

CHAPTER 4: ANIMAL MODELS OF HEPATIC FIBROSIS

Introduction

In this section we describe the development of animal models of fibrosis that may be used to evaluate both the progression and treatment of hepatic fibrosis. There remains a need to develop models of alcoholic fibrosis that are both easy to use and mimic the phenotype observed in human patients. Thus we performed various durations of ethanol feeding coupled with LPS injections to evaluate a "two-hit" model of ethanol-induced hepatic fibrosis. We also used a BDL model of hepatic fibrosis that results in rapid development of liver fibrosis, providing a means to test the efficacy of SAMe as a treatment for the resolution of fibrosis.

Ethanol model of hepatic fibrosis

With a high prevalence of hepatic fibrosis and cirrhosis world-wide, there is a need to develop animal models that mimic the pathophysiology of human disease. In particular, there remains a need to develop a clinically-relevant animal model of ethanol consumption that generates the peri-cellular fibrosis, and ultimately, "chicken-wire" fibrosis seen in humans. Despite the development of the nutritionally complete Lieber-DeCarli (L-D) liquid ethanol diet that overcomes the natural aversion of rodents to ethanol consumption, ethanol alone does not lead to fibrosis, regardless of the length of administration [258]. L-D did, however, generate peri-venular steatosis, apoptosis, MEOS induction, reactive oxygen species, and glutathione depletion.

Increasing evidence points to a “two-hit” model of ethanol-induced fibrosis and a number of ethanol models have demonstrated fibrosis when augmented with a secondary stress such as iron [40] or vitamin A [36]. However, these secondary stresses are not considered clinically relevant to the majority of cases of ALD. LPS is frequently observed to be elevated in patients with ALD [259]. Ethanol consumption disrupts the gut epithelium, allowing LPS leakage into the bloodstream [260]. LPS can interact with various liver cells such as the SECs, Kupffer cells, and HSCs to promote cytokine production and infiltration of inflammatory cells, which may ultimately lead to fibrosis. This position is further augmented by the observation that treatment of rodents with oral antibiotics lessens the damage due to ethanol intake [261].

In animal studies utilizing ethanol and LPS there is increasing evidence that LPS can enhance damage due to ethanol. Mice maintained on an ethanol diet for 5 weeks followed by a one-time dose of LPS experienced greater fat accumulation, inflammatory cell infiltration, and hemorrhage than pair-fed controls [262]. In a model of chronic ethanol priming (2 weeks of ethanol feeding alone using a low carbohydrate/high fat diet) followed by 4 weeks of ethanol feeding with a continuous infusion of LPS, there were only minor histopathological changes; mainly polymorphonuclear cell infiltration [263]. This suggests that continuous elevated endotoxin exposure may induce tolerance and desensitization of target cells, blunting the effects. By utilizing an intragastric ethanol infusion model that provides continuous ethanol feeding (9 weeks) coupled with weekly 5 mg/kg injections with LPS, Tsukamoto et al. showed centri-lobular fibrosis [264]. Despite the ability to generate fibrosis in a model that may more closely mimic the progression of ALD in humans, the intragastric feeding model is limited by the invasive

nature of the intragastric feeding tube, requiring personnel trained in the surgery and maintenance of the feeding tube. Also, this model does not represent the traditional delivery of ethanol through *ad libitum* consumption. Thus, it would be beneficial to develop a "two-hit" animal model of liver fibrosis utilizing ethanol and LPS that is easy for investigators to utilize and more closely follows the normal pattern of ethanol consumption. We hypothesized that utilizing the L-D *ad libitum* liquid ethanol diet coupled with weekly or biweekly injections of a mild dosage of LPS (0.5 or 1.0 mg/kg) would lead to hepatic fibrosis within 7 weeks.

Materials and Methods

7 week ethanol model of fibrosis pilot study

For the 7 week ethanol plus LPS (*E. coli* serotype 026:B6, Sigma) pilot study, male Sprague-Dawley rats weighing 200-250 g were used. Animals were split into four groups: control (C), ethanol alone (E), ethanol plus weekly i.p. injections of 0.5 mg/kg LPS (EL 0.5), and ethanol plus weekly i.p. injections of 1.0 mg/kg LPS (EL 1.0) (n=3 for all groups).

10 week ethanol model of fibrosis pilot study

For the 10 week ethanol plus LPS pilot study, male Sprague-Dawley rats weighing 250-350 g were used due to an unanticipated delay in initiating the study. Animals were split into six groups: control (C), control plus 1.0 mg/kg LPS semi-weekly (L), control plus 10 mg/kg SAMe chloride (Sigma) injected i.p. every other day (S), ethanol alone (E), ethanol plus 1.0 mg/kg LPS injected i.p. semi-weekly (EL), and ethanol plus i.p. injections of 1.0 mg/kg LPS semi-weekly and 10 mg/kg SAMe chloride (ELS) every other day (n=3 for all groups).

8 week ethanol model of fibrosis pilot study

For the 8 week ethanol plus LPS pilot study, male Sprague-Dawley rats weighing 225-275 g were used. Animals were split into five groups: control (C), control plus 10 mg/kg SAMe toluene-sulfonate (Sigma) injected i.p. daily (S), ethanol alone (E), ethanol plus 0.5 mg/kg LPS injected i.p. semi-weekly (EL), and ethanol plus i.p. injections of 0.5 mg/kg LPS semi-weekly and 10 mg/kg SAMe toluene-sulfonate (ELS) daily (n=6 for all groups).

Lieber-DeCarli liquid ethanol diet

Animals were permitted *ad libitum* access to either an ethanol liquid diet (Lieber-DeCarli Regular Ethanol, Dyets Inc., Bethlehem, PA) providing 36% of daily calories in the form of ethanol or an isocaloric control diet (Dyets Inc.) where calories provided by ethanol were replaced by dextrin-maltose. To allow animals to acclimate to receiving ethanol liquid diets, the amount of ethanol in the diet was increased 25% every two days until receiving the full 36% of their calories from ethanol. This time-point was designated as the start of the experiment. To control caloric consumption of control rats, it was necessary to limit the amount of liquid control diet they received based on the average daily consumption across all ethanol groups. Animals were weighed weekly to monitor weight gain. At the conclusion of the feeding period (7 weeks, 8 weeks, or 10 weeks), animals were sacrificed by exsanguination under anesthesia and tissues were collected. Samples for histology were fixed for 20 hours in 10% neutral-buffered formalin, washed with tap H_2O, and stored for processing in 70% ethanol. Samples for protein and isolation of RNA were snap-frozen in liquid nitrogen. Masson's trichrome, Sirius red (except for the 8 week ethanol study, which was performed by Amel Karaa),

and hematoxylin and eosin (H&E) staining was performed by the image technician in the UNC Charlotte Department of Biology. Examination of histological samples was performed by an investigator blinded to the study.

Results

Animal weights for the 7 week ethanol pilot study.

To monitor the weights of animals on the liquid control and ethanol diets, animals were weighed weekly. Because the pilot study was conducted with the assistance of the laboratory of Dr. Mark Clemens, UNC-Charlotte, it was necessary conclude the experiment after 4 weeks for the C and E animals. EL 0.5 and EL 1.0 animals were continued on the diet for 7 weeks. For the first 4 weeks, animals in groups fed ethanol had similar weights while control animals had higher weights, despite consuming equal amounts of a nutritionally-complete isocaloric diet. Following termination of the study for animals in the C and E groups, animals in the EL 0.5 and EL 1.0 groups had similar weights throughout the remainder of the study (Fig. 22). One animal in the EL 1.0 group died two days after the 3rd i.p. LPS injection. We suspected this was a consequence of injection error as opposed to mortality associated with the experimental conditions.

When comparing weight gain, there were broad differences. EL 0.5 animals had the largest weight gain in the study (123.3 g ± 28.7), followed by C animals (120.7 g ± 7.6) despite only being included in the study for 4 weeks. Animals in the EL 1.0 group had a weight gain of 96 g ± 5.7 and E animals, which again were only subjected to 4 weeks of liquid diet, had the smallest weight gain at 72 g ± 6 (Fig. 23).

Ethanol coupled with LPS injections induces early hepatic fibrosis.

To evaluate livers for fibrosis, Masson's Trichrome staining was performed on sections from formalin-fixed livers. There was minimal staining in C and E groups except around central veins and portal triads, as expected (Fig. 24). Treatment with LPS resulted in mild fibrosis accumulating mostly peri-sinusoidally (Fig. 25).

Animal weights for the 10 week Ethanol study.

To monitor the weights of animals on the liquid control and ethanol diets, animals were weighed weekly. Animals in each group gained weight throughout the study, although animals in the ELS group initially gained weight at a slower rate in the first two weeks of the study (Fig. 26). Because there was a broad range of starting weights at the beginning of the study, weight change was evaluated. Animals had a consistent amount of weight gain over the course of the study. Only animals in the ELS had a noticeably lower weight gain during the study (Fig. 27); however, this was not a statistically significant amount.

Hepatic fibrosis was not induced by ethanol and LPS in the 10 week ethanol study.

Histological analysis following the 10 week ethanol study revealed only minor damage. H&E staining of animals in the E group exhibited micro- and macrovesicular steatosis while addition of both LPS and LPS in conjunction with SAMe to ethanol-fed rats abolished this effect (Fig. 28). In all groups normal liver architecture was preserved and there was no observable infiltration of inflammatory cells or areas of necrosis.

To assess if hepatic fibrosis was induced by 10 weeks of ethanol administration coupled with semi-weekly injections of 1.0 mg/kg LPS, Sirius red staining of formalin-fixed sections was performed. Surprisingly, there was no observable staining for

collagen in any group, except for small staining around vessels as normally found in the healthy adult liver (Fig. 29).

Animal weights for the 8 week ethanol study.

To monitor the weights of animals on the liquid control and ethanol diets, animals were weighed weekly. Animals in the control groups had higher weights throughout the study than animals in ethanol-fed groups (Fig. 30). This trend was also evident in weight gain during the course of the study. The highest weight gains were animals receiving control diets and there was a statistically significant difference it weight gain between animals in the EL (194.6 g ± 6.2) and ELS (184 g ± 1.2) groups with animals in the S group (218.7 g ± 2.3) (Fig. 31).

Animals fed diets containing ethanol had detectable levels of ethanol ranging from 18 mM ±2.47 (EL) to 24.5 mM ± 4.53 (ELS) to 25.1 mM ± 2.28 (E) (Fig. 32). These levels correspond with blood alcohol contents of 0.11%, 0.14%, and 0.15% respectively, which in humans are suitable levels to cause motor impairment. Ethanol consumption alone compared to control and control animals receiving daily SAMe injections resulted in a significant increase in liver:body weight ratio, suggesting hepatomegaly, an indicator of liver injury. Animals receiving ethanol in combination with LPS semi-weekly, or ethanol and LPS semi-weekly in addition to daily SAMe administration also had hepatomegaly; however, this increase was not statistically significant (Fig. 33).

Evaluation of ALT levels, a marker for hepatic injury, revealed significant damage caused by ethanol feeding and the combination of ethanol plus LPS compared to

control animals. Treatment with SAMe significantly reduced hepatic injury as assessed by ALT levels (Fig. 34).

Effects of SAMe on markers of oxidative stress.

The expression of key enzymes involved in the metabolism of ethanol and generation of oxidative stress were examined. Ethanol consumption and ethanol coupled with LPS injections led to a significant increase in CYP2E1 expression. This effect was attenuated significantly by treatment with daily SAMe (Fig. 35). Levels of ADH were unchanged across all groups. Expression of ALDH was significantly elevated in animals fed ethanol and ethanol plus LPS (Fig. 35). Treatment with SAMe slightly decreased ALDH expression as compared to animals receiving ethanol plus LPS; however, this change was not statistically significant (Fig. 35).

To examine the effect on the redox status of livers from the ethanol diet, GSSG/GSH ratio was determined. Animals from control and control plus SAMe groups showed low GSSG/GSH ratios, suggesting low levels of oxidative stress. Consumption of ethanol significantly elevated the GSSG/GSH ratio, suggesting an increase in oxidative stress. This ratio was further increased by consumption of ethanol with semi-weekly LPS injections. Treatment with SAMe, however, restored normal GSSG/GSH ratios (Fig. 36).

To indirectly evaluate oxidative stress the presence of 4-hydroxy-2-nonenal (4-HNE), a marker of lipid peroxidation was determined. Immunofluorescent histochemistry using an antibody that recognizes 4-HNE showed minimal staining in animals on the control diet. Ethanol-fed rats had a mild increase in the amount of 4-HNE staining, which was further exacerbated by the combination of ethanol and LPS. SAMe

injections, however, markedly reduced the amount of 4-HNE staining suggesting that SAMe administration can decrease lipid peroxidation in our model of fibrosis (Fig. 37).

SAMe inhibits ethanol-induced hepatic fibrosis.

Histological changes following the 8 week ethanol study were assessed by H&E staining of formalin-fixed tissue samples. Sections from C and S groups demonstrated normal liver architecture. Ethanol consumption alone resulted in micro- and macrovesicular steatosis similar to that observed from both the 7 week ethanol pilot and 10 week ethanol study. However, unlike previous studies semi-weekly i.p. injection of LPS at 0.5 mg/kg resulted in areas of focal infiltration of small cells. Treatment with SAMe at 10 mg/kg daily abolished both the inflammation and micro- and macrovesicular steatosis observed in EL animals (Fig. 38).

To determine if hepatic fibrosis was induced by 8 weeks of ethanol administration coupled with semi-weekly injections of 0.5 mg/kg LPS, Sirius red staining of formalin-fixed sections was performed. Minimal collagen staining was observed in control and animals treated with SAMe alone. Ethanol resulted in an increase in perivenular collagen staining. Treatment of ethanol-fed animals with LPS increased perivenular fibrosis and led to marked perisinusoidal fibrosis compared to animals fed ethanol alone. SAMe-administration abolished both perivenular and perisinusoidal fibrosis compared to ethanol and ethanol plus LPS animals (Fig. 39). Quantitation of areas positive for collagen staining revealed a significant increase in collagen staining for animals fed ethanol compared to controls. This was further exacerbated by the combination of LPS plus ethanol. SAMe treatment, however, restored collagen staining to normal levels (Fig. 40).

Infiltration of PMNs and activation of HSCs is inhibited by SAMe.

Chronically-injured liver often results in activation of HSCs and infiltration of inflammatory cells, such as polymorphonuclear leukocytes (PMNs). Animals on diets containing ethanol alone had mild staining for PMNs, suggesting inflammation. This effect was exacerbated by the combination of ethanol plus semi-weekly LPS. Treatment with SAMe diminished this effect, suggesting a decrease in inflammation (Fig. 41).

Animals on control diet and control plus daily SAMe injections had low levels of αSMA protein expression. Ethanol consumption resulted in a significant increase in αSMA expression, which was further significantly increased by the combination of ethanol plus semi-weekly LPS injections. Administration of SAMe restored αSMA protein expression to control levels (Fig. 42).

Effects of SAMe on TGF-β signaling pathway.

Because numerous studies have established a link between oxidative stress and lipid peroxidation with an increase in the production and signaling of TGF-β [265-268], we examined the effects of SAMe administration on the expression of members of the TGF-β signaling pathway. Animals on control diets had similar mRNA expression levels of TGF-β. Chronic ethanol consumption resulted in significantly elevated TGF-β mRNA levels; however, ethanol coupled with semi-weekly LPS injections resulted in no further increase. Treatment with SAMe significantly reduced TGF-β mRNA expression (Fig. 43).

To examine the effects of SAMe on downstream TGF-β signaling components, mRNA expression for Smad3 and Smad7 were determined. Animals receiving control diet, control diet plus SAMe, and ethanol feeding alone had similar levels of Smad3

mRNA expression. LPS injections coupled with chronic ethanol feeding, however, resulted in a significant increase in Smad3 expression, suggesting that the combination of LPS and ethanol may enhance TGF-β signaling. Treatment with SAMe resulted in a significant decrease in Smad3 expression compared to animals in the EL group (Fig. 43). Expression of the Smad3 inhibitor, Smad7, was consistent between animals receiving control diet and control diet plus daily SAMe injections. Animals in the ethanol-fed group and ethanol-fed group plus semi-weekly LPS injections had a significant decrease in Smad7 expression, suggesting that ethanol feeding can also enhance TGF-β signaling by downregulating a key inhibitory molecule of Smad3 signaling. This effect was abolished by SAMe treatment, resulting in a significant increase compared to the E and EL groups (Fig 43).

BDL model of hepatic fibrosis

Therapies to evaluate hepatic fibrosis must be evaluated to determine their efficacy as both a preventative treatment and curative treatment. Because a model of ethanol-induced hepatic fibrosis required 8 weeks to induce mild fibrosis, we wished to develop a model for evaluating SAMe as a curative treatment to verify results observed *in vitro* using culture-activated HSCs. We opted to use a bile duct-ligated model of experimental fibrosis using Spague-Dawley rats. This model results in an increase of both type I collagen message (α1(I) procollagen mRNA) and protein production within 5 days [29] and has been used to evaluate the efficacy of SAMe as a treatment using gross histological markers [237]. The molecular mechanisms of the inhibitory actions of SAMe were not evaluated, however. We sought to develop a BDL model where 7 days

of BDL alone were followed by 7 additional days of treatment with SAMe or an equal volume of saline.

Materials and Methods

BDL model of hepatic fibrosis

Using male Sprague-Dawley rats between 350 and 450 g, a mid-line laparotomy was performed under anesthesia and the bile duct was identified, doubly-ligated with silk suture, and transected. The abdominal incision was closed using absorbable suture in a continuous pattern and the skin closed with non-absorbable suture in an interrupted pattern. Sham operations were performed in an identical manner, except without ligation and transaction of the bile duct. Animals were followed for 7, 14, or 21 days and sacrificed by exsanguination under anesthesia to collect tissue. To test the efficacy of SAMe as a therapeutic for hepatic fibrosis, BDL or Sham operations were again performed. Animals were allowed to recover for 7 days. On post-operative day 7 animals were treated daily with injections of 10 mg/kg SAMe-toluene sulfonate or an equal volume of saline. On post-operative day 14 animals were sacrificed by exsanguination under anesthesia and tissues were collected. Samples for histology were fixed for 20 hours in 10% neutral-buffered formalin, washed with tap H_2O, and stored for processing in 70% ethanol. Samples for protein and isolation of RNA were snap-frozen in liquid nitrogen. Picro-sirius red staining, and hematoxylin and eosin (H&E) staining were performed by the image technician in the UNC Charlotte Department of Biology.

Results

BDL results in hepatic fibrosis.

To validate the efficacy of our model to induce hepatic damage, a small pilot study was performed. Animals (n=8) were subjected to either sham operation or BDL and allowed to recuperate for 7, 14, or 21 days. H&E staining revealed normal liver architecture in the sham operated animals. BDL resulted in disruption of normal liver architecture in as little as 7 days with proliferation of bile duct epithelial cells around the portal triad and infiltration of small cells with maximum duct formation at 21 days (Fig. 44). Sirius red staining showed very little staining in all three zones of the sham operated animal, except for some collagen in the portal triad. By day 7 there was extensive staining for collagen, predominantly in the portal region (zone 1). Samples from day 14 and day 21 showed an increase in collagen staining compared to day 7 but little apparent difference between the two (Fig. 45).

SAMe attenuates liver fibrosis in BDL animals.

To assess SAMe as a potential reversing agent for hepatic fibrosis, we utilized the BDL model for fibrosis. Animals were subjected to either sham operation or BDL. At post-operative day 7, sham and BDL animals were further sub-divided into two additional groups, one set receiving SAMe 10 mg/kg i.p. daily and the other set receiving an equal volume of saline i.p. daily for an additional 7 days. Sirius red staining revealed that BDL CTRL animals had significantly higher levels of type I collagen versus both sham groups (3.196% area vs. 0.627% and 0.629% respectively for sham CTRL and sham SAMe). SAMe treatment significantly abrogated this effect (1.484% vs. 3.196%)

(Fig. 46). ANOVA on the ranks was performed to determine significance (n=8 for all groups).

SAMe decreases procollagen and αSMA steady-state mRNA levels in BDL rats

To determine if SAMe altered the expression of key mediators of fibrosis following BDL, RT-PCR was performed to analyze steady-state mRNA levels of α1(I) procollagen, α2(I) procollagen, and αSMA. BDL resulted in a significant increase in the levels of all three messages. Treatment with SAMe led to a significant decrease of αSMA expression compared to the BDL vehicle group. No significant decreases were observed when comparing levels of α1(I) and α2(I) procollagen expression between BDL vehicle and BDL SAMe-treated animals (Fig. 47). Two-way ANOVA was performed to determine statistical significance (n=8 for all groups).

Expression of MMPs and their inhibitors in BDL rats.

The expression of MMPs and their inhibitors, TIMPs, are altered by bile duct ligation. In particular, MMP-2 and TIMP-1 are strongly upregulated following BDL [147]. An increase in MMP-2 is hypothesized to degrade basement membrane, allowing infiltration of activated HSCs and inflammatory cells to areas of injury, facilitating repair. Sustained MMP expression, however, may contribute to injury. Previous studies in our lab support a role for MMP production by HSCs treated with SAMe. SAMe administration resulted in an increase in MMP-13 expression in culture-activated HSCs (Cross, MS Thesis, 2004), suggesting SAMe may resolve hepatic fibrosis through increased MMP-13 production, which has been shown to be fibrolytic.

To examine the effect of SAMe administration in the resolution of hepatic fibrosis, we utilized our BDL model. BDL resulted in a significant increase in MMP-2

mRNA expression (Fig. 48). BDL also increased MMP-13 expression; however, this was not a significant increase. Treatment with SAMe attenuated MMP-2 expression but had no effect on MMP-13 expression. Levels of both TIMP-1 and -2 were elevated by BDL. Daily injections of SAMe starting with post-operative day 7, however, failed to reduce expression of TIMP levels (Fig. 49).

Discussion

We sought to develop an animal model of alcoholic liver fibrosis that was easy to conduct and mimicked the pathophysiology observed in humans. Previous studies have demonstrated ethanol consumption increases translocation of LPS from the gut into the blood stream [260] and endotoxin levels are increased in patients with ALD [259]. Animals have shown chronic ethanol primes the liver for greater injury when challenged with a single dose of LPS [269]. However, chronic ethanol consumption coupled with continuous exposure to LPS results in minor injury [263], possibly due to an increased tolerance to endotoxin. We proposed a "two-hit" model of alcoholic liver fibrosis combining chronic *ad libitum* ethanol consumption and intermittent exposure to LPS.

To test our hypothesis we first established an ethanol feeding pilot. Animals were subjected to 7 weeks of either the L-D ethanol liquid diet, isocaloric control diet where calories from ethanol were replaced with dextrin-maltose, or L-D diet plus weekly i.p. injection of 0.5 mg/kg or 1.0 mg/kg of LPS. Ethanol consumption in our model reproduced the micro- and macrovesicular steatosis originally reported by Lieber et al. [33]. Ethanol consumption causes an increase in reducing equivalents through the oxidative generated by its metabolism and can down-regulate key regulators of lipid metabolism in cells, such as peroxisome proliferator-activated receptor-alpha (PPAR-α)

[270]. No inflammation was observed in the ethanol only group, also consistent with previous findings. Masson's trichrome staining revealed no collagen staining outside the small amounts normally found around the portal triads, central veins, and larger blood vessels in animals from ethanol feeding alone and their pair-fed controls. In animals fed ethanol combined with weekly injections of 0.5 mg/kg or 1.0 mg/kg of LPS there was evidence of peri-sinusoidal accumulation of collagen, indicating fibrogenesis.

The study was limited by the lack of appropriate control groups. Animals in the C and E groups were sacrificed at 4 weeks and the tissue shared with the laboratory of Dr. Mark Clemens (UNC-Charlotte, our collaborators in the study. Future studies will require appropriate control groups maintained throughout the study). Additionally, one animal in the E LPS 1.0 group died 2 days after the 3rd weekly i.p. LPS injection. 1.0 mg/kg LPS is considered a sub-acute dose (LD_{50} for LPS is approximately 40-50 mg/kg) and alone would not cause mortality. The most likely cause of death was improper injection technique and additional care was taken to avoid sudden movements of rats while receiving injections.

To examine the effect of longer duration of ethanol feeding coupled with an increased frequency of injection, we lengthened the study to 10 weeks and changed the injections to 1.0 mg/kg of LPS i.p. semi-weekly and added a group of animals on the isocaloric control diet receiving LPS injections to ensure LPS alone was not causing the fibrosis observed. Treatment with SAMe chloride was also added to the study to determine if fibrosis could be prevented with a 10 mg/kg dose injected i.p. every other day. A group of animals receiving SAMe injections on control diets was also added to evaluate the effects of SAMe injection alone. SAMe chloride was chosen over the

toluene sulfonate form used *in vitro*. We hypothesized that a chloride salt would be more soluable and safer *in vivo* than the aromatic form.

Histological analysis of the 10 week ethanol study revealed mirco- and macrovesicular steatosis, as expected. However, the combination of longer chronic ethanol consumption and the increased dosage and frequency of LPS failed to result in fibrosis and instead there was a marked reduction in the amount of steatosis present. This observation was also found in animals treated with SAMe, though to a lesser degree. The improvement in steatosis due to SAMe administration may be due to its ability to act as an antioxidant, restore the normal redox state in the liver, an important condition for the normal metabolism of lipids. The lack of steatosis observed in LPS-treated animals may be due to de-sensitization of LPS targets in the liver. Chronic exposure to circulating LPS diminishes injury in a chronic ethanol model. By increasing the frequency and dosage of LPS, the response of Kupffer cells may be diminished through the down-regulation of CD14 and toll-like receptor 4. Chronic LPS exposure has also been shown to decrease signaling through toll-like receptor 4 through an increase in suppression of cytokine signaling-1 (SOCS1) [271]. Longterm effects due to chronic LPS exposure may also in part be due to changes in hormonal production from the hypothalamus-pituitary-adrenal axis [272]. To overcome the problem of potential LPS tolerance and to improve the stability of the SAMe in hopes of achieving better therapeutic event, modifications were made to the experimental design and the ethanol study was repeated.

In the third, 8 week ethanol study, animals were fed either L-D ethanol liquid diet or isocaloric control diet. One subset of control animals received daily SAMe toluene-sulfonate injections i.p. The toluene-sulfonate form of SAMe has a larger anion

stabilizing the SAMe molecule than SAMe chloride, which has been shown to increase the stability of the compound [273]. At ambient and body temperature, SAMe rapidly decomposes, thus stable forms of the compound are necessary [274]. We hypothesized that using a more stable form coupled with an increased frequency of administration would provide a greater therapeutic benefit than SAMe chloride administered every other day. To reduce the risk of tolerance to LPS, the dosage was reduced from 1.0 mg/kg to 0.5 mg/kg i.p. semi-weekly. Because the effects of LPS alone are well-documented in the literature, we omitted the control group receiving LPS injections.

Chronic ethanol consumption for 8 weeks again led to marked steatosis micro- and macrovesicular steatosis. This was accompanied by mild infiltration of PMNs activation of HSCs. Addition of semi-weekly LPS injections exacerbated the hepatic infiltration and resulted in greater cell damage. Furthermore, LPS led to an increase in HSC activation and collagen production. Detailed examination of histological staining for collagen revealed preferential pericellular localization for collagen, which is an indicator of advanced fibrosis. These data suggest that our 8 week ethanol model is appropriate for examining the development of ALD and hepatic fibrosis. Although the extensive “chicken-wire” fibrosis did not develop, future experiments can focus with extending the length of the ethanol feeding to see if further progression of the disease occurs, or if as experienced in the 10 week ethanol study, there is actually blunting of injury with continued LPS injection. Although the L-D resulted in chronically elevated ethanol levels, the extent of intoxication was mild. Studies utilizing ethanol-preferring rats may demonstrate increased injury through higher levels of circulating ethanol levels. Genetic approaches to overcome the natural tolerance of rats to LPS may also be

utilizied, such as targeting SOCS1 expression. However, care must be taken to specificially target SOCS1 expression in the liver to prevent systemic consequences of SOCS1 inhibition.

Treatment with daily injections of 10 mg/kg SAMe toluene-sulfonate significantly ameliorated injury caused by the combination of ethanol and LPS. There was a significant reduction in the amount of collagen accumulation, steatosis, and inflammation compared to ethanol and LPS treated animals. This suggests that SAMe is an effective preventative treatment for initiation of alcoholic fibrosis. Examination of the mechanism of SAMe-mediated attenuation of injury revealed a decrease in oxidative stress generated by the combination of ethanol and LPS. Levels of CYP2E1 were reduced with SAMe administration and there was a significant reduction in the GSSG/GSH ratio and 4-HNE accumulation, demonstrating that SAMe can act as an antioxidant in an ethanol model of liver fibrosis.

SAMe treatment also decreased the expression of a key mediator of fibrogenesis, TGF-β, as well as diminishing the expression of key TGF-β signaling molecules, Smad3 and Smad7. SAMe treatment decreased Smad3 which has been implicated in the transdifferentiation of HSCs as well as collegen production and organization of stress fibers. The inhibitor of TGF-β signaling, Smad7, was reduced by ethanol consumption while SAMe treatment restored Smad7 to normal levels. TGF-β from both HSCs and Kupffer cells is a key mediator of hepatic fibrosis. Although LPS did not elevate TGF-β in our model of alcoholic fibrosis, LPS did alter the expression of key TGF-β signaling molecules, possibly potentiating the effects of TGF-β on HSCs. Administration of SAMe inhibited both the production of TGF-β in the livers of ethanol-fed rats as well as

restoring the normal expression patterns of Smad3 and Smad7, potentially limiting the signaling of TGF-β in target cells such as the HSCs. Further investigation of the relationship between ethanol, LPS, TGF-β, and the downstream regulators of TGF-β signaling should be investigated further in cultured HSCs and Kupffer cells.

These studies established a model for producing hepatic fibrosis from a rat model of chronic ethanol consumption by the addition of semi-weekly administration of a low dose of LPS. This model will provide a means for studying the initiation and progression of alcoholic hepatic fibrosis as well as a platform for evaluating treatments to both prevent and resolve fibrosis. Our model also has the advantages of utilizing the widely-available Lieber-Decarli liquid ethanol diet as well as being minimally invasive. Other methods to overcome the natural aversion of rodents to ethanol consumption such as the Tsukamoto-French intragastric ethanol infusion model are costly and require intensive surgical intervention and upkeep. We also established a role for the antioxidant SAMe as a therapeutic treatment to prevent the development of alcoholic liver fibrosis utilizing our model. These data show that SAMe can diminish oxidative stress through the restoration of reduced glutathione as well as inhibiting, in part, the increase in expression of CYP2E1, a key enzyme in the metabolism of ethanol that has been implicated in generating oxidative stress. 4-HNE, a marker of lipid peroxidation often associated with oxidative stress, was also diminished by SAMe. SAMe treatment also decreased the expression and downstream signaling of a key fibrogenic cytokine, TGF-β. This cytokine can be produced by several cell types in the liver, such as the Kupffer cell and HSCs. SAMe may be exerting effects on both cell types. Further investigation using *in vitro* cell culture may help elucidate this mechanism more clearly.

To examine SAMe as a therapeutic treatment to reverse established fibrosis we established a BDL model of hepatic fibrosis. BDL mimics cholestasis in humans and causes injury through the blocking of free bile flow, resulting in injury to hepatocyte membranes due to the detergent action of hydrophobic bile acids [25]. Inflammation is also considered a key component of cholestasis-mediated fibrosis with neutrophils, Kupffer cells, and lymphocytes all playing a contributing role [29].

Prior to testing the effects of SAMe, we sought to validate our model based on previously reported findings. BDL is reported to result in the accumulation of peri-portal (zone 3) collagen, proliferation of bile duct epithelium, infiltration of inflammatory cells, and mild biliary infarcts [29]. In comparison to the sham-operated animal, there was accumulation of peri-portal collagen beginning with day 7, and increased in days 14 and 21. H&E staining also confirmed the previously reported findings of ductular proliferation and small cell inflammation, with the latter most prevalent at day 7.

We then sought to evaluate the antioxidant SAMe as a treatment for already established fibrosis utilizing our BDL model. Animals subjected to either sham or BDL operations were allowed to recover for 7 days. One week BDL in our pilot as well as previously described in the literature is enough time to begin fibrogenesis. On post-operative day 7 animals received daily injections of either 10 mg/kg SAMe or an equal volume of saline as a vehicle. Treatment continued for 7 days before animals were sacrificed and analyzed.

Because previous investigators have established a link between MMPs and their inhibitors (TIMPs), we sought to investigate the role SAMe administration may play in the expression levels of MMP-2, -13, TIMP-1, and -2 in a BDL model of hepatic fibrosis.

BDL as expected increased MMP-2 and TIMP-1 and -2. SAMe decreased MMP-2 expression, however, it had no influence on TIMP-1 or -2. SAMe administration also had no influence on MMP-13 steady state mRNA levels. The observation that SAMe decreases MMP-2 may contribute to the decrease in injury seen in BDL animals treated with SAMe. MMP-2 is associated with basement membrane degredation, allowing migration of activated HSCs and infiltration of inflammatory cells. By decreasing levels of MMP-2, SAMe might be acting to decrease inflammation to attenuate injury.

Although SAMe treatment of culture-activated HSCs resulted in MMP-13 production *in vitro*, no change in mRNA expression was observed in animals subjected to BDL followed by daily treatment with SAMe. Although this data would suggest SAMe does not increase expression of interstitial collagenase *in vivo*, further experimentation should be performed. Collagenase and gelatinase activity *in vivo* is regulated by the balance of MMP activity and expression of TIMPs. Because MMPs have multiple regulatory "checkpoints" such as cleavage of the pro-MMP to the active form, zymographys should be performed on tissue samples to determine MMP activity. Combining gene expression data with measurement of MMP activity will give a more complete picture of the effects of SAMe on MMP expression as opposed to analysis by Western blot or RT-PCR.

Analysis through Sirius red staining revealed that BDL induces marked proliferation of bile duct epithelium, inflammation, and collagen deposition. Treatment with SAMe significantly decreased the amount of type I collagen secretion. SAMe treatment, however, did not significantly decrease the mRNA expression of α(1)I and α(2)I procollagens. SAMe did, however, decrease the expression of αSMA mRNA.

These results seemingly pattern the results seen with SAMe treatment of culture-activated HSCs; a decrease in type I collagen secretion, decrease in αSMA mRNA expression, but no change in procollagen mRNAs. This suggests that SAMe is a suitable treatment for the resolution of established fibrosis. Furthermore, in established fibrosis SAMe may have similar effects on HSCs *in vivo* as it does on culture-activated HSCs *in vitro*. Therefore we conclude that we developed an appropriate model for examining the treatment with SAMe in a model of established fibrosis. These results may also be appropriate with drawing parallels with observations noted in treating culture-activated HSCs with SAMe.

Future studies to isolate HSCs from our ethanol model of hepatic fibrosis will allow us to characterize the *in vivo* mechanism of SAMe, allowing us to make comparisons to *in vitro* observations. Our ethanol model will also permit the evaluation of other candidate treatments for fibrosis, as well as further investigation the progression of disease.

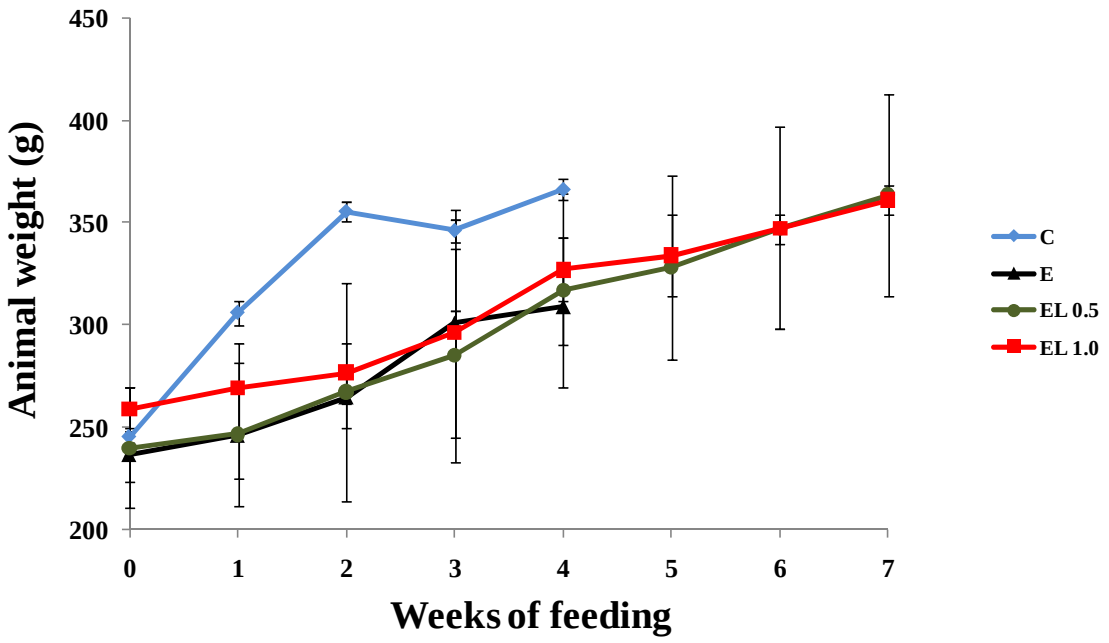

Figure 22. Weekly weights of animals on the 7 week ethanol pilot study. Animals were permitted *ad libitum* access to the Lieber-DeCarli liquid ethanol diet (E) with 36% of the total calories provided by ethanol. Control animals (C) received an isocaloric diet where calories from ethanol were replaced by dextrin-maltose. Two subsets of animals on the ethanol diet received either 0.5 mg/kg LPS i.p. weekly (EL 0.5) or 1.0 mg/kg LPS i.p. weekly (EL 1.0). Animals were weighed weekly throughout the study.

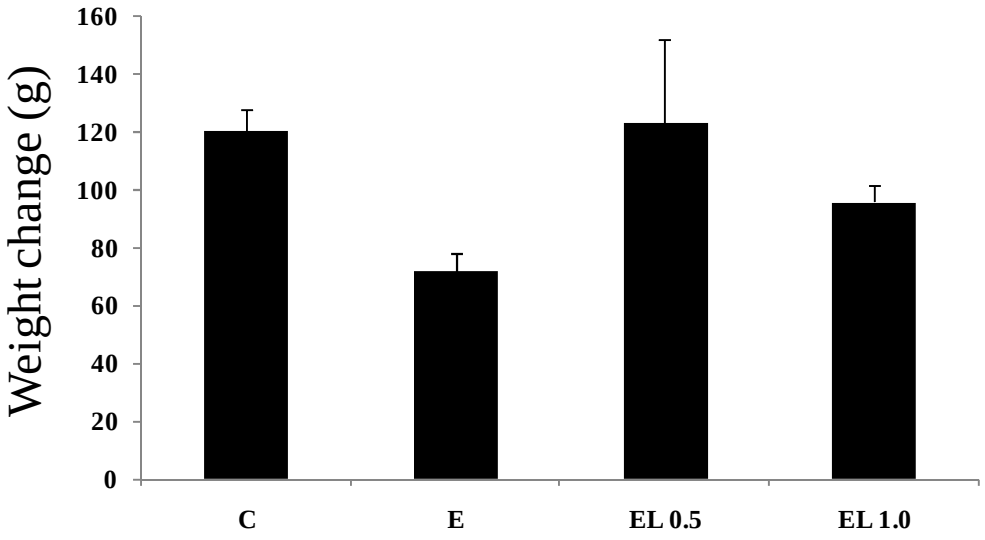

Figure 23. Weight change for animals on the 7 week ethanol pilot study. To compare weight change of animals in the study, the difference in weights from initiation of the study to its conclusion were determined. Animals were permitted *ad libitum* access to the Lieber-DeCarli liquid ethanol diet (E) with 36% of the total calories provided by ethanol. Control animals (C) received an isocaloric diet where calories from ethanol were replaced by dextrin-maltose. Two subsets of animals on the ethanol diet received either 0.5 mg/kg LPS i.p. weekly (EL 0.5) or 1.0 mg/kg LPS i.p. weekly (EL 1.0).

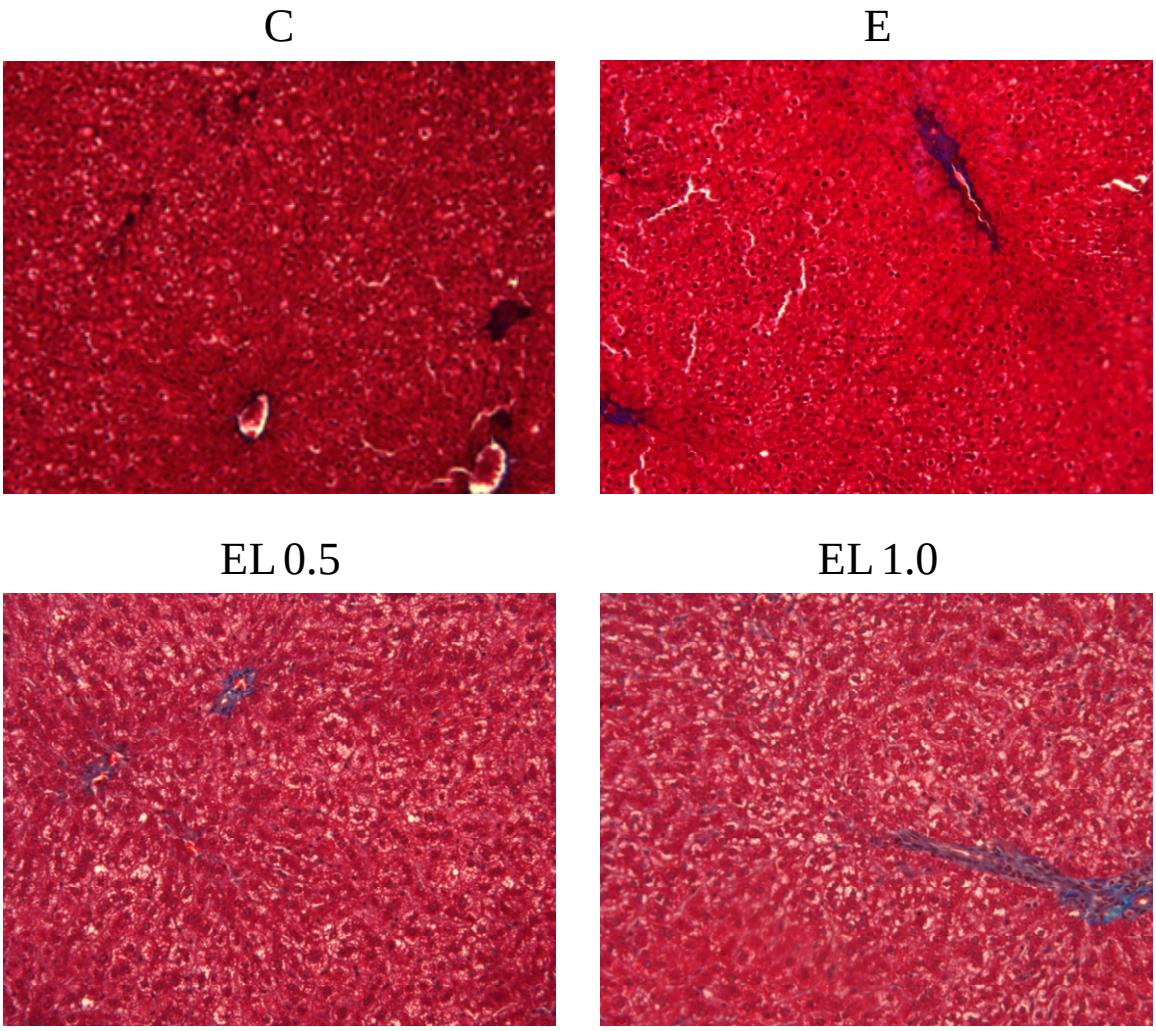

Figure 24. Ethanol liquid diet plus LPS induces early fibrosis. Formalin-fixed samples were embedded in paraffin and sectioned. Masson's trichrome staining was performed on slides and 10X micrographs taken. Sections from control (C) and ethanol (E) animals showed minimal type I collagen deposition. Treatment of ethanol-fed rats with either 0.5 (EL 0.5) or 1.0 (EL 1.0) mg/kg LPS resulted in a mild fibrosis.

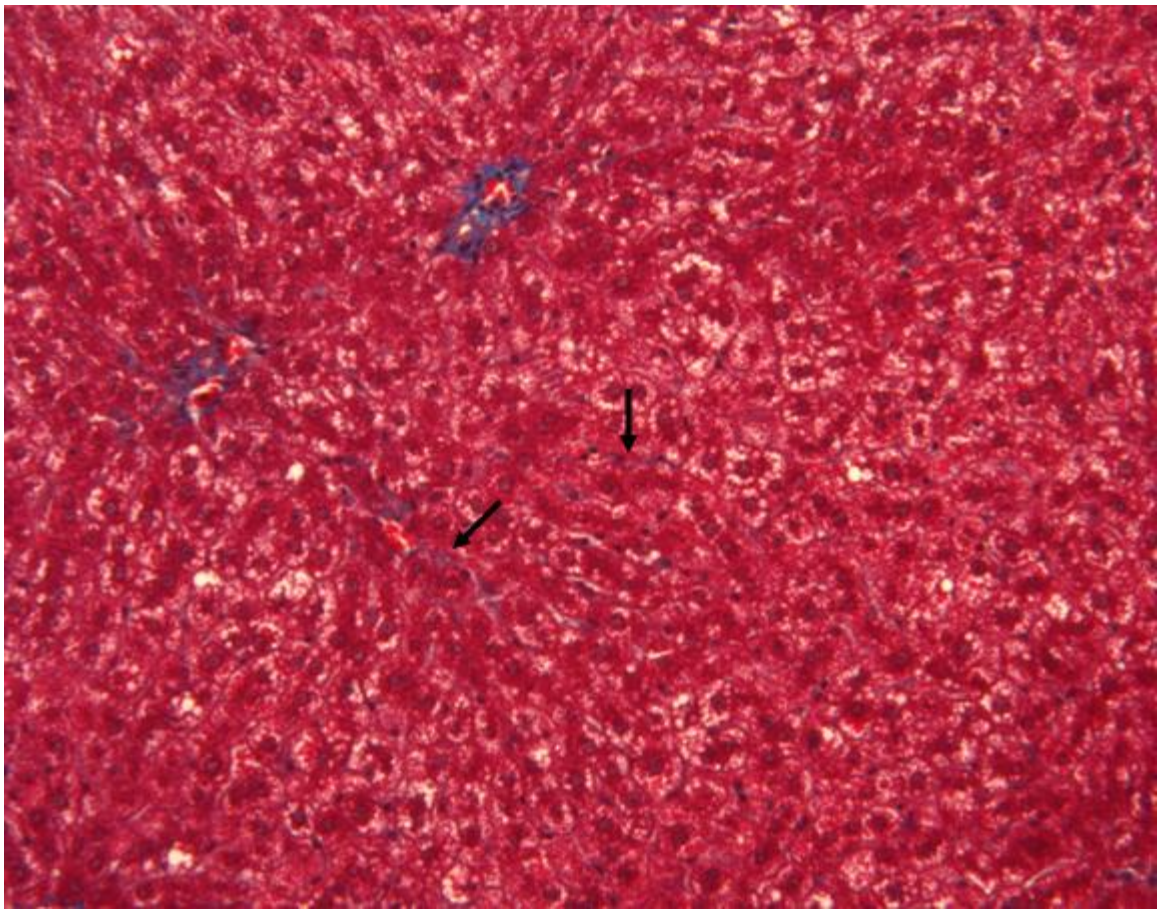

Figure 25. Early fibrosis in animals fed in conjunction with LPS injections occurs peri-sinusoidally. Formalin-fixed samples were embedded in paraffin and sectioned. Masson's trichrome staining collagen was performed on slides and 20X micrographs taken. Large size image is presented to better display peri-sinusoidal collagen staining (arrows) from an animal fed ethanol in conjunction with weekly LPS injections.

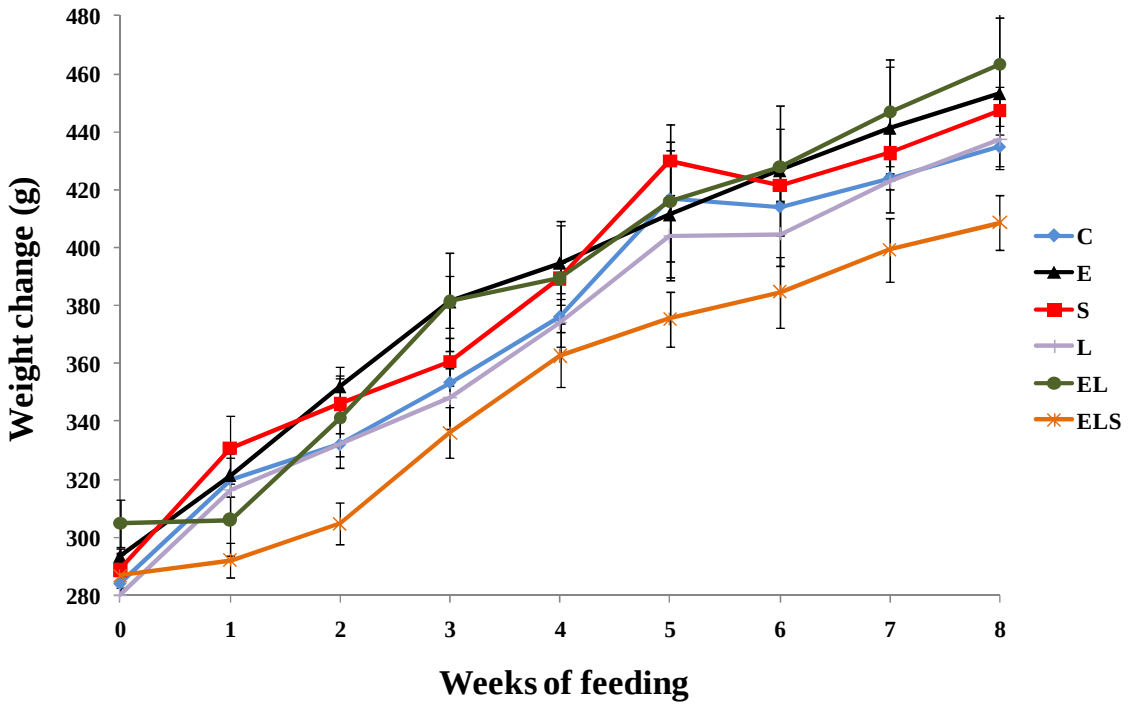

Figure 26. Weekly animal weights from the 10 week ethanol study. Animals were permitted *ad libitum* access to the Lieber-DeCarli liquid ethanol diet (E) with 36% of the total calories provided by ethanol. Control animals (C) received an isocaloric diet where calories from ethanol were replaced by dextrin-maltose. Two subsets of animals on the control diet received either 1.0 mg/kg LPS i.p. semi-weekly (L) or 10.0 mg/kg SAMe chloride i.p. every other day (S). Two subsets of animals on the ethanol diet received either 1.0 mg/kg LPS i.p. semi-weekly (EL) or 1.0 mg/kg LPS i.p. semi-weekly and 10.0 mg/kg SAMe chloride i.p. every other day (ELS). Animals were weighed weekly throughout the study.

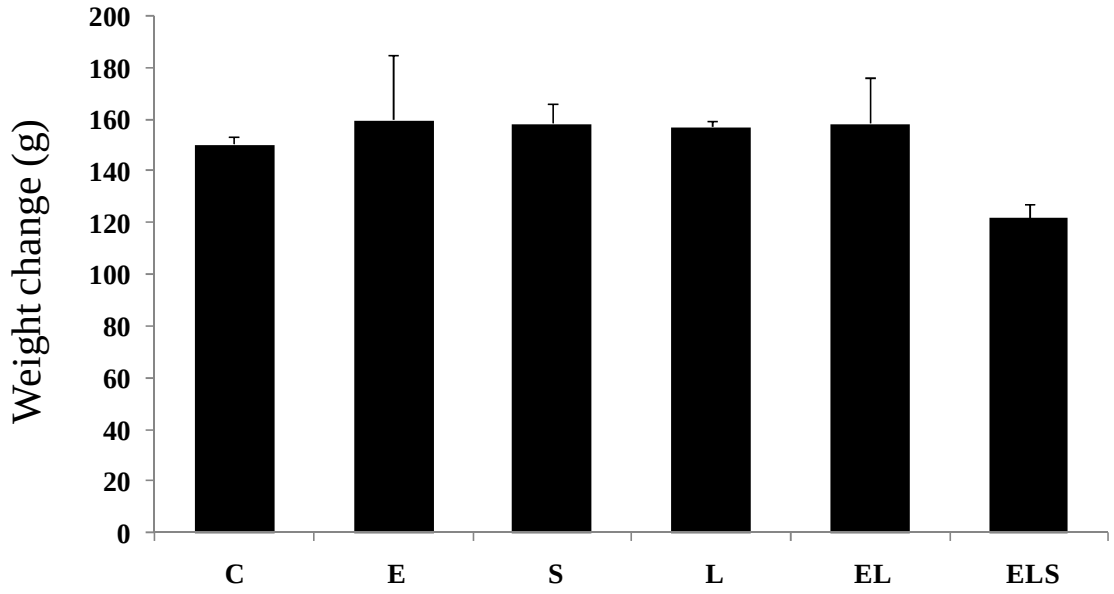

Figure 27. Weight change for animals on the 10 week ethanol study. To compare weight change of animals in the study, the difference in weights from initiation of the study to its conclusion were determined. Animals were permitted *ad libitum* access to the Lieber-DeCarli liquid ethanol diet (E) with 36% of the total calories provided by ethanol. Control animals (C) received an isocaloric diet where calories from ethanol were replaced by dextrin-maltose. Two subsets of animals on the control diet received either 1.0 mg/kg LPS i.p. semi-weekly (L) or 10.0 mg/kg SAMe chloride i.p. every other day (S). Two subsets of animals on the ethanol diet received either 1.0 mg/kg LPS i.p. semi-weekly (EL) or 1.0 mg/kg LPS i.p. semi-weekly and 10.0 mg/kg SAMe chloride i.p. every other day (ELS).

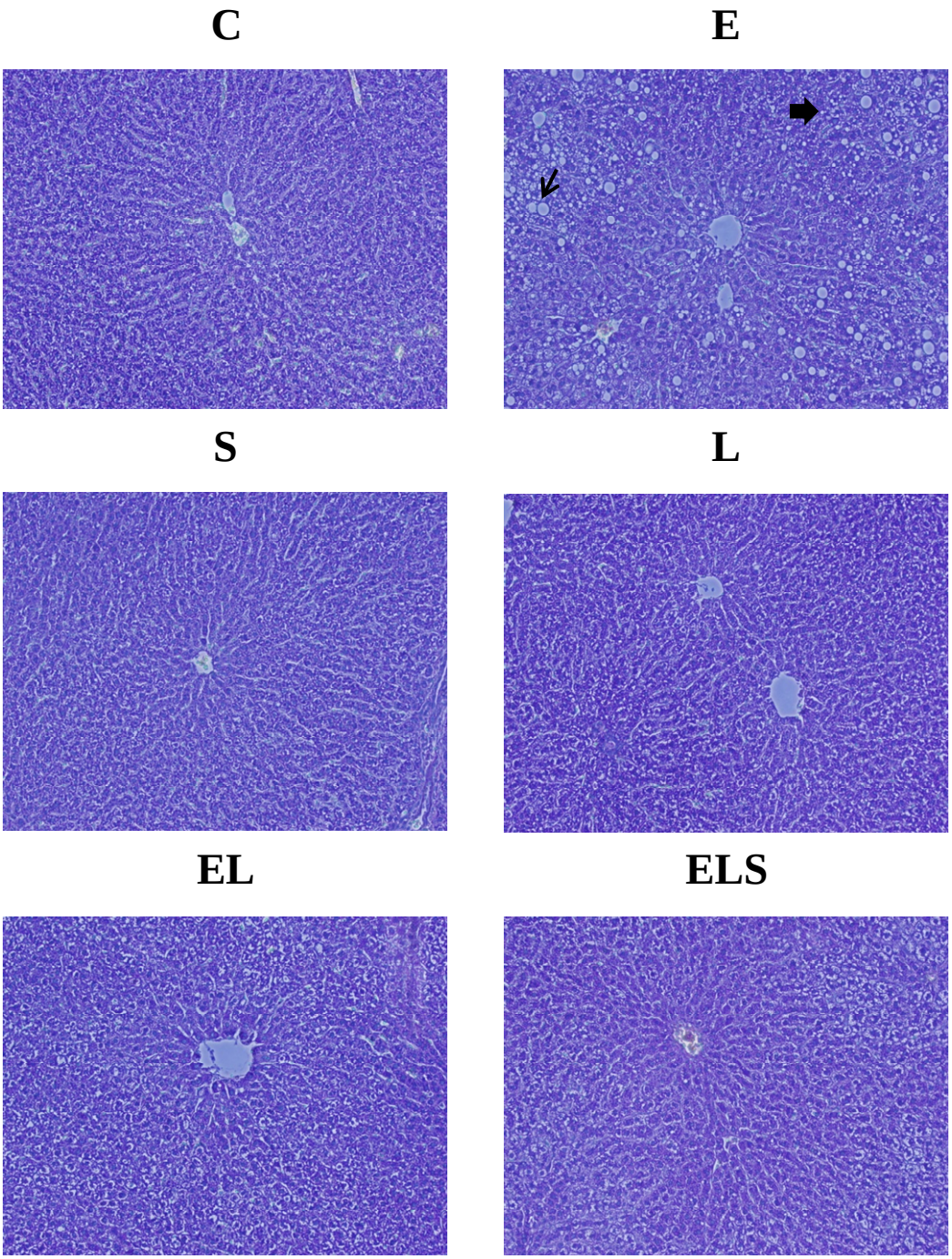

Figure 28. Ethanol results in micro- and macrovesicular steatosis. Formalin-fixed samples were embedded in paraffin and sectioned. H&E staining was performed on slides and 10X micrographs taken. Micro- (narrow arrow) and macrovesicular steatosis (bold arrow) were seen in animals receiving ethanol (E) alone. No inflammation was observed in any group and normal liver architecture was preserved.

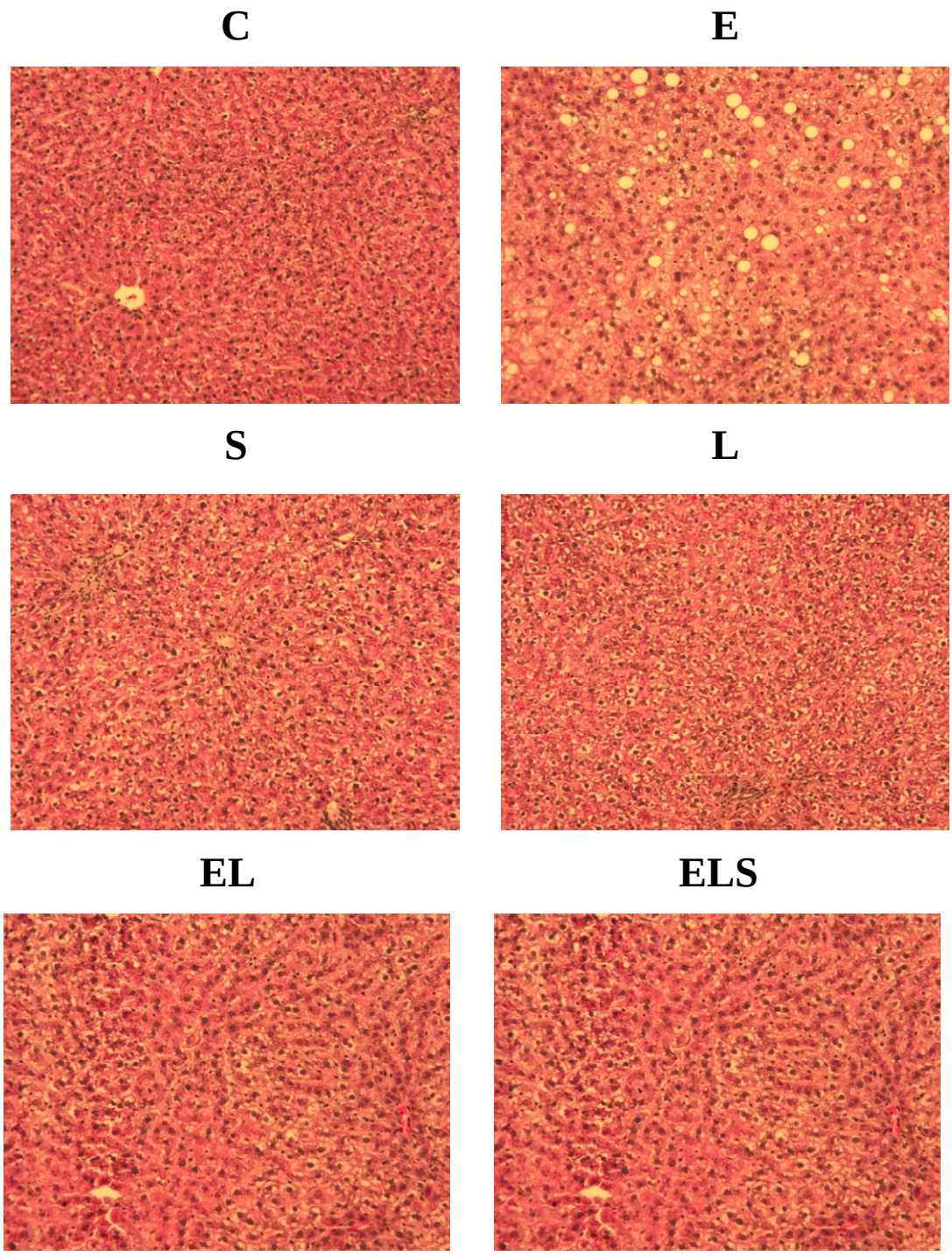

Figure 29. Ethanol and LPS does not lead to hepatic fibrosis. Formalin-fixed samples from 10 week ethanol study animals were embedded in paraffin and sectioned. Sirius red staining for collagen was performed on slides and 10X micrographs taken. No collagen staining was observed in any group, except vessel-associated collagen normally found around portal triads and central veins.

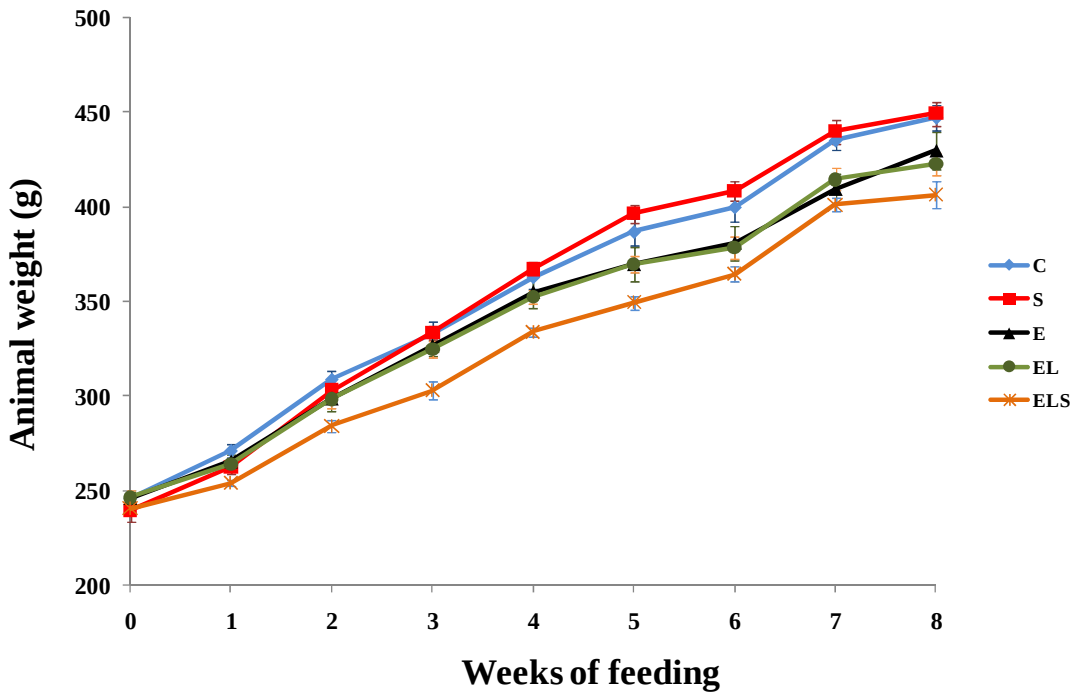

Figure 30. Animal weights for the 8 week ethanol study. Animals were permitted *ad libitum* access to the Lieber-DeCarli liquid ethanol diet (E) with 36% of the total calories provided by ethanol. Control animals (C) received an isocaloric diet where calories from ethanol were replaced by dextrin-maltose. One subset of animals on the control diet received 10.0 mg/kg SAMe toluene-sulfonate i.p. daily (S). Two subsets of animals on the ethanol diet received either 0.5 mg/kg LPS i.p. semi-weekly (EL) or 0.5 mg/kg LPS i.p. semi-weekly and 10.0 mg/kg SAMe toluene-sulfonate i.p. daily (ELS). Animals were weighed weekly throughout the study.

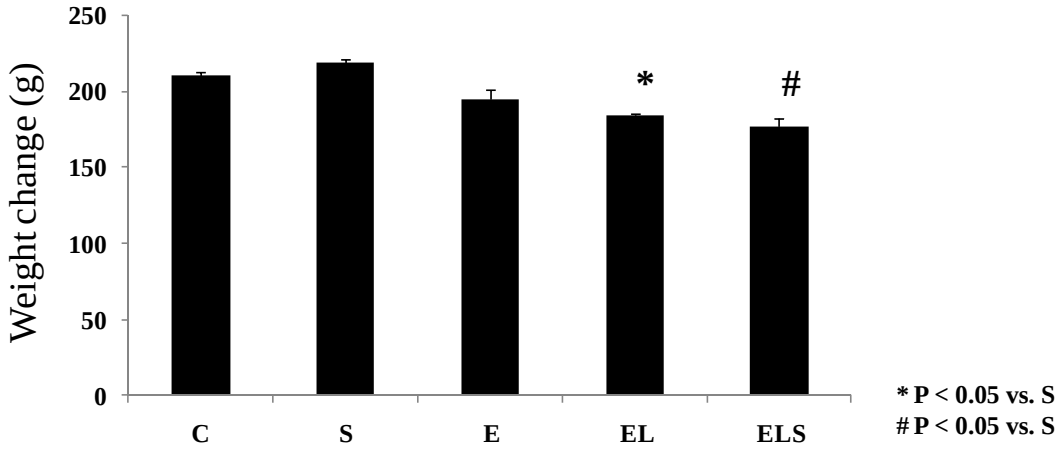

Figure 31. Animal weight change during 8 week ethanol study. Weight change comparison for each animal group in the study. Animals were permitted *ad libitum* access to the Lieber-DeCarli liquid ethanol diet (E) with 36% of the total calories provided by ethanol. Control animals (C) received an isocaloric diet where calories from ethanol were replaced by dextrin-maltose. One subset of animals on the control diet received 10.0 mg/kg SAMe toluene-sulfonate i.p. daily (S). Two subsets of animals on the ethanol diet received either 0.5 mg/kg LPS i.p. semi-weekly (EL) or 0.5 mg/kg LPS i.p. semi-weekly and 10.0 mg/kg SAMe toluene-sulfonate i.p. daily (ELS). Animals were weighed weekly throughout the study.

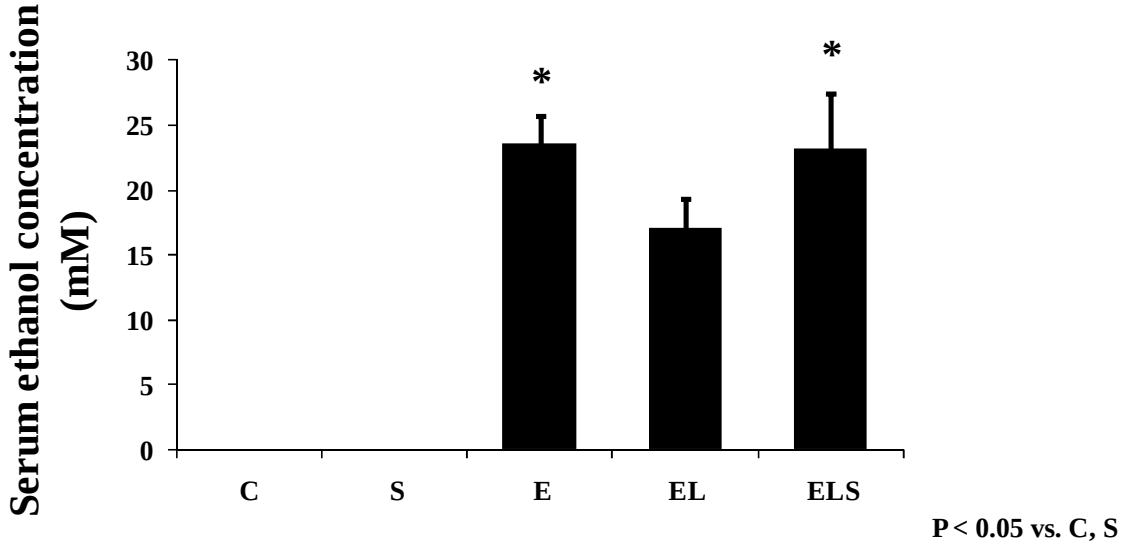

Figure 32. Serum ethanol concentrations from 8 week ethanol study. Animals on control (C) and a subset of control animals receiving 10 mg/kg SAMe injections daily had undetectable levels of ethanol. Animals on diets containing ethanol alone (E), ethanol plus LPS injected semi-weekly (EL), and animals fed ethanol in combination with semi-weekly LPS injections and daily SAMe injections (ELS) all had detectable levels of serum ethanol. (Karaa and Thompson et al. 2008)

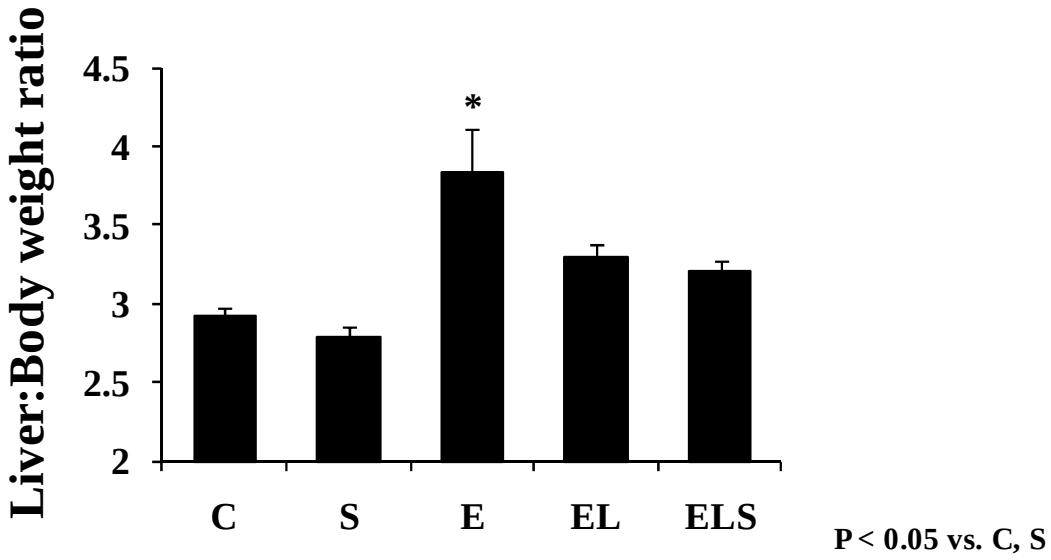

Figure 33. Liver:body weight ratio from 8 week ethanol study. Animals fed control diets (C) or control diets coupled with daily injections of SAMe had similar liver:body weight ratios. Animals receiving ethanol alone (E) had significantly higher liver:body weight ratios. Animals receiving ethanol and semi-weekly LPS injections (EL) as well as the combination of ethanol, semi-weekly LPS, and daily SAMe (ELS) had elevated liver:body weight ratios; however, these were not significantly increased. (Karaa and Thompson et al. 2008)

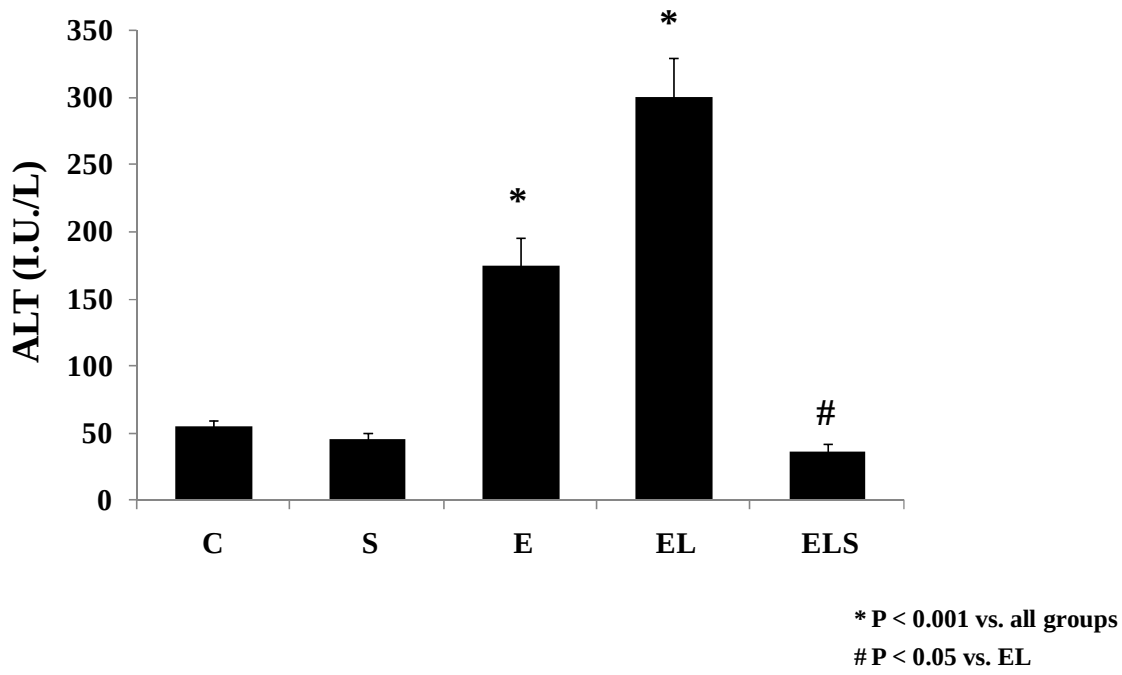

Figure 34. SAMe decreases cellular injury in an animal model of alcoholic liver fibrosis. Plasma was collected and assayed for ALT, a marker of liver injury. Control animals (C, S) had normal levels of ALT. Ethanol administration (E) significantly increased liver injury, which was further increased with semi-weekly LPS injection (EL). SAMe treatment reduced cellular injury to normal levels (ELS). (Karaa and Thompson et al. 2008)

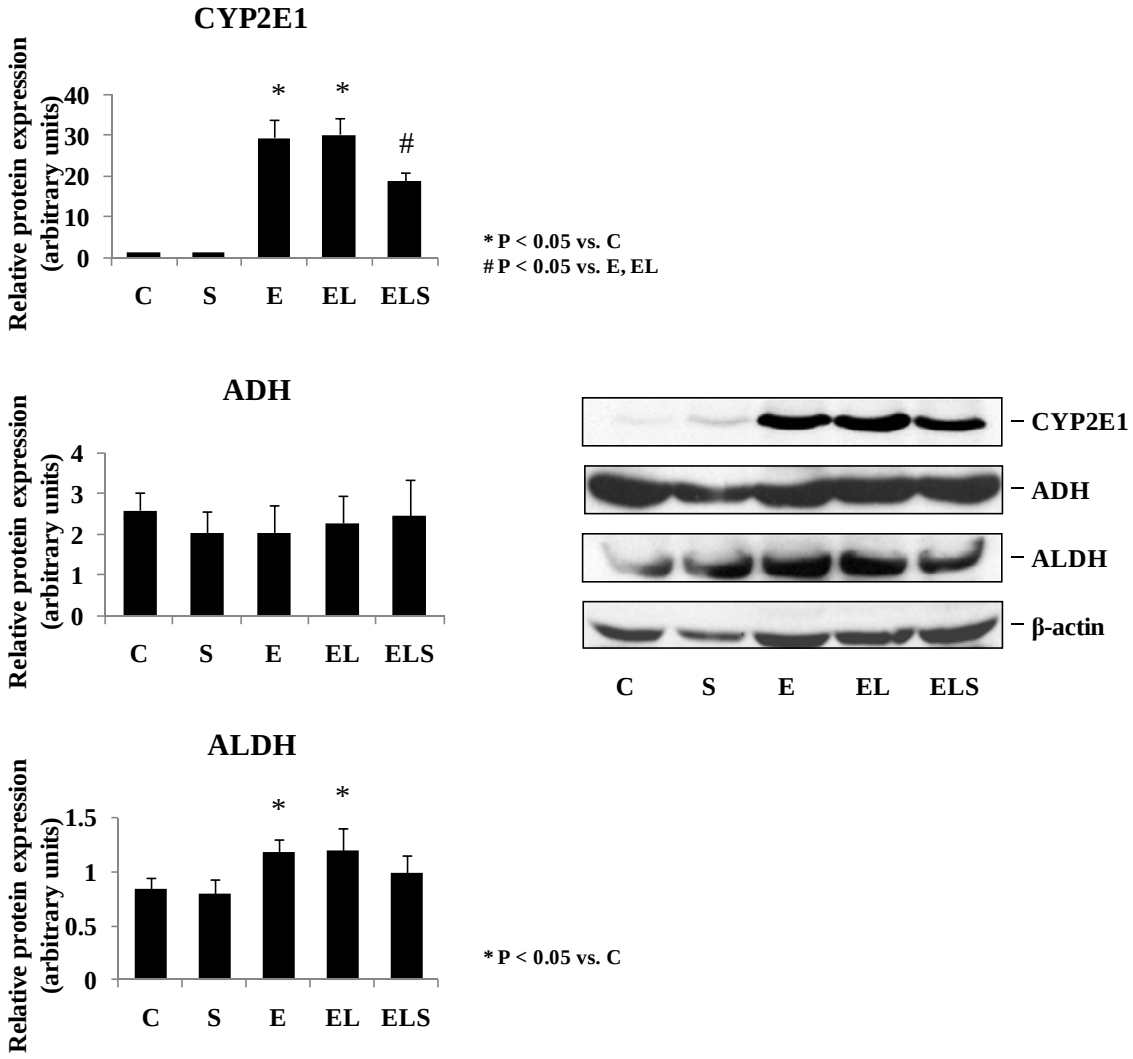

Figure 35. Expression of key enzymes involved in the metabolism of ethanol. Protein expression of CYP2E1, ADH, and ALDH were determined from whole liver. Ethanol significantly increased CYP2E1 in the livers of ethanol-fed (E) and ethanol-fed plus semi-weekly LPS (EL) compared to control animals (C) and animals receiving control diets plus SAMe (S). SAMe administration (ELS) significantly decreased CYP2E1 expression. Levels of ADH were unchanged across all groups. ALDH levels were significantly increased in E and EL. SAMe decreased ALDH compared to E and EL, but this was not significant. (Karaa and Thompson et al. 2008)

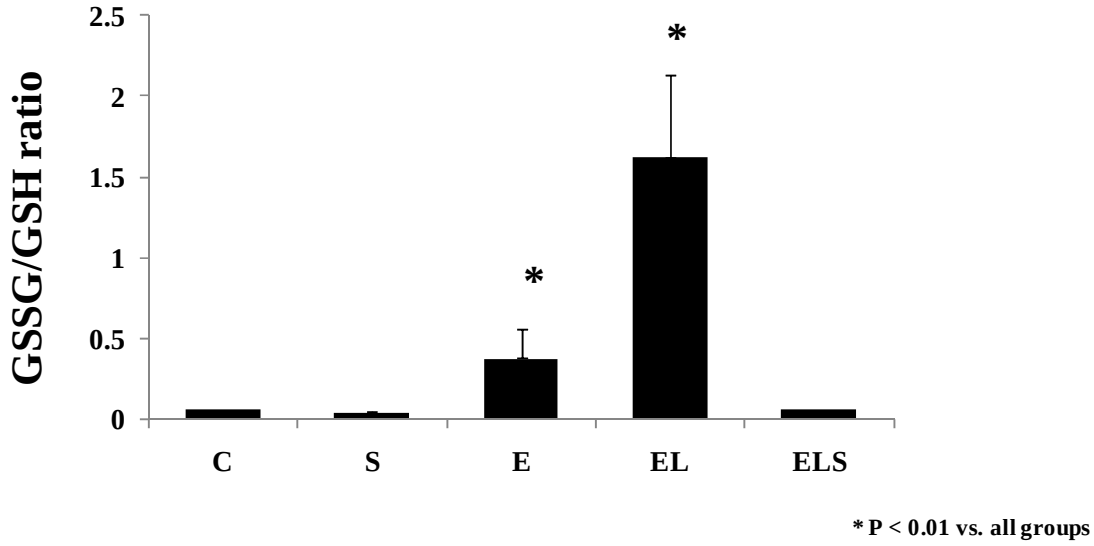

Figure 36. GSSG/GSH is reduced with SAMe administration. The ratio of oxidized glutathione (GSSG) to reduced glutathione (GSH) was determined from whole livers. Control animals and control animals treated with SAMe (C, S) had low GSSG/GSH ratios. Ethanol feeding (E) increased this ratio, with a further increase due to semi-weekly LPS injections (EL). Treatment with daily SAMe (ELS) significantly reduced the GSSG/GSH ratio. (Karaa and Thompson et al. 2008)

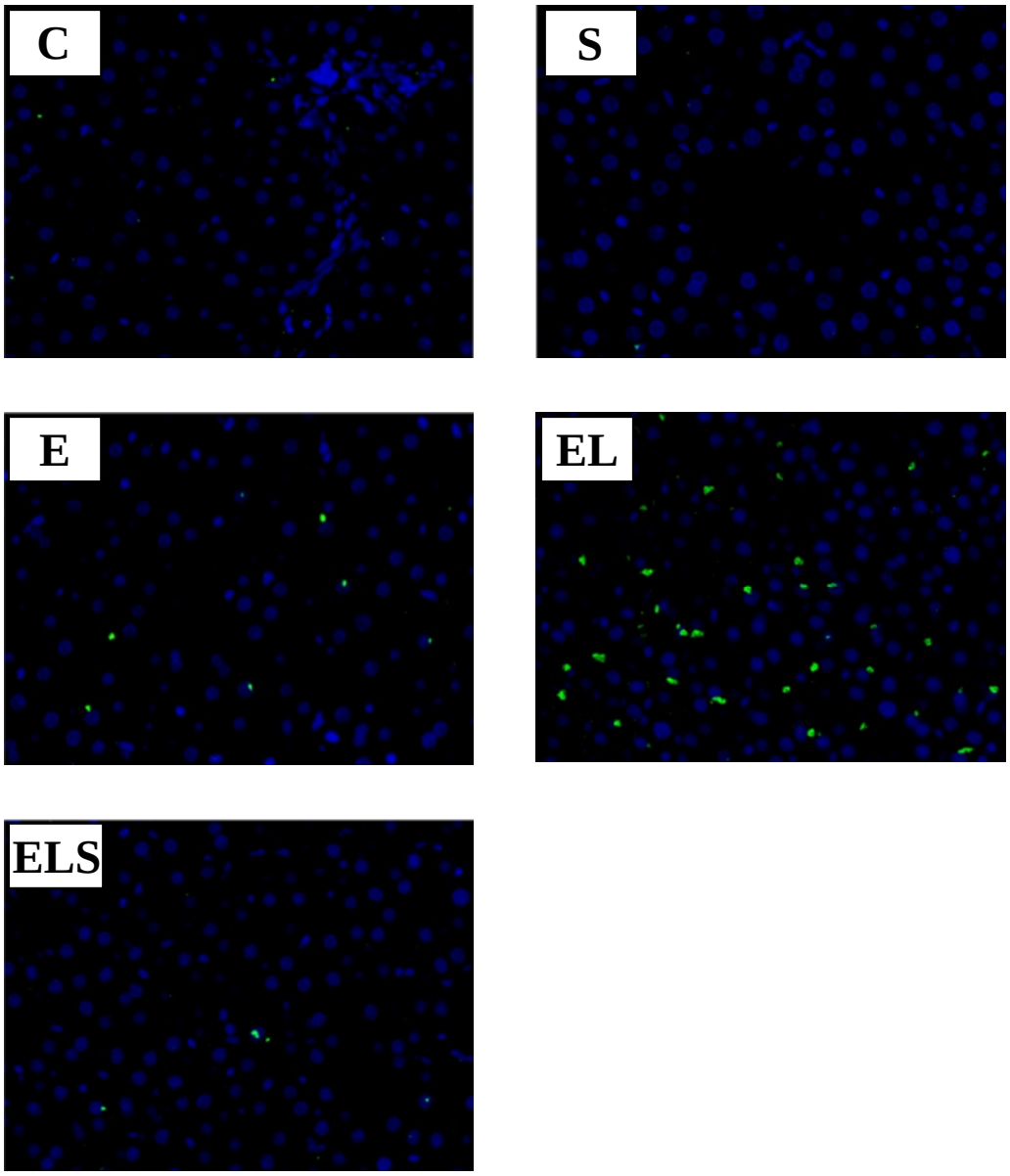

Figure 37. SAMe decreases lipid peroxidation in an alcoholic model of fibrosis. Formalin-fixed samples were embedded in paraffin and sectioned. Anti-4-HNE staining (green) was performed on slides and 20X micrographs taken. Minimal staining for 4-HNE was observed with animals on control diet (C) and control diet with daily injection of 10 mg/kg SAMe (S). Ethanol (E) feeding resulted in a mild increase in 4-HNE staining, which was further increased by semi-weekly LPS administration (EL). Treatment with SAMe (ELS) attenuated this effect. DAPI (blue) was used to counterstain nuclei. (Karaa and Thompson et al. 2008)

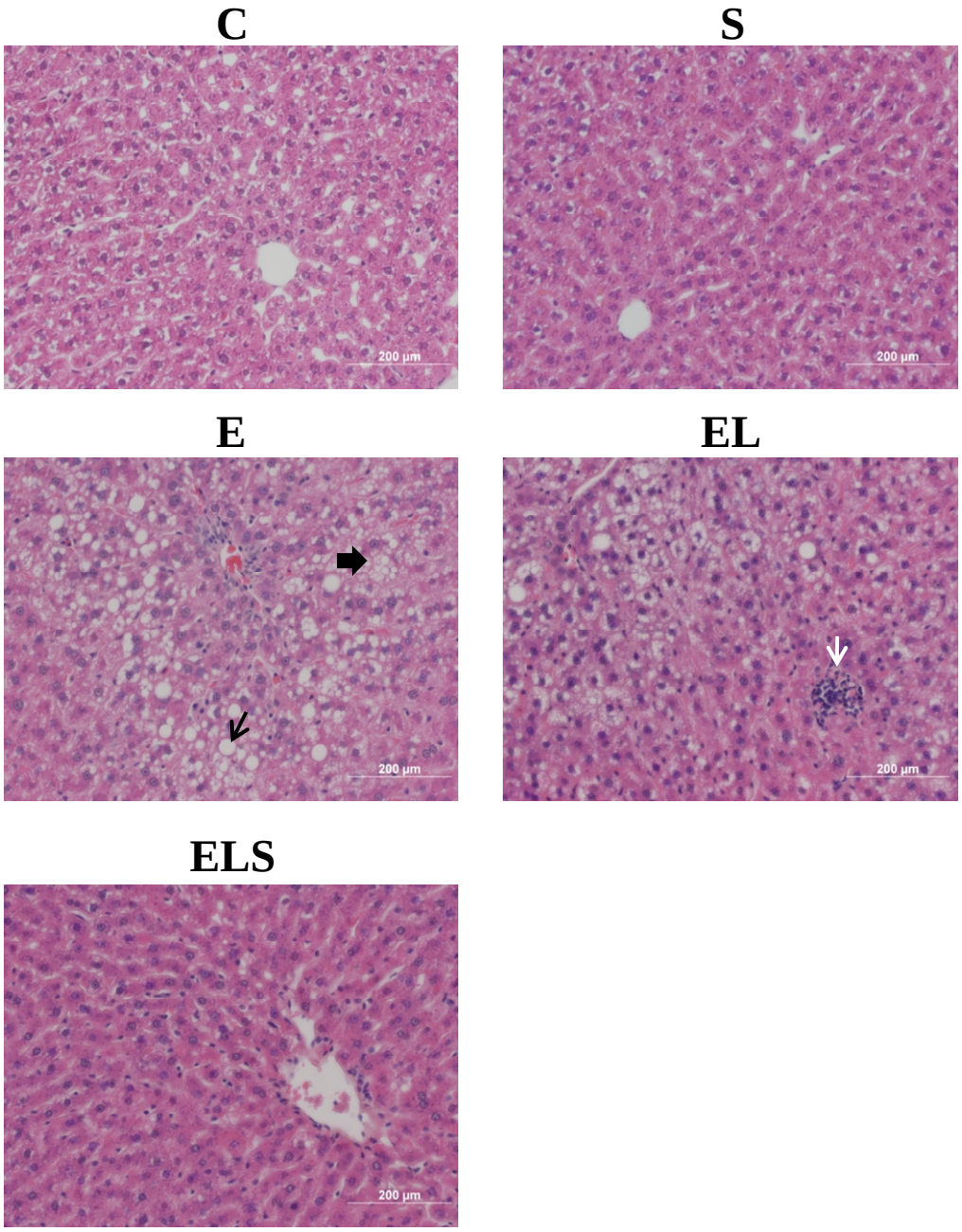

Figure 38. SAMe restores normal histology in animals treated with ethanol and LPS. Formalin-fixed samples were embedded in paraffin and sectioned. H&E staining was performed on slides and 20X micrographs taken. Normal histology was observed with animals on control diet (C) and control diet with daily injection of 10 mg/kg SAMe (S). Micro- (black thin arrow) and macrovesicular (black bold arrow) steatosis was seen in animals receiving ethanol alone (E). Steatosis was reduced in animals on ethanol diets receiving LPS injections (EL), however, areas of focal infiltration of small cells (white arrow) were observed. SAMe administration reversed both steatosis and inflammation in animals receiving ethanol and LPS injections (ELS).

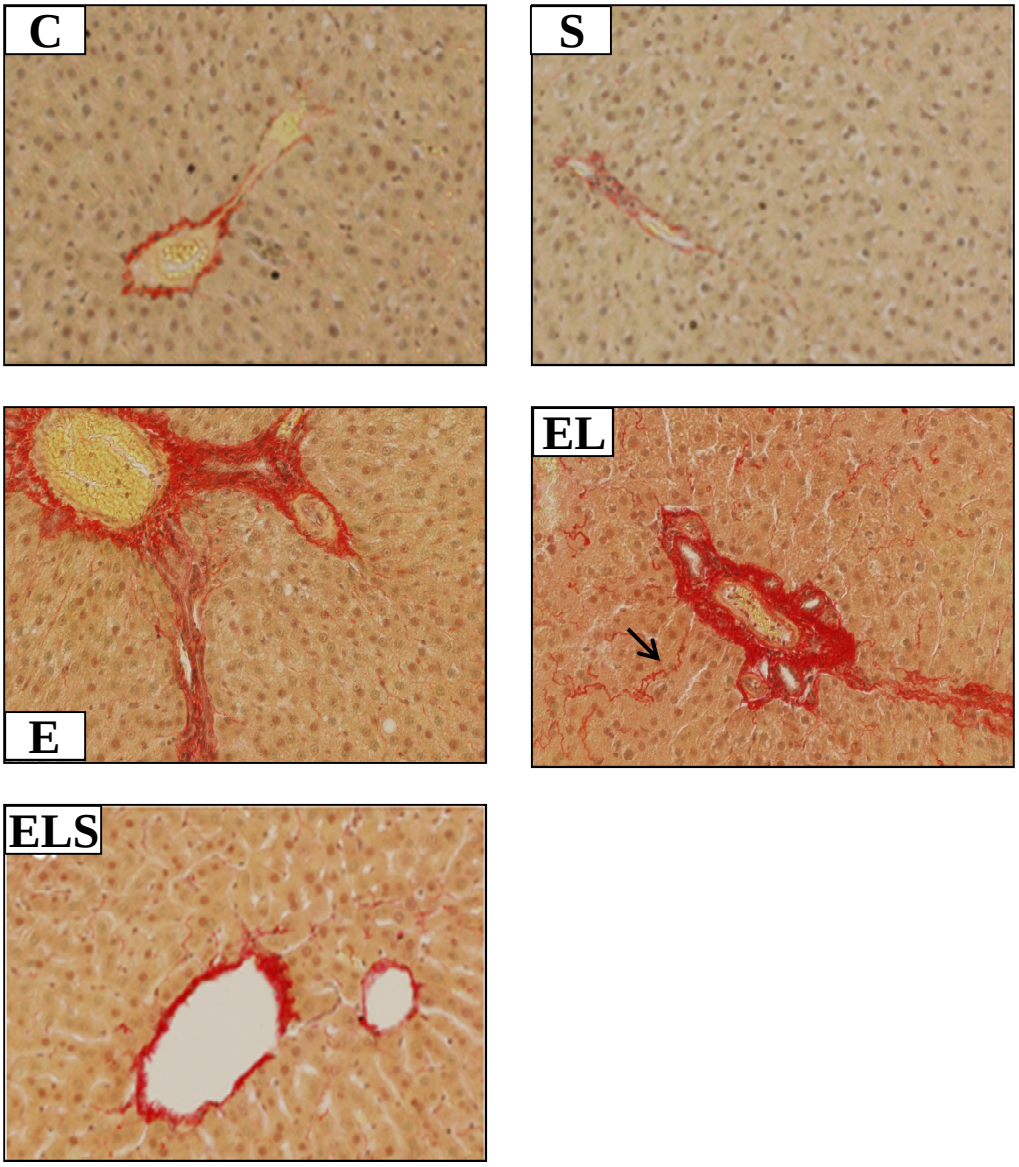

Figure 39. 8 week ethanol liquid diet plus LPS induces fibrosis. Formalin-fixed samples from 8 week ethanol study animals were embedded in paraffin and sectioned. Sirius red staining for collagen was performed on slides and 20X micrographs taken. Animals from control (C) and control plus SAMe (S) showed minimal collagen staining. Ethanol feeding (E) resulted in an increase in perivenular collagen. Semi-weekly injections of 0.5 mg/kg LPS (EL) led to perisinusoidal collagen staining as well as increased perivenualar collagen. Treatment with 10 mg/kg of SAMe (ELS) daily inhibited this effect. (Karaa and Thompson et al. 2008)

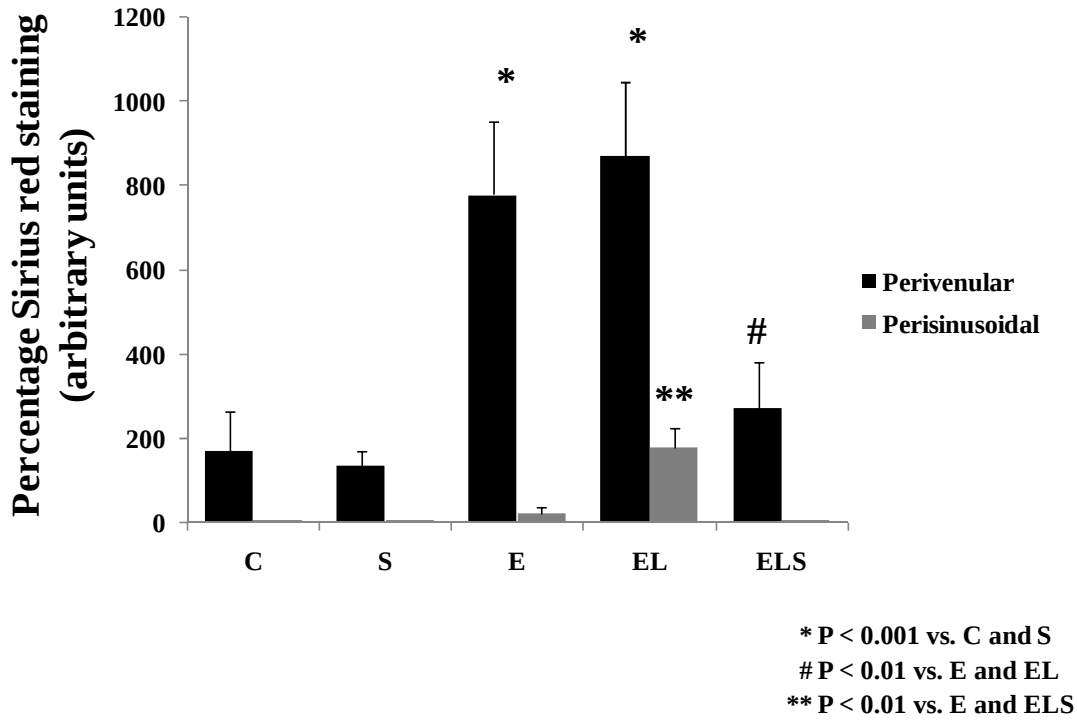

Figure 40. SAMe attenuates collagen deposition in ethanol fed animals challenged with LPS. Collagen content was quantitated by Sirius red staining. Control (C) animals and control animals injected with SAMe (S) showed low collagen staining. Ethanol treatment (E) resulted in a significant increase in perivenular collagen staining; however, LPS administration did result in an increase (EL). SAMe administration significantly diminished collagen staining (ELS). Analysis of perisinusoidal collagen staining revealed similar levels across all groups except LPS-treated animals. This increase was again abolished by SAMe. (Karaa and Thompson et al. 2008)

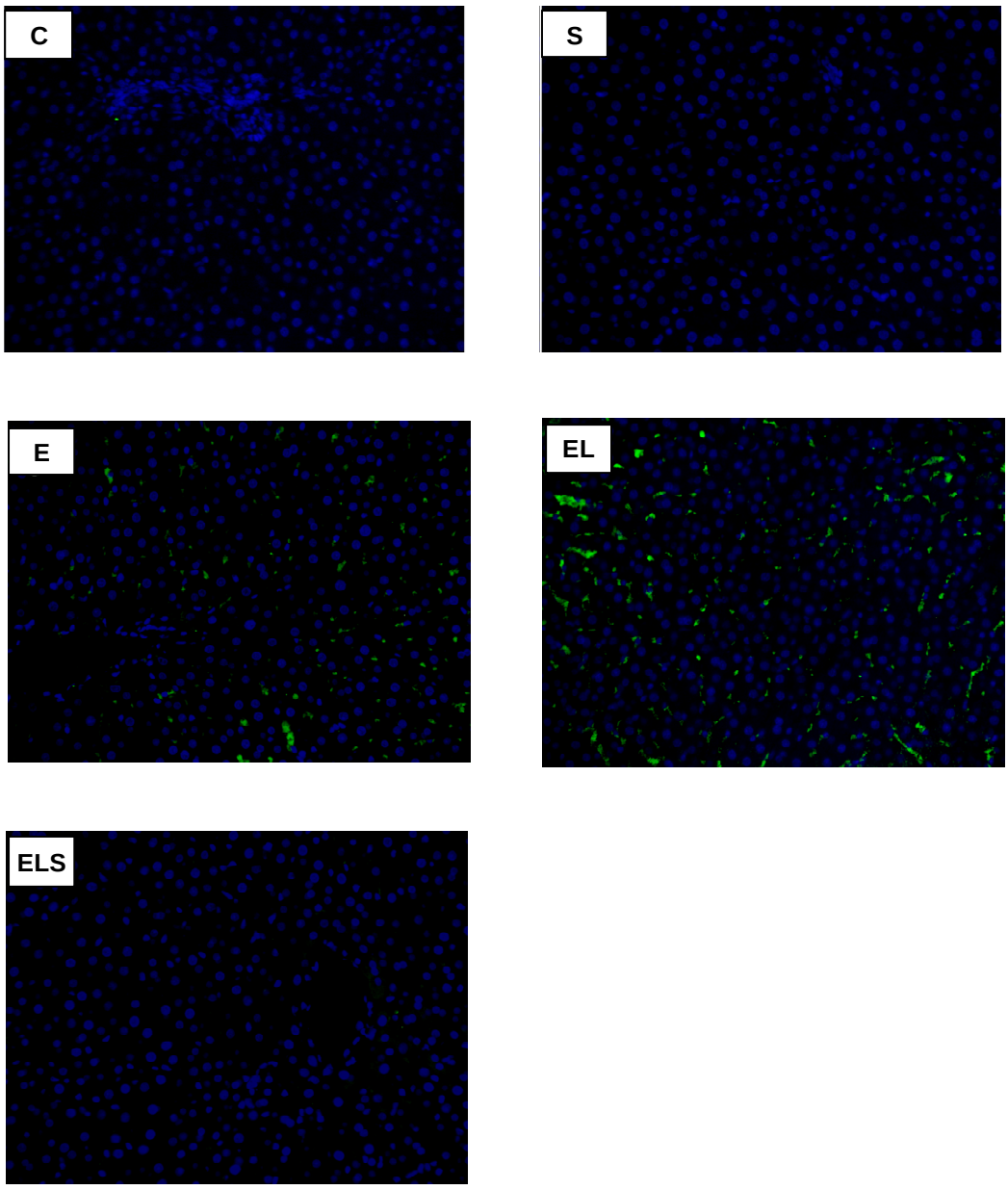

Figure 41. SAMe decreases polymorphonuclear cell infiltration in an ethanol model of hepatic fibrosis. Formalin-fixed samples were embedded in paraffin and sectioned. Anti-PMN staining (green) was performed on slides and 20X micrographs taken. Minimal infiltration of PMN was observed with animals on control diet (C) and control diet with daily injection of 10 mg/kg SAMe (S). Ethanol (E) feeding resulted in extensive perivenual and intrasinusoidal infiltration, which was increased by semi-weekly LPS administration (EL). Treatment with SAMe (ELS) abolished this effect. DAPI (blue) was used to counterstain nuclei. (Karaa and Thompson et al. 2008)

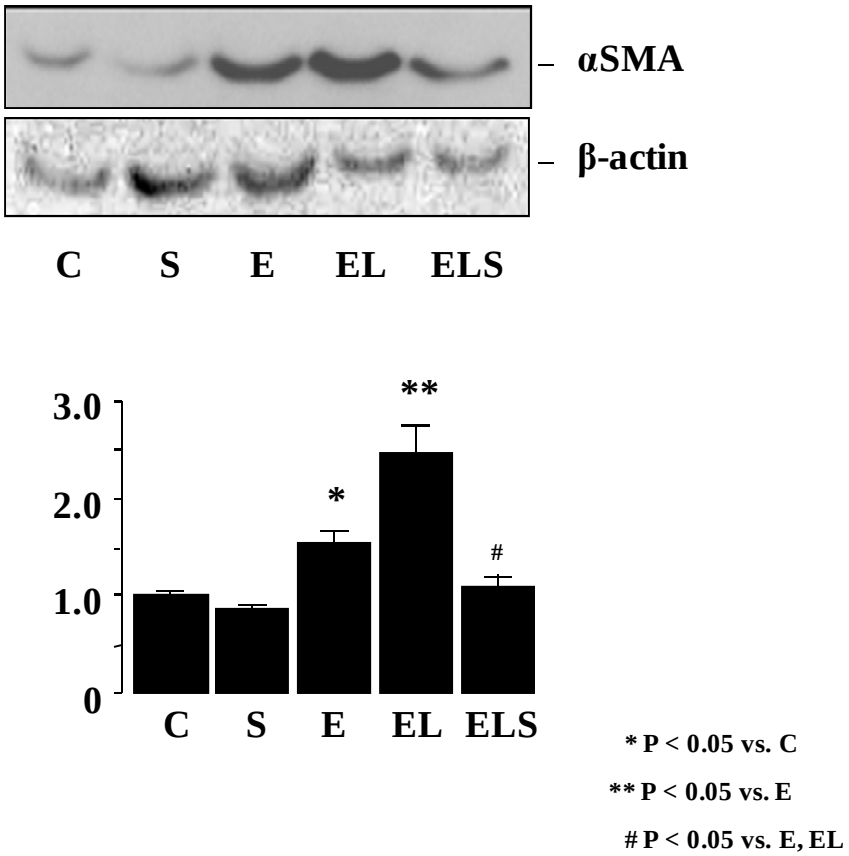

Figure 42. Effect of SAMe on activation of HSCs in livers from an animal model of alcoholic liver fibrosis. Whole tissue was analyzed by Western blot to determine αSMA expression as a marker for activation of HSCs. Ethanol feeding resulted in a signficant activation of HSCs (E), which was enhanced by treatment with LPS (EL). SAMe administration abrogated this effect (ELS). (Karaa and Thompson et al. 2008)

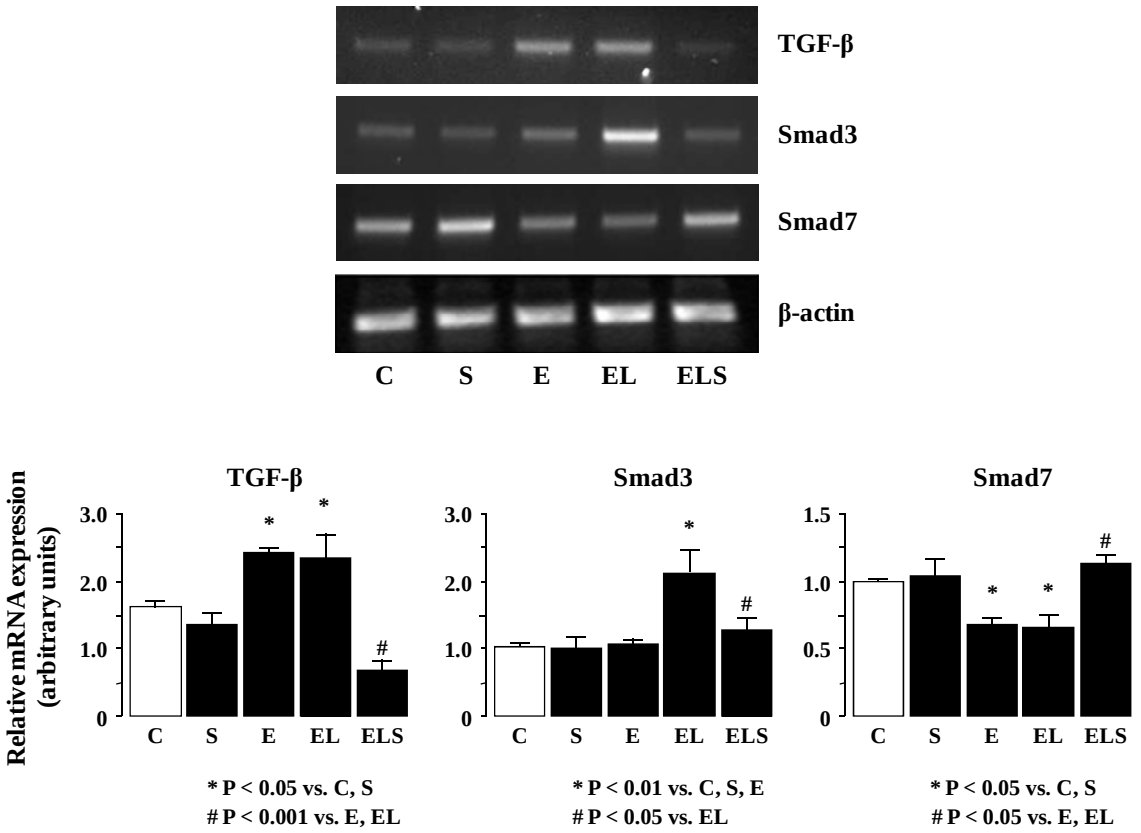

Figure 43. TGF-β signaling in an ethanol model of fibrosis. mRNA expression of members of the TGF-β signaling pathway in whole liver. Ethanol treatment alone (E) and combined with LPS injections (EL) resulted in a significant increase in TGF-β expression compared to control animals (C) and control animals receiving SAMe injections (S). Treatment with SAMe (ELS) significantly reduced the expression of TGF-β in animals fed ethanol with semi-weekly injections of LPS. Smad3 expression was unchanged in C, S, and E animals, however was elevated in EL animals. This effect was significantly inhibited by SAMe (ELS) treatment. Smad7 expression was significantly decreased in E and EL animals, however, SAMe treatment (ELS) restored Smad7 expression. (Karaa and Thompson et al. 2008)

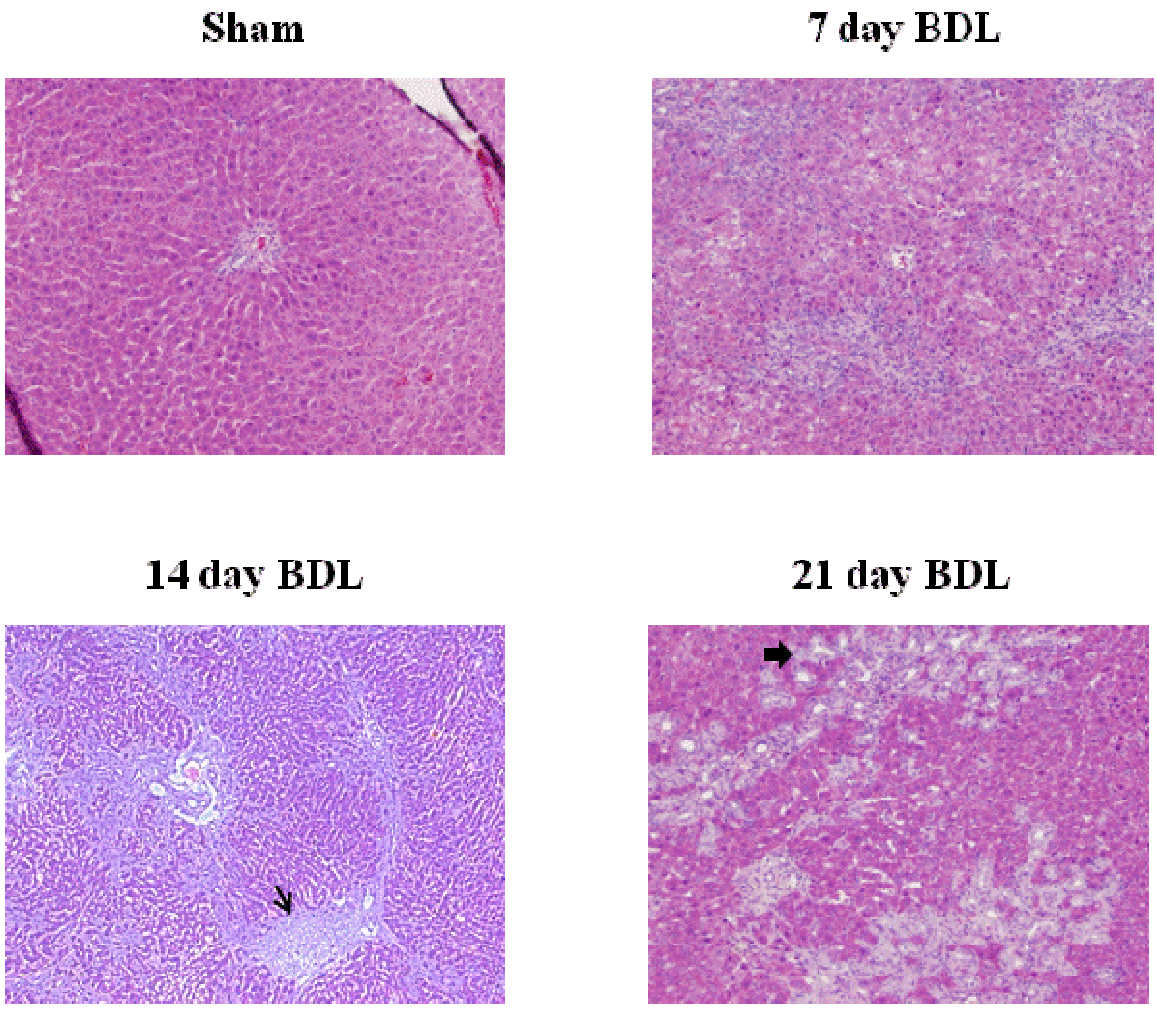

Figure 44. BDL induces liver damage and disrupts the normal hepatic architecture. Formalin-fixed samples were embedded in paraffin and sectioned. H&E staining was performed on slides and 10X micrographs taken. Sham sections showed normal architecture and no inflammation. Sections from BDL animals showed infiltration of small cells near portal triads (all time points, wide arrows) and proliferation of bile duct epithelium (predominantly at days 14 and 21). Areas of focal necrosis were also seen (all time points, narrow areas).

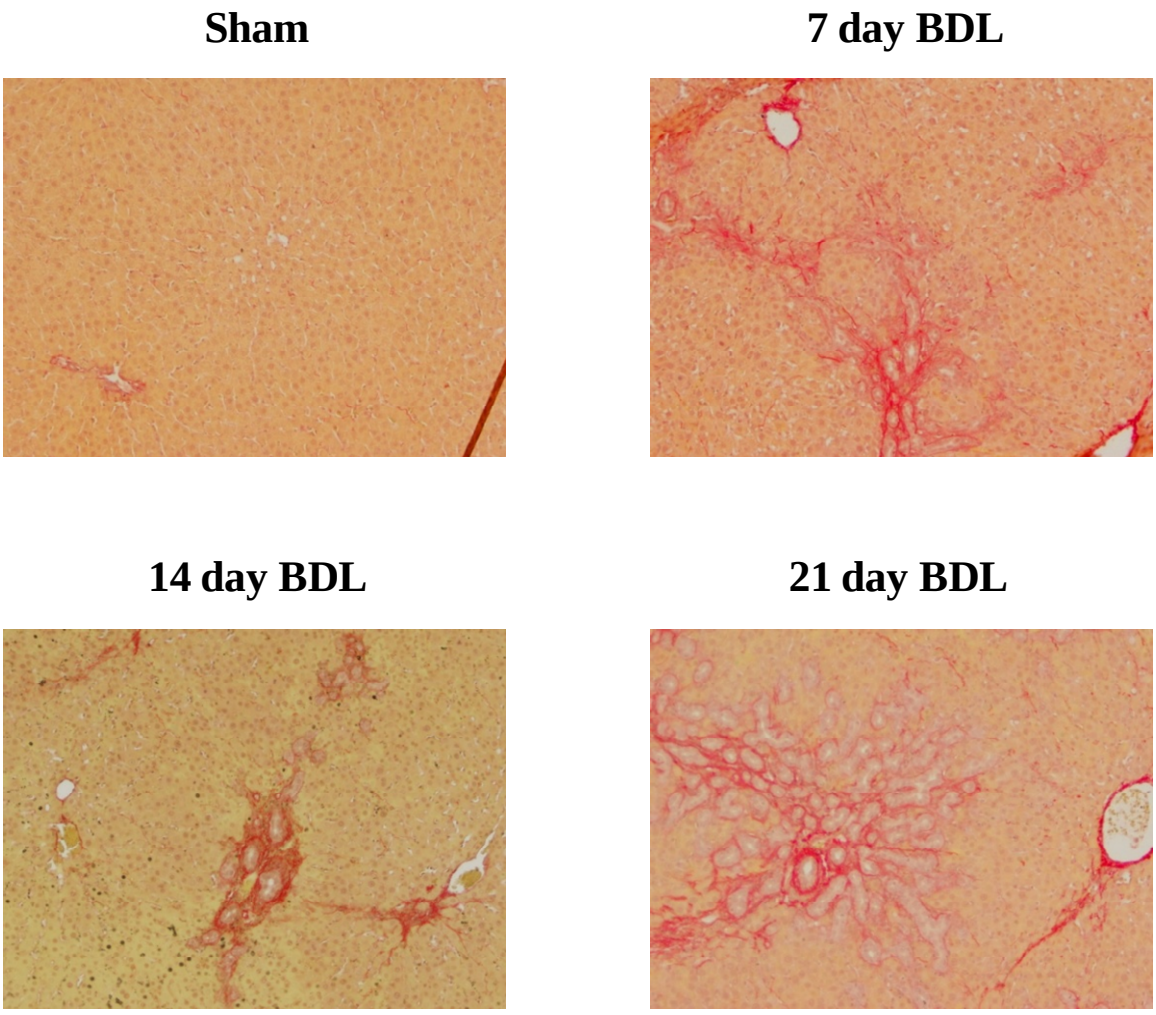

Figure 45. BDL increases type I collagen. Formalin-fixed samples were embedded in paraffin and sectioned. Sirius red staining was performed on slides and 10X micrographs taken. Sham sections showed minimal type I collagen deposition. Sections from BDL animals showed fibrosis beginning at day 7 and continuing at days 14 and 21. The majority of type I collagen accumulation occurred in zone 1 near proliferating bile duct epithelium. Some branching fibrosis appeared to occur at day 21.

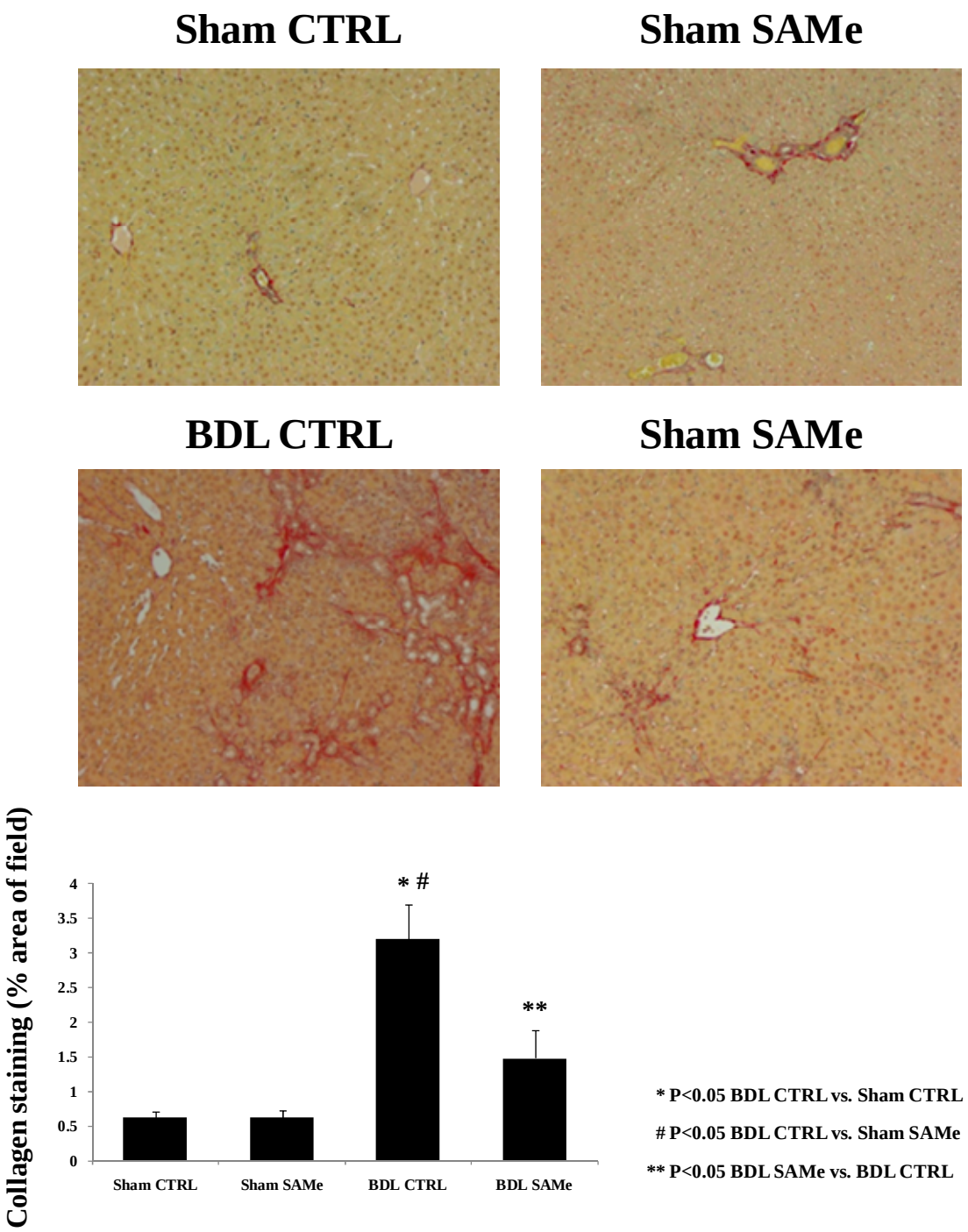

Figure 46. SAMe attenuates hepatic fibrosis in BDL rats. Sham or BDL surgery was performed on male Sprague-Dawley rats. At post-operative day 7 animals were treated either with vehicle (CTRL) or 10 mg/kg SAMe daily for 7 days. Sirius red staining was performed to quantitate type I collagen accumulation.

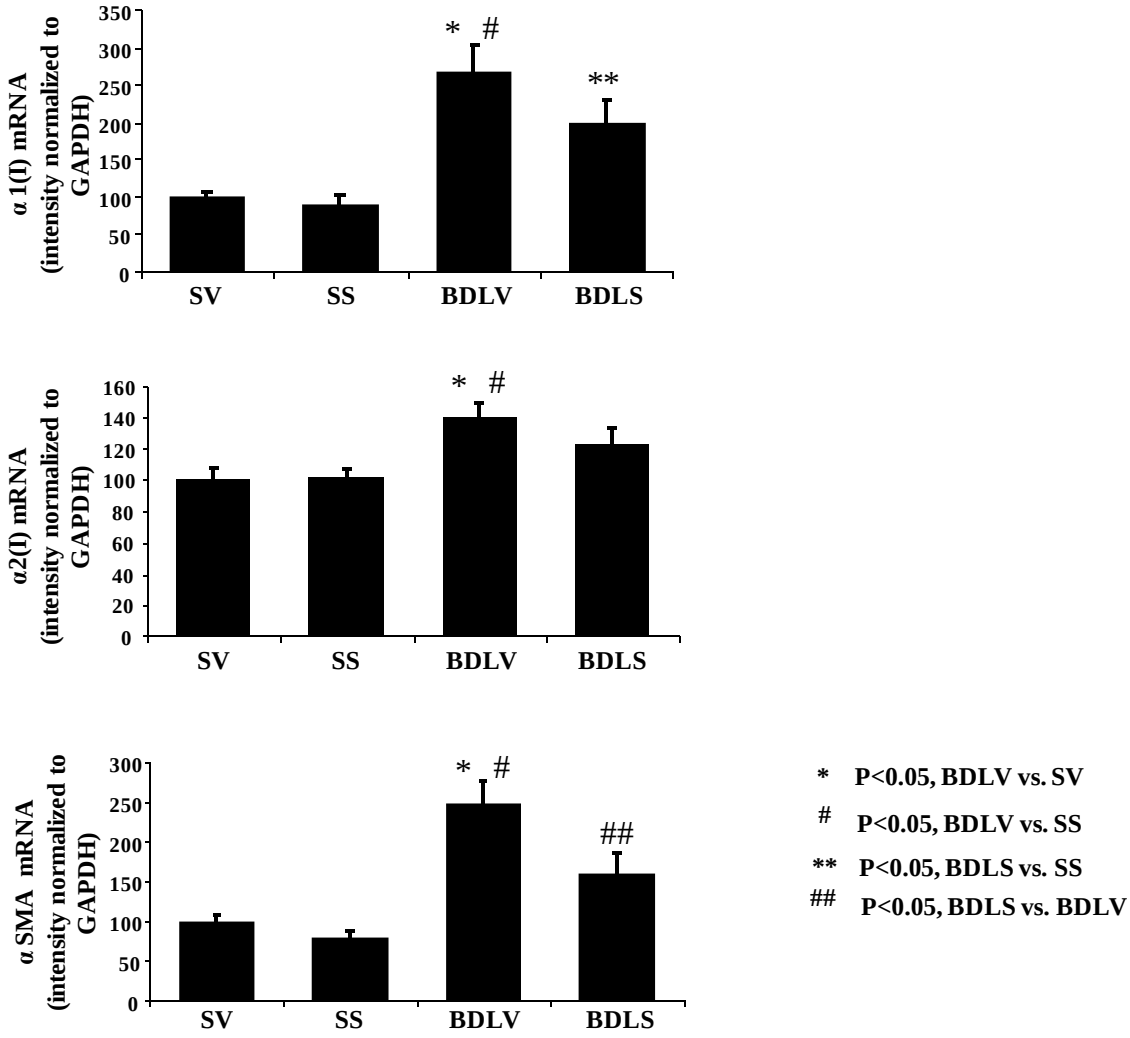

Figure 47. SAMe decreases procollagen and αSMA mRNA expression in BDL rats. RT-PCR on total RNA reversed transcribed from whole liver revealed a significant increase in the messages of α(1)I and α(2)I procollagen mRNAs, and αSMA in animals subjected to BDL with vehicle treatment. Administration of daily SAMe starting on post-operative day 7 of BDL animals (BDLS) resulted in a significant decrease in αSMA levels, but not α(1)I or α(2)I procollagen mRNA. Sham vehicle (SV), Sham SAMe (SS), BDL vehicle (BDLV).

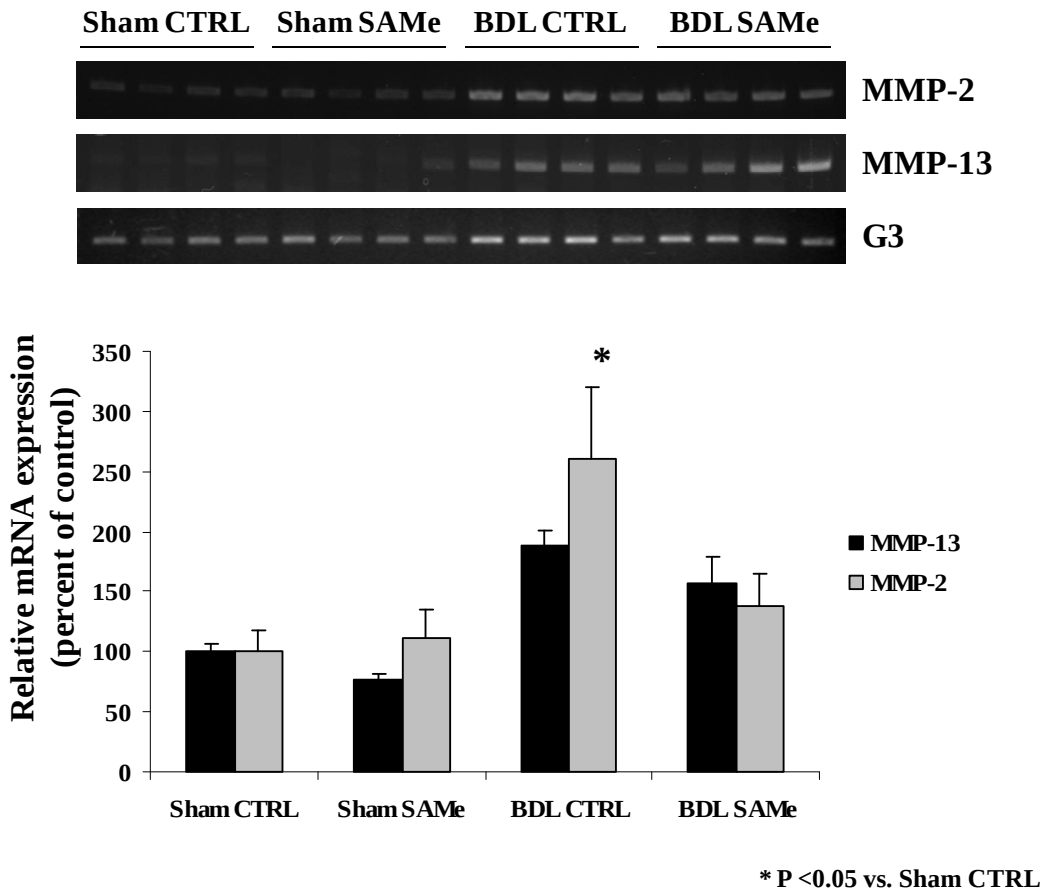

Figure 48. Two week BDL increases MMP-2 expression. RNA reversed transcribed from whole liver revealed a significant increase in the message of MMP-2 in animals subjected to BDL with vehicle treatment. Administration of daily SAMe starting on post-operative day 7 of BDL animals diminished this effect. Levels of MMP-13 were increased by BDL, however, this increase was not significant.

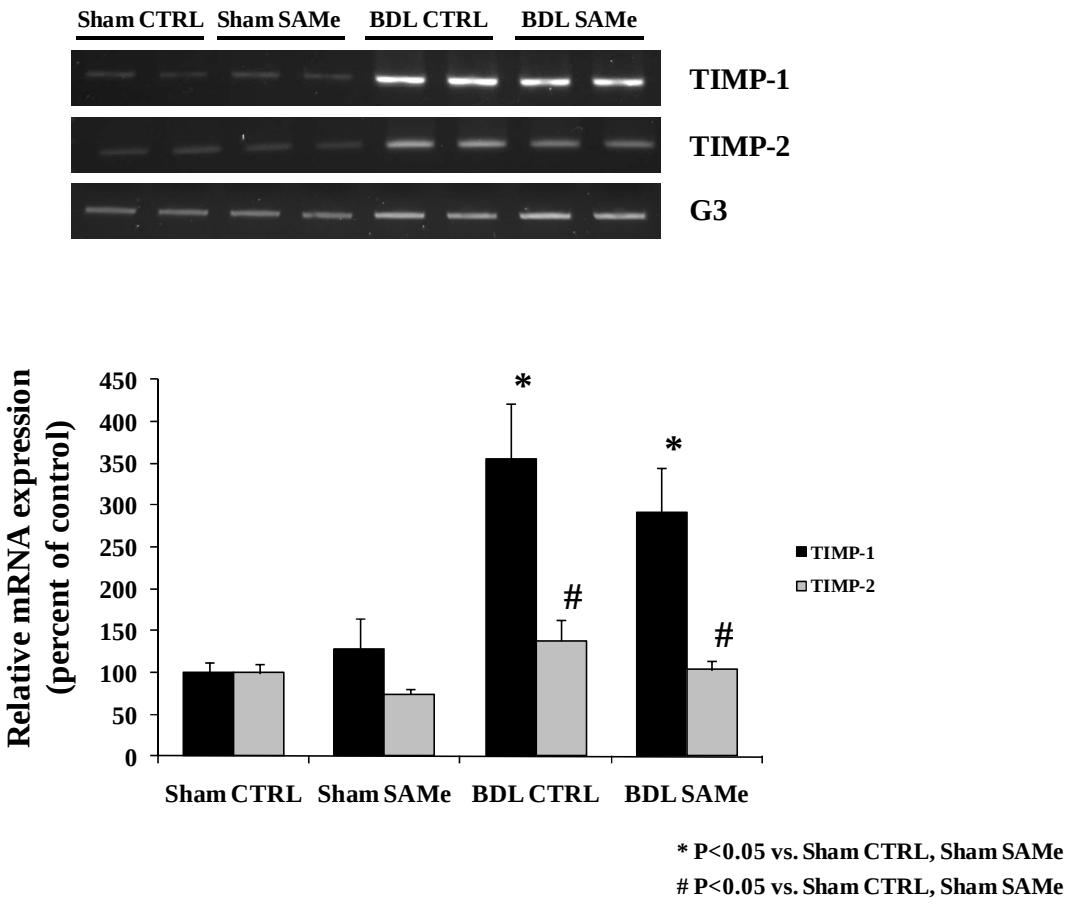

Figure 49. TIMP expression is increased by BDL. RT-PCR on total RNA reversed transcribed from whole liver showed a significant increase in the messages of TIMP-1 and TIMP-2 in animals subjected to BDL with vehicle treatment. Administration of daily SAMe starting on post-operative day 7 of BDL animals attenuated TIMP-1 and TIMP-2 expression, but not significantly.

CHAPTER 5: SUMMARY AND FUTURE DIRECTIONS

In the normal liver, hepatic stellate cells (HSCs) are quiescent and reside in the space of Disse. Quiescent HSCs store vitamin A in the form of retinyl esters [18], maintain the basement membrane, and regulate sinusoidal diameter through their cytoplasmic projections and contractile properties [41]. Upon a noxious stimulus, HSCs activate to a myofibroblast-like cell capable of proliferating extensively, migrating to areas of injury, producing proinflammatory cytokines, and secreting extracellular matrix (ECM) products to facilitate healing [6]. Withdrawl of the stimulus results in a reduction of activated HSCs, either by apoptosis or reversion back to a quiescent phenotype. However, chronic injury results in the accumulation of ECM components, including type I collagen, disrupting the normal liver architecture resulting in impairment of nutrient delivery and further injury leading to fibrosis. Unresolved hepatic fibrosis can progress to cirrhosis, which is an end-stage liver disease with considerable morbidity and mortality. Removal or treatment of the underlying cause of liver fibrosis can lead to spontaneous recovery [9-12]; however, in the case of alcoholic liver disease (ALD) recovery is hampered by continued ethanol abuse. Thus therapies that can treat hepatic fibrosis in the setting of continued fibrogenic stimuli are attractive.

The antioxidant S-adenosyl-L-methionine (SAMe) has received attention as a candidate therapy for alcoholic fibrosis. SAMe is a precursor to the intracellular principal intracellular antioxidant glutathione and may prevent fibrosis through a

reduction in reactive oxygen species (ROS) generated through ethanol metabolism, injury to hepatocytes, and activation of Kupffer cells. Previous studies have shown SAMe can attenuate liver injury in experimental models of hepatic fibrosis [210, 237, 275] and is well tolerated in human trials [209]. Although the effects of SAMe have been investigated *in vitro* utilizing HSCs, these studies focused on early-activated HSCs, which may be more consistent with investigating SAMe as a preventative agent. Culturing primary HSCs on plastic results in the spontaneous activation of HSCs from a quiescent to myofibroblast-like phenotype and is considered the best model for mimicking the phenotype of HSCs in the fibrotic liver. Therefore, we took a mechanistic approach to determine the effects of SAMe on culture-activated HSCs.

Treatment of culture-activated HSCs with increasing doses of SAMe resulted in a decrease in intracellular type I collagen protein expression over time; however, this attenuation was not significant. Since hepatic fibrosis is defined by the accumulation of ECM products, we examined the effects of a single concentration of SAMe on type I collagen secretion in culture-activated HSCs. SAMe resulted in a highly significant ($P < 0.001$) decrease in the amount of type I collagen secreted into culture media. These results suggest SAMe may be useful in resolving hepatic fibrosis in a setting of sustained insult, such as chronic ethanol abuse in humans. Our findings also demonstrated that SAMe-mediated type I collagen inhibition in Rat-1 fibroblasts requires NF-κB activity. Because of the difficulty in inhibiting NF-κB activity in culture-activated HSCs, the precise role of NF-κB in mediating SAMe-induced type I collagen inhibition will be difficult to examine. Future experiments utilizing HSCs isolated from the livers of

fibrotic animals treated with SAMe will help determine if the observation that SAMe increases NF-κB also occurs *in vivo*.

Although treatment of culture-activated HSCs with SAMe failed to diminish steady-state mRNA levels of procollagen gene products as hypothesized, SAMe treatment resulted in the polyubiquitination of intracellular type I collagen. This finding led us to investigate ER proteins to determine if SAMe administration could modulate their expression, potentially suggesting a role for ER stress in the mechanism of SAMe-mediated type I collagen inhibition. Our data showed SAMe treatment resulted in a significant decrease at 24 hours in the expression of protein disulfide isomerase (PDI) and the 78-kDa glucose-regulated protein (Grp78). SAMe has been shown to increase levels of glutathione both *in vitro* and *in vivo*. The redox status of the ER is important for its proper function. High levels of glutathione may suppress the oxidizing activity of PDI, limiting disulfide bond formation [256, 257]. These findings may suggest a novel mechanism for type I collagen inhibition in activated HSCs through the selective retention of secretory proteins requiring precise disulfide-bond formation for proper assembly. Further studies utilizing SAMe and other agents capable of producing a more reducing environment in the ER should be conducted to more precisely examine a connection between redox status changes and inhibition of type I collagen secretion in activated HSCs.

Additionally, the role of polyubiquitination of type I collagen should be further examined *in vivo*. Although SAMe-treatment failed to demonstrate co-localization of type I collagen and polyubiquitin, these findings are not conclusive. Varying the time points at which animals are analyzed following the initiation of SAMe administration will

give a more accurate assessment, as the kinetics of SAMe-induced increases in type I collagen polyubiquitination were not uniform. Furthermore, because HSCs represent only 15% of the liver's cellular population, analysis of HSCs directly either through *in situ* isolation or laser capture dissection microscopy may provide more definitive results than analysis of whole liver tissue.

The second aim of this dissertation was the development of experimental models of hepatic fibrosis. These models will allow us to evaluate treatments of hepatic fibrosis as well as better our understanding of disease progression. Bile duct ligation (BDL) is a well established model of hepatic fibrosis. To determine if we could reproduce the phenotype observed in BDL, as well as evaluate if SAMe could attenuate already-established fibrosis, we subjected animals to either sham or BDL surgery, followed by 7 days of recovery. On post-operative day 7, animals were treated with either 10 mg/kg of SAMe or a saline vehicle daily for an additional 7 days. As expected, BDL resulted in an increase in collagen production, as demonstrated by Sirius red staining. SAMe administration decreased type I collagen expression at the protein level; however, there was not a significant decrease in either α1(I) or α2(I) procollagen mRNA levels. SAMe treatment did decrease αSMA expression, suggesting either a reduction in the number of activated HSCs or a reversion of HSCs to a quiescent phenotype in the livers of BDL animals.

Because there was a reduction in type I collagen at the protein level, but not mRNA level, we investigated the expression of matrix metalloproteinases (MMPs) and their inhibitors, tissue inhibitors of metalloproteinases (TIMPs) in our BDL model of hepatic fibrosis. BDL resulted in a significant increase in profibrotic MMP-2, TIMP-1,

and TIMP-2 and no significant change in fibrolytic MMP-13 expression. SAMe treatment attenuated MMP-2 expression in BDL animals, but the difference was not significantly lower than MMP-2 expression in BDL animals treated with vehicle alone. Although these findings do not support a major role for SAMe in the modulation of MMPs and their inhibitors, TIMPs, further investigation examining the activity level of the respective MMPs should be conducted. MMPs have multiple steps of regulation, including mRNA expression, cleavage of the pro-MMP to form the active MMP, and an inverse relationship between TIMP expression and MMP activity. Studies utilizing zymographies should be conducted on samples from SAMe-treated animals subjected to BDL to better ascertain the role SAMe plays in their expression and activity.

We also sought to develop an ethanol model of hepatic fibrosis. Current models of alcoholic fibrosis suffer from a combination of difficulty in administration and a lack of relevance to the clinical progression of disease in humans. To develop a "two-hit" model of alcoholic fibrosis, we administered lipopolysaccharide (LPS) injections concurrently with chronic ethanol feeding utilizing the Lieber-DeCarli (LD) liquid ethanol diet. LPS was chosen based on observations that ethanol consumption increases the permeability of the gut to endotoxin [276] and an increase in plasma endotoxin in patients with ALD as well as following acute ethanol consumption [259].

The initial pilot study comprised of daily ethanol consumption and weekly injections of either 0.5 mg/kg or 1.0 mg/kg LPS resulted in the formation of mild fibrosis. To evaluate if increasing both the frequency of LPS injection and duration of the study resulted in greater fibrosis, the study was repeated using semi-weekly injections of 1.0 mg/kg LPS in conjunction with 10 weeks of ethanol feeding. This model failed to

demonstrate hepatic fibrosis. We hypothesized that the combination of increased LPS dosage coupled with an increase in the frequency of administration may have induced tolerance to LPS in the liver, blunting its effects. This is supported by findings that continuous LPS infusion diminishes injury in a model of chronic ethanol feeding [263].

We then modified our hypothesis to semi-weekly low-dosage (0.5 mg/kg) LPS injections in animals on the LD diet would produce hepatic fibrosis. Following 8 weeks of feeding and injections of LPS, animals were evaluated for hepatic fibrosis. Ethanol feeding alone resulted in increased activated HSCs and perivenular collagen production. Treatment with LPS increased both these measures of hepatic fibrosis. In particular, ethanol plus LPS resulted in a highly significant increase in perisinusoidal collagen staining. Fibrosis was associated with increased inflammation, a higher ratio of oxidized glutathione (GSSG) to reduced glutathione (GSH), and increased expression of mediators of transforming growth factor-beta (TGF-β) signaling.

To evaluate if SAMe administration concomitantly with ethanol consumption and LPS injections would inhibit hepatic fibrosis, animals were injected daily with 10 mg/kg SAMe. Treatment with SAMe significantly decreased markers of hepatic fibrosis, including collagen staining, αSMA expression, and inflammation. SAMe also restored the normal ratio of GSSG/GSH, suggesting a decrease in oxidative stress. Finally, SAMe decreased TGF-β expression, and expression of a key downstream signaling molecule of TGF-β, Smad3.

These findings demonstrate that the combination of chronic ethanol consumption utilizing the LD diet coupled with semi-weekly injections of LPS can produce hepatic fibrosis within 8 weeks. This “two-hit” model of alcoholic liver fibrosis provides a

simple and easily administered model to evaluate the development and prevention of hepatic fibrosis. Although this model did not result in extensive “chicken-wire” fibrosis that links adjacent lobules in the liver, future experiments focusing on increasing the duration of ethanol feeding with LPS injections can evaluate the extent of fibrosis that can be generated. We also demonstrated that our model can be modulated with administration of the antioxidant, SAMe. This suggests our model can be used as a platform to prevent the onset of hepatic fibrosis in a “two-hit” model. Future studies to evaluate the efficacy of other treatments both alone and in comparison with more established treatments such as SAMe will allow us to increase the pool of candidate anti-fibrotic agents. Finally, studies utilizing this model can be used to examine the role of SAMe in the reversal of already-established alcoholic fibrosis.

REFERENCES

1. Albanis, E. and S.L. Friedman, *Hepatic fibrosis. Pathogenesis and principles of therapy.* Clin Liver Dis, 2001. **5**(2): p. 315-334.

2. Ginès, P., et al., *Management of cirrhosis and ascites.* N Engl J Med, 2004. **350**: p. 1646-1654.

3. McKillop, I.H. and L.W. Schrum, *Alcohol and liver cancer.* Alcohol, 2005. **35**(3): p. 195-203.

4. Ginés, P., et al., *Compensated cirrhosis: natural history and prognostic factors.* Hepatology, 1987. **7**(1): p. 122-8.

5. Brunt, E.M., *Nonalcoholic steatohepatitis.* Semin Liver Dis., 2004. **24**: p. 3-20.

6. Friedman, S.L., *Liver fibrosis - from bench to bedside.* J Hepatol, 2003. **38**(Suppl 1): p. S38-S53.

7. Abdel-Aziz, G., et al., *Reversibility of hepatic fibrosis in experimentally induced cholestasis in rat.* Am J Pathol, 1990. **137**(6): p. 1333-42.

8. Iredale, J.P., et al., *Mechanisms of spontaneous resolution of rat liver fibrosis. Hepatic stellate cell apoptosis and reduced hepatic expression of metalloproteinase inhibitors.* J Clin Invest, 1998. **102**(3): p. 538-49.

9. Dufour, J.F., R. DeLellis, and M.M. Kaplan, *Reversibility of hepatic fibrosis in autoimmune hepatitis.* Ann Intern Med, 1997. **127**(11): p. 981-985.

10. Duchatelle, V., et al., *Changes in liver fibrosis at the end of alpha interferon therapy and 6 to 18 months later in patients with chronic hepatitis C: quantitative assessment by a morphometric method.* J Hepatol, 1998. **29**(1): p. 20-8.

11. Hammel, P., et al., *Regression of liver fibrosis after biliary drainage in patients with chronic pancreatitis and stenosis of the common bile duct.* N Engl J Med, 2001. **344**(6): p. 418-23.

12. Wanless, I.R., E. Nakashima, and M. Sherman, *Regression of human cirrhosis. Morphologic features and the genesis of incomplete septal cirrhosis.* Arch Pathol Lab Med, 2000. **124**(11): p. 1599-607.

13. Thampanitchawong, P. and T. Piratvisuth, *Liver biopsy:complications and risk factors.* World J Gastroenterol, 1999. **5**(4): p. 301-4.

14. Bedossa, P., D. Dargere, and V. Paradis, *Sampling variability of liver fibrosis in chronic hepatitis C.* Hepatology, 2003. **38**(6): p. 1449-57.

15. Poynard, T., et al., *Biochemical surrogate markers of liver fibrosis and activity in a randomizd trial of peginterferon alfa-2b and ribavirin.* Hepatology, 2003. **38**(2): p. 481-92.

16. Yin, M., et al., *Assessment of hepatic fibrosis with magnetic resonance elastography.* Clin Gastroenterol Hepatol, 2007. **5**(10): p. 1207-13.e2.

17. Otto, D.A. and R.L. Veech, *Isolation of a lipocyte-rich fraction from rat liver nonparenchymal cells.* Adv Exp Med Biol, 1980. **132**: p. 509-17.

18. Friedman, S.L., et al., *Hepatic lipocytes: the principal collagen-producing cells of normal rat liver.* Proc Natl Acad Sci U S A, 1985. **82**(24): p. 8681-5.

19. Maher, J.J., et al., *Collagen measured in primary cultures of normal rat hepatocytes derives from lipocytes within the monolayer.* J Clin Invest, 1988. **82**(2): p. 450-9.

20. Desmoulière, A., et al., *Extracellular matrix deposition, lysyl oxidase expression, and myofibroblastic differentiation during the initial stages of cholestatic fibrosis in the rat.* Lab Invest, 1997. **76**(6): p. 765-78.

21. Milani, S., et al., *Procollagen expression by nonparenchymal rat liver cells in experimental biliary fibrosis.* Gastroenterology, 1990. **98**(1): p. 175-84.

22. Kinnman, N., et al., *The myofibroblastic conversion of peribiliary fibrogenic cells distinct from hepatic stellate cells is stimulated by platelet-derived growth factor during liver fibrogenesis.* Lab Invest, 2003. **83**(2): p. 163-73.

23. Ramadori, G. and B. Saile, *Portal tract fibrogenesis in the liver.* Lab Invest, 2004. **84**(2): p. 153-9.

24. Forbes, S.J., et al., *A significant proportion of myofibroblasts are of bone marrow origin in human liver fibrosis.* Gastroenterology, 2004. **126**(4): p. 955-63.

25. Trauner, M., P. Fickert, and R.E. Stauber, *Inflammation-induced cholestasis.* J Gastroenterol Hepatol., 1998. **14**(10): p. 946-59.

26. Iredale, J.P., et al., *Tissue inhibitor of metalloproteinase-1 messenger RNA expression is enhanced relative to interstitial collagenase messenger RNA in experimental liver injury and fibrosis.* Hepatology, 1996. **24**(1): p. 176-84.

27. Saito, J.M., et al., *Infiltrating neutrophils in bile duct-ligated livers do not promote hepatic fibrosis.* Hepatol Res., 2003. **25**(2): p. 180-91.

28. Gurjal, J.S., et al., *Neutrophils aggravate acute liver injury during obstructive cholestasis in bile duct-ligated mice.* Hepatology, 2003. **38**(2): p. 355-63.

29. Georgiev, P., et al., *Characterization of time-related changes after experimental bile duct ligation.* Br J Surg, 2008. **95**(5): p. 646-56.

30. Constandinou, C., N. Henderson, and J.P. Iredale, *Modeling liver fibrosis in rodents.* Methods Mol Med, 2005. **117**: p. 237-50.

31. Tsukamoto, H., M. Matsuoka, and S.W. French, *Experimental models of hepatic fibrosis: a review.* Semin Liver Dis., 1990. **10**(1): p. 56-65.

32. Perez-Tamayo, R., *Is cirrhosis of the liver experimentally produced by CCl4 an adequate model of human cirrhosis?* Hepatology, 1983. **3**(1): p. 112-20.

33. Lieber, C.S. and L.M. DeCarli, *Fatty liver in the rat after prolonged intake of ethanol with a nutritionally adequate new liquid diet.* J Nutr., 1967. **91**(3): p. 331-6.

34. Iseri, O.A., C.S. Lieber, and L.S. Gottlieb, *The ultrastructure of fatty liver induced by prolonged ethanol ingestion.* Am J Pathol, 1966. **48**(4): p. 535-555.

35. Lieber, C.S., *Alcohol and Liver: 1994 update.* Gastroenterology, 1994. **106**(4): p. 1085-1105.

36. Leo, M.A., et al., *Hepatotoxicity of vitamin A and ethanol in the rat.* Gastroenterology, 1982. **82**(2): p. 194-205.

37. Leo, M.A. and C.S. Lieber, *Hepatic fibrosis after long-term administration of ethanol and moderate vitamin A supplementation in the rat.* Hepatology, 1983. **3**(1): p. 1-11.

38. Best, C.H., et al., *Liver damage produced by feeding alcohol or sugar and its prevention by choline.* Br Med J, 1949. **2**(4635): p. 1001-1006.

39. Tsukamoto, H., et al., *Severe and progressive steatosis and focal necrosis in rat liver induced by continuous intragastric infusion of ethanol and low fat diet.* Hepatology, 1985. **5**(2): p. 224-232.

40. Tsukamoto, H., et al., *Experimental liver cirrhosis induced by alcohol and iron.* J Clin. Invest., 1995. **96**(1): p. 620-630.

41. Rockey, D.C., C.N. Housset, and S.L. Friedman, *Activation-dependent contractility of rat hepatic lipocytes in culture and in vivo.* J Clin Invest., 1993. **92**(4): p. 1795-1804.

42. Perez-Pomares, J.M., et al., *Contribution of mesothelium-derived cells to liver sinusoids in avian embryos.* Dev Dyn, 2004. **229**(3): p. 465-74.

43. Geerts, A., *On the origin of stellate cells: mesodermal, endodermal or neuro-ectodermal?* J Hepatol, 2004. **40**(2): p. 331-4.

44. Kobold, D., et al., *Expression of reelin in hepatic stellate cells and during hepatic tissue repair: a novel marker for the differentiation of HSC from other liver myofibroblasts.* J Hepatol, 2002. **36**(5): p. 607-13.

45. Niki, T., et al., *Class VI intermediate filament protein nestin is induced during activation of rat hepatic stellate cells.* Hepatology, 1999. **29**(2): p. 520-7.

46. Knittel, T., et al., *Cell-type-specific expression of neural cell adhesion molecule (N-CAM) in Ito cells of rat liver. Up-regulation during in vitro activation and in hepatic tissue repair.* Am J Pathol, 1996. **149**(2): p. 449-62.

47. Oben, J.A., et al., *Hepatic fibrogenesis requires sympathetic neurotransmitters.* Gut, 2004. **53**(3): p. 438-45.

48. Echelard, Y., G. Vassileva, and A.P. McMahon, *Cis-acting regulatory sequences governing Wnt-1 expression in the developing mouse CNS.* Development, 1994. **120**(8): p. 2213-24.

49. Srinivas, S., et al., *Cre reporter strains produced by targeted insertion of EYFP and ECFP into the ROSA26 locus.* BMC Dev Biol, 2001. **1**(1): p. 4.

50. Cassiman, D., et al., *Hepatic stellate cells do not derive from the neural crest.* J Hepatol, 2006. **44**: p. 1098-1104.

51. Saga, Y., et al., *MesP1: a novel basic helix-loop-helix protein expressed in the nascent mesodermal cells during mouse gastrulation.* Development, 1996. **122**(9): p. 2769-78.

52. Asahina, K., et al., *Mesenchymal origin of hepatic stellate cells, submesothelial cells, and perivascular mesenchymal cells during mouse liver development.* Hepatology, 2009. **49**(3): p. 998-1011.

53. Kalinichenko, V.V., et al., *Foxf1 +/- mice exhibit defective stellate cell activation and abnormal liver regeneration following CCl4 injury.* Hepatology, 2003. **37**: p. 107-17.

54. Suskind, D.L. and M.O. Muench, *Searching for common stem cells of the hepatic and hematopoietic systems in the human fetal liver: CD34+ cytokeratin 7/8+ cells express markers for stellate cells.* J Hepatol, 2004. **40**: p. 261-8.

55. Jezequel, A.M., et al., *Quantitative analysis of the perisinusoidal cells in the human liver; the lipocytes.* Front Gastrointestinal Res, 1984. **8**: p. 85-90.

56. Wake, K., *Cell-cell organization and functions of "sinusoids" in liver microcirulation system.* J Electron Microsc, 1999. **48**: p. 89-98.

57. Zou, Z., W. Ekataksin, and K. Wake, *Zonal and regional differences identified from precision mapping of vitamin A-storing lipid droplets of the hepatic stellate*

cells in pig liver: A novel concept of addressing the intralobular area of heterogeneity. Hepatology, 1998. **27**: p. 1098-1108.

58. Thurman, R.G., *II. Alcoholic liver injury involves activation of Kupffer cells by endotoxin.* Am J Physiol, 1998. **275**: p. G605-11.

59. Paik, Y.H., et al., *Toll-like receptor 4 mediates inflammatory signaling by bacterial lipopolysaccharide in human hepatic stellate cells.* Hepatology, 2003. **37**(5): p. 1043-55.

60. Friedman, S.L., *Hepatic stellate cells: protean, multifunctional, and enigmatic cells of the liver.* Physiol Rev, 2008. **88**: p. 125-72.

61. Stefanovic, B., et al., *Posttranscriptional regulation of collagen alpha1(I) mRNA in hepatic stellate cells.* Mol Cell Biol, 1997. **17**(9): p. 5201-9.

62. Gressner, A.M., et al., *Roles of TGF-beta in hepatic fibrosis.* Front Biosci, 2002. **7**: p. d793-807.

63. Inagaki, Y. and I. Okazaki, *Emerging insights into transforming growth factor beta smad signal in hepatic fibrogenesis.* Gut. **56**: p. 284-92.

64. Ritzenthaler, J.D., et al., *Transforming-growth-factor-beta activation elements in the distal promoter regions of the rat alpha 1 type I collagen gene.* Biochem J, 1991. **280**: p. 157-62.

65. Inagaki, Y., S. Truter, and F. Ramirez, *Regulation of the alpha 2(I) collagen gene transcription in fat-storing cells derived from a cirrhotic liver.* Hepatology, 1995. **22**(2): p. 573-9.

66. Friedman, S.L. and J.L. Arthur, *Activation of cultured rat hepatic lipocytes by Kupffer cell conditioned medium. Direct enhancement of matrix synthesis and stimulation of cell proliferation via induction of platelet-derived growth factor receptors.* J Clin. Invest., 1989. **84**: p. 1780-5.

67. Pinzani, M., et al., *Effects of platelet-derived growth factor and other polypeptide mitogens on DNA synthesis and growth of cultured rat liver fat-storing cells.* J Clin. Invest., 1989. **84**: p. 1786-93.

68. Shah, V., *Cellular and molecular basis of portal hypertension.* Clin Liver Dis, 2001. **5**: p. 629-44.

69. Gaca, M.D., et al., *Basement membrane-like matrix inhibits proliferation and collagen synthesis by activated rat hepatic stellate cells: evidence for matrix-dependent deactivation of stellate cells.* Matrix Biol, 2003. **22**: p. 229-239.

70. Saile B, K.T., Matthes N, Schott P, Ramadori G, *CD95/CD95L-mediated apoptosis of the hepatic stellate cell. A mechanism terminating uncontrolled*

hepatic stellate cell proliferation during hepatic tissue repair. Am J Pathol, 1997. **151**(5): p. 1265-72.

71. Di Lullo, G.A., et al., *Mapping the ligand-binding sites and disease-associated mutations on the most abundant protein in the human, type I collagen.* J Biol Chem, 2002. **277**: p. 4233-31.

72. Imai, K., T. Sato, and H. Senoo, *Adhesion between cells and extracellular matrix with special reference to hepatic stellate cell adhesion to three-dimensional collagen fibers.* Cell Struct Funct, 2000. **25**: p. 329-36.

73. Van Der Rest, M. and M. Garrone, *Collagen family of proteins.* FASEB J, 1991. **5**: p. 2814-23.

74. Sweeney, S.M., et al., *Candidate cell and matrix interaction domains on the collagen fibril, the predominat protein of vertebrates.* J Biol Chem, 2008. **283**: p. 21187-97.

75. Prockop, D.J. and K.I. Kivirikko, *Collagens: Molecular biology, diseases, and potentials for therapy.* Annu Rev Biochem, 1995. **64**: p. 403-34.

76. Fleischmajer, R., B.R. Olsen, and K. Kuhn, *Structure, molecular biology, and pathology of collagen.* Ann NY Acad Sci, 1990. **580**: p. 1-592.

77. Wynn, T.A., *Cellular and molecular mechanisms of fibrosi.* J Pathol, 2008. **214**: p. 199-210.

78. Alexakis, C., P. Maxwell, and G. Bou-Gharios, *Organ-specific collagen expression: implications for renal diseas.* Nephron Exp Nephrol, 2006. **102**: p. 71-5.

79. Ghosh, A.K., *Factors involved in the regulation of type I collagen gene expression: implication in fibrosis.* Exp Biol Med, 2002. **227**: p. 301-14.

80. Lindquist, J.N., W.F. Marzluff, and B. Stefanovic, *Fibrogenesis. III. Posttranscriptional regulation of type I collagen.* Am J Physiol Gastrointest Liver Physiol, 2000. **279**: p. G471-6.

81. Karsenty, G., *Conservation of binding sites for regulatory factors in the coordinately expressed alpha 1 (I) and alpha 2 (I) collagen promoters.* Biochem Biophys Res Commun, de Crombrugghe, B. **177**: p. 538-44.

82. de Wet, W.J., et al., *Synthesis of a shortened pro-alpha 2(I) chain and decreased synthesis of pro-alpha 2(I) chains in a proband with osteogenesis imperfecta.* J Biol Chem, 1983. **258**: p. 7721-8.

83. Rossouw, C.M., et al., *DNA sequences in the first intron of the human pro-alpha 1(I) collagen gene enhance transcription* J Biol Chem, 1987. **262**: p. 15151-15157.

84. Sherwood, A.L., et al., *Structural and functional analysis of the first intron of the human alpha 2(I) collagen-encoding gene.* Gene, 1990. **89**: p. 239-44.

85. Bornstein, P., *Regulation of expression of the alpha 1 (I) collagen gene: a critical appraisal of the role of the first intron.* Matrix Biol, 1996. **15**(1): p. 3-10.

86. Rhodes, K., et al., *DNA methylation represses the murine alpha 1(I) collagen promoter by an indirect mechanism.* Mol Cell Biol., 1994. **14**: p. 5950-60.

87. Sengupta, P., et al., *Collagen alpha 1(I) gene (COL1A1) is repressed by RFX family.* J Biol Chem, 2005. **280**: p. 21004-14.

88. Blomhoff, R. and K. Wake, *Perisinusoidal stellate cells of the liver: important roles in retinol metabolism and fibrosis.* FASEB J, 1991. **5**: p. 271-7.

89. Armendariz-Borunda, J., K. Katayama, and J.M. Seyer, *Transcriptional mechanisms of type I collagen gene expression are differentially regulated by interleukin-1 beta, tumor necrosis factor alpha, and transforming growth factor beta in Ito cells.* J Biol Chem, 1992. **267**: p. 14316-21.

90. Tsukamoto, H., *Cytokine regulation of hepatic stellate cells in liver fibrosis.* Alcohol Clin Exp Res, 1999. **23**(5): p. 911-6.

91. Choi, I., et al., *IL-6 induces hepatic inflammation and collagen synthesis in vivo.* Clin Exp Immunol, 1994. **95**(3): p. 530-5.

92. Rossi, P., et al., *A nuclear factor 1 binding site mediates the transcriptional activation of a type I collagen promoter by transforming growth factor-beta.* Cell, 1988. **52**: p. 405-14.

93. Tamaki, T., et al., *Characterization of a GC-rich region containing Sp1 binding site(s) as a constitutive responsive element of the alpha 2(I) collagen gene in human fibroblasts.* J Biol Chem, 1995. **270**: p. 4299-304.

94. Chen, A. and B.H. Davis, *The DNA binding protein BTEB mediates acetaldehyde-induced, jun N- terminal kinase-dependent alphaI(I) collagen gene expression in rat hepatic stellate cells.* Mol Cell Biol, 2000. **20**(8): p. 2818-26.

95. Mathurin, P., et al., *IL-10 receptor and coreceptor expression in quiescent and activated hepatic stellate cells.* Am J Physiol Gastrointest Liver Physiol, 2002. **282**: p. G981-90.

96. Rosenbloom, J., et al., *Transcriptional control of human diploid fibroblast collagen synthesis by gamma-interferon.* Biochem Biophys Res Commun, 1984. **123**: p. 365-72.

97. Tan, E.M., et al., *Acidic and basic fibroblast growth factors down-regulate collagen gene expression in keloid fibroblasts.* Am J Pathol., 1993. **142**: p. 463-70.

98. Dalgleish, R., *The human type I collagen mutation database.* Nucleic Acids Res., 1997. **25**: p. 181-7.

99. Hendershot, L.M. and N.J. Bulleid, *Protein-specific chaperones: the role of hsp47 begins to gel.* Curr. Biol., 2000. **10**: p. R912-5.

100. Chessler, S.D. and P.H. Byers, *BiP binds type I procollagen pro alpha chains with mutations in the carboxyl-terminal propeptide synthesized by cells from patients with osteogenesis imperfecta.* J Biol Chem, 1993. **268**: p. 18226-33.

101. Lamande, S.R. and J.F. Bateman, *Procollagen folding and assembly: the role of endoplasmic reticulum enzymes and molecular chaperones.* Semin Cell Dev Biol, 1999. **10**: p. 455-64.

102. Wilson, R., J.F. Lees, and N.J. Bulleid, *Protein disulfide isomerase acts as a molecular chaperone during the assembly of procollagen.* J Biol Chem, 1998. **279**: p. 9637-43.

103. John, D.C., M.E. Grant, and N.J. Bulleid, *Cell-free synthesis and assembly of prolyl 4-hydroxylase: the role of the beta-subunit (PDI) in preventing misfolding and aggregation of the alpha-subunit.* EMBO J, 1993. **12**: p. 1587-95.

104. Privalov, P.L., *Stability of proteins. Proteins which do not present a single cooperative system.* Adv Protein Chem, 1982. **35**: p. 1-104.

105. Bella, J., B. Brodsky, and H.M. Berman, *Hydration structure of a collagen peptide.* Structure, 1995. **3**: p. 893-906.

106. Nagata, K., S. Saga, and K.M. Yamada, *Characterization of a novel transformation-sensitive heat-shock protein (HSP47) that binds to collagen.* Biochem Biophys Res Commun, 1988. **31**: p. 428-34.

107. Nagai, N., et al., *Embryonic lethality of molecular chaperone hsp47 knockout mice is associated with defects in collagen biosynthesis.* J Cell Biol., 2000. **150**: p. 1499-1506.

108. Leung, M.K., et al., *Separate amino acid and carboxyl procollagen peptidases in chick embryo tendon.* J Biol Chem, 1979. **254**: p. 224-232.

109. Kadler, K.E., Y. Hojima, and D.J. Prockop, *Assembly of collagen fibrils de novo by cleavage of the type I pC-collagen with procollagen C-proteinase. Assay of critical concentration demonstrates that collagen self-assembly is a classical example of an entropy-driven process.* J Biol Chem, 1987. **262**: p. 15696-701.

110. Elsharkawy, A.M. and D.A. Mann, *Nuclear factor-kappaB and the hepatic inflammation-fibrosis-cancer axis.* Hepatology, 2007. **46**: p. 590-7.

111. Verma, I.M., et al., *Rel/NF-kappa B/I kappa B family: intimate tales of association and dissociation.* Genes Dev., 1995. **9**: p. 2723-35.

112. Kang, S.M., et al., *NF-kappa B subunit regulation in nontransformed CD4+ T lymphocytes.* Science, 1992. **256**(5062): p. 1452-6.

113. Franzoso, G., et al., *The candidate oncoprotein Bcl-3 is an antagonist of p50/NF-kappa B-mediated inhibition.* Nature, 1992. **359**: p. 339-42.

114. DiDonato, J.A., et al., *A cytokine-responsive IkappaB kinase that activates the transcription factor NF-kappaB.* Nature, 1997. **388**(6642): p. 548-54.

115. Hoffmann, A. and D. Baltimore, *Circuitry of nuclear factor κB signaling.* Immunol Rev., 2006. **210**: p. 171-86.

116. Lee, K.S., et al., *Activation of hepatic stellate cells by TGF alpha and collagen type I is mediated by oxidative stress through c-myb expression.* J Clin. Invest., 1995. **96**: p. 2561-8.

117. Roman, J., et al., *Enhanced DNA binding and activation of transcription factors NF-kappa B and AP-1 by acetaldehyde in HEPG2 cells.* J Biol Chem, 2000. **275**(19): p. 14684-90.

118. Lang, A., et al., *Nuclear factor kappaB in proliferation, activation, and apoptosis in rat hepatic stellate cells.* J Hepatol, 2000. **33**(1): p. 49-58.

119. Hellerbrand, C., et al., *Expression of intercellular adhesion molecule I by activated hepatic stellate cells.* Hepatology, 1996. **24**: p. 670-6.

120. Rippe, R.A., et al., *NF-kappaB inhibits expression of the alpha1(I) collagen gene.* DNA Cell Biol, 1999. **18**(10): p. 751-61.

121. Novitskiy, G., et al., *Identification of a novel NF-kappaB-binding site with regulation of the murine alpha2(I) collagen promoter.* J Biol Chem, 2004. **279**: p. 15639-44.

122. Aimes, R.T. and J.P. Quigley, *Matrix metalloproteinase-2 is an interstitial collagenase. Inhibitor-free enzyme catalyzes the cleavage of collagen fibrils and soluble native type I collagen generating the specific 3/4- and 1/4-length fragments.* J Biol Chem, 1995. **270**: p. 5872-6.

123. Itoh, Y. and M. Seiki, *MT1-MMP: a potent modifier of pericellular environment.* J Cell Physiol, 2005. **206**(1): p. 1-8.

124. Sternlicht, M.D. and Z. Werb, *How matrix metalloproteinases regulate cell behavior.* Annu Rev Cell Dev Biol, 2001. **17**: p. 463-516.

125. Visse, R. and H. Nagase, *Matrix metalloproteinases and tissue inhibitors of metalloproteinases: structure, function, and biochemistry.* Circ Res, 2003. **92**(8): p. 827-39.

126. Nagase, H. and J.F. Woessner, *Matrix metalloproteinases.* J Biol Chem, 1999. **274**: p. 21491-4.

127. Nagase, H., et al., *Stepwise activation mechanisms of the precursor of matrix metalloproteinase 3 (stromelysin) by proteinases and (4-aminophenyl)mercuric acetate.* Biochemistry, 1990. **29**: p. 5783-9.

128. Peppin, G.J. and S.J. Weiss, *Activation of the endogenous metalloproteinase, gelatinase, by triggered human neutrophils.* Proc Natl Acad Sci U S A, 1986. **83**: p. 4322-6.

129. Gu, Z., et al., *S-nitrosylation of matrix metalloproteinases: signaling pathway to neuronal cell death.* Science, 2002. **297**(5584): p. 1186-90.

130. Baker, A.H., D.R. Edwards, and G. Murphy, *Metalloproteinase inhibitors: biological actions and therapeutic opportunities.* J Cell Sci, 2002. **115**: p. 3719-27.

131. Nagase, H., R. Visse, and G. Murphy, *Structure and function of matrix metalloproteinases and TIMPs.* Cardiovasc Res, 2006. **69**(3): p. 562-73.

132. Will, H., et al., *The soluble catalytic domain of membrane type 1 matrix metalloproteinase cleaves the propeptide of progelatinase A and initiates autoproteolytic activation: regulation by TIMP-2 and TIMP-3.* J Biol Chem, 1996. **271**: p. 17119-23.

133. Schuppan, D., et al., *Matrix as a modulator of hepatic fibrogensis.* Semin Liver Dis, 2001. **21**(3): p. 351-72.

134. Hemmann, S., et al., *Expression of MMPs and TIMPs in liver fibrosis - a systematic review with special emphasis on anti-fibrotic strategies.* J Hepatol, 2007. **46**: p. 955-75.

135. Knittel, T., et al., *Expression patterns of matrix metalloproteinases and their inhibitors in parenchymal and non-parenchymal cells of rat liver: regulation by TNF-alpha and TGF-beta1.* J Hepatol, 1999. **30**: p. 48-60.

136. Han, Y.P., et al., *Essential role of matrix metalloproteinases in interleukin-1-induced myofibroblastic activation of hepatic stellate cell in collagen.* J Biol Chem, 2004. **279**(6): p. 4820-28.

137. Lee, H.S., et al., *Differential role of p38 in IL-1alpha induction of MMP-9 and MMP-13 in an established liver myofibroblast cell line.* J Biomed Sci, 2003. **10**(6 Part 2): p. 757-65.

138. Yasui, H., et al., *Role of fibroblast growth factor-2 in the expression of matrix metalloproteinases and tissue inhibitors of metalloproteinases in human intestinal myofibroblasts.* Digestion, 2004. **69**: p. 34-44.

139. Overall, C.M., J.L. Wrana, and J. Sodek, *Independent regulation of collagenase, 72-kDa progelatinase, and metalloendoporteinase inhibitor expression in human fibroblasts by transforming growth factor-beta.* J Biol Chem, 1989. **264**: p. 1860-1869.

140. Yan, S., et al., *Expression pattern of matrix metalloproteinases-13 in a rat model of alcoholic liver fibrosis.* Hepatolbiliary Pancreat Dis Int, 2005. **28**: p. 505-13.

141. Uchinami, H., et al., *Loss of MMP 13 attenuates murine hepatic injury and fibrosis during cholestasis.* Hepatology, 2006. **44**(2): p. 420-9.

142. Fallowfield, J.A., et al., *Scar-associated macrophages are a major source of hepatic matrix metalloproteinase-13 and facilitate the resolution of murine hepatic fibrosis.* J Immunol, 2007. **178**(8): p. 5288-95.

143. Wang, D.R., et al., *Stimulation of pro-MMP-2 production and activation by native form of extracellular type I collagen in cultured hepatic stellate cells.* Cell Struct Funct, 2003. **28**: p. 505-13.

144. Strongin, A.Y., et al., *Mechanism of cell surface activation of 72-kDa type IV collagenase. Isolation of the activated form of the membrane metalloprotease.* J Biol Chem, 1995. **270**: p. 5331-8.

145. Takahara, T., et al., *Increased expression of matrix metalloproteinase-II in experimental liver fibrosis in rats.* Hepatology, 1995. **21**(3): p. 787-95.

146. Watanabe, T., et al., *Dynamic change of cells expressing MMP-2 mRNA and MT1-MMP mRNA in the recovery from liver fibrosis in the rat.* J Hepatol, 2001. **35**(4): p. 465-73.

147. Kossakowska, A.E., et al., *Altered balance between matrix metalloproteinases and their inhibitors in experimental biliary fibrosis.* Am J Pathol, 1998. **153**(6): p. 1895-902.

148. Parola, M. and G. Robino, *Oxidative stress-related molecules and liver fibrosis.* J Hepatol, 2001. **35**: p. 297-306.

149. Zhou, X., et al., *Expression of matrix metalloproteinase-2 and -14 persists during early resolution of experimental liver fibrosis and might contribute to fibrolysis.* Liver Int, 2004. **24**: p. 492-501.

150. Giannelli, G., et al., *Antifibrogenic effect of IFN-alpha2b on hepatic stellate cell activation by human hepatocytes.* J Interferon Cytokine Res, 2006. **26**(5): p. 301-8.

151. Yu, Q. and I. Stamenkovic, *Cell surface-localized matrix metalloproteinase-9 proteolytically activates TGF-beta and promotes turor invasion and angiogenesis.* Genes Dev, 2000. **14**: p. 163-76.

152. Knittel, T., et al., *Expression of matrix metalloproteinases and their inhibitors during hepatic tissue repair in the rat.* Histochem Cell Biol, 2000. **113**: p. 443-453.

153. Roeb, E., et al., *Regulation of tissue inhibitor of metalloproteinases-1 gene expression by cytokines and dexamethasone in rat hepatocyte primary cultures.* Hepatology, 1993. **18**: p. 1437-42.

154. Roderfeld, M., et al., *Cytokine blockade inhibits hepatic tissue inhibitor of metalloproteinase-1 exprssion and up-regulates matrix metalloproteinase-9 in toxic liver injury.* Liver Int, 2006. **26**: p. 579-86.

155. Roeb, E., et al., *TIMP expression in toxic and cholestatic liver injury in rat.* J Hepatol, 1997. **27**: p. 535-44.

156. Iredale, J.P., *Tissue inhibitors of metalloproteinases in liver fibrosis.* Int J Biochem Cell Biol, 1997. **29**: p. 43-54.

157. Yoshiji, H., et al., *Tissue inhibitor of metalloproteinases-1 promotes liver fibrosis development in a transgenic mouse model.* Hepatology, 2000. **32**(6): p. 1248-54.

158. Yoshiji, H., et al., *Tissue inhibitor of metalloproteinases-1 attenuates spontaneous liver fibrosis resolution in the transgenic mouse.* Hepatology, 2002. **36**: p. 850-60.

159. Parsons, C.J., et al., *Antifibrotic effects of a tissue inhibitor of metalloproteinase-1 antibody on established liver fibrosis in rats.* Hepatology, 2004. **40**: p. 1106-15.

160. Nie, Q.H., et al., *Inhibiting effect of antisense oligonucleotides phosphorthioate on gene expression of TIMP-1 in rat liver fibrosis.* World J Gastroenterol, 2001. **7**: p. 363-69.

161. Murphy, F.R., et al., *Inhibition of apoptosis of activated hepatic stellate cells by tissue inhibitor of metalloproteinase-1 is mediated via effects on matrix metalloproteinase inhibition: implications for reversibility of liver fibrosis.* J Biol Chem, 2002. **277**(13): p. 11069-76.

162. Mohammed, F.F., et al., *Metalloproteinase inhibitor TIMP-1 affects hepatocyte cell cycle via HGF activation in murine liver regeneration.* Hepatology, 2005. **41**: p. 857-67.

163. Lindquist, S., *The heat-shock response.* Annu Rev Biochem, 1986. **55**: p. 1151-91.

164. Ma, Y. and L.M. Hendershot, *The unfolding tale of the unfolded protein response.* Cell, 2001. **107**: p. 827-30.

165. Kostova, Z. and D.H. Wolf, *For whom the bell tolls: protein quality control of the endoplasmic reticulum and the ubiquitin-proteasome connection.* EMBO J, 2003. **22**: p. 2309-17.

166. Kurzchalia, T.V., et al., *The signal sequence of nascent preprolactin interacts with the 54K polypeptide of the signal recognition particle.* Nature, 1986. **320**: p. 634-6.

167. Sommer, T. and D.H. Wolf, *Endoplasmic reticulum degradation: reverse protein flow of no return.* FASEB J, 1997. **11**: p. 1227-33.

168. Kaplowitz, N. and C. Ji, *ER stress: Can the liver cope?* J Hepatol, 2006. **45**: p. 321-33.

169. Tirasophon, W., A.A. Welihinda, and R.J. Kaufman, *A stress response pathway from the endoplasmic reticulum to the nucleus requires a novel bifunctional protein kinase/endoribonuclease (Ire1p) in mammalian cells.* Genes Dev., 1998. **12**: p. 1812-24.

170. Wang, X.Z., et al., *Cloning of mammalian Ire1 reveals diversity in the ER stress responses.* EMBO J, 1998. **17**: p. 5708-17.

171. Haze, K., et al., *Mammalian transcription factor ATF6 is synthesized as a transmembrane protein and activated by proteolysis in response to endoplasmic reticulum stress.* Mol Biol Cell, 1999. **10**: p. 3787-99.

172. Shi, Y., et al., *Identification and characterization of pancreatic eukaryotic initiation factor 2 alpha-subunit kinase, PEK, involved in translational control.* Mol Cell Biol, 1998. **18**: p. 7499-509.

173. Werner, E.D., J.L. Brodsky, and A.A. McCracken, *Proteasome-dependent endoplasmic reticulum-associated protein degradation: an unconventional route to a familiar fate.* Proc Natl Acad Sci U S A, 1996. **93**: p. 13797-801.

174. Dorner, A.J., L.C. Wasley, and R.J. Kaufman, *Protein dissociation from GRP78 and secretion are blocked by depletion of cellular ATP levels.* Proc Natl Acad Sci U S A, 1990. **87**: p. 7429-32.

175. Boyce, M. and J. Yuan, *Cellular response to endoplasmic reticulum stress: a matter of life or death.* Cell Death Differ., 2006. **13**: p. 363-73.

176. Pahl, H.L. and P.A. Baeuerle, *The ER-overload response: activation of NF-kappa B.* Trends Biochem Sci, 1997. **22**: p. 63-7.

177. Ji, C. and N. Kaplowitz, *Betaine decreases hyperhomocysteinemia, endoplasmic reticulum stress, and liver injury in alcohol-fed mice.* Gastroenterology, 2003. **124**: p. 1488-99.

178. Ji, C. and N. Kaplowitz, *Hyperhomocysteinemia, endoplasmic reticulum stress, and alcoholic liver injury.* World J Gastroenterol, 2004. **10**: p. 1699-709.

179. Lieber, C.S. and L.M. DeCarli, *Ethanol oxidation by hepatic microsomes: adaptive increase after ethanol feeding.* Science, 1968. **162**: p. 917-18.

180. Keilin, D. and E.F. Hartree, *Properties of catalse: Catalysis of coupled oxidation of alcohols.* Biochem J., 1945. **39**: p. 293-301.

181. Crabb, D.W., *Ethanol oxidizing enzymes: roles in alchol metabolism and alcoholic liver disease.* Prog Liver Dis, 1995. **13**: p. 151-72.

182. Lieber, C.S., *Hepatic and other medical disorders of alcoholism: From pathogenesis to treatment.* J Stud Alcohol, 1998. **59**: p. 9-25.

183. Lieber, C.S., *Relationships between nutrition, alcohol use, and liver disease.* Alcohol Res Health, 2003. **27**: p. 220-31.

184. Koop, D.R., *Oxidative and reductive metabolism by cytochrome P450 2E1.* FASEB J, 1992. **6**: p. 724-30.

185. Tsutsumi, M., et al., *The intralobular distribution of ethanol-inducible P450IIE1 in rat and human liver.* Hepatology, 1989. **10**: p. 437-46.

186. Lieber, C.S., *Alcoholic fatty liver: its pathogenesis and mechanism of progression to inflammation and fibrosis.* Alcohol, 2004. **34**: p. 9-19.

187. Lieber, C.S., *Microsomal ethanol-oxidizing system (MEOS): the first 30 years (1968-1998)--a review.* Alcohol Clin Exp Res, 1999. **12**: p. 991-1007.

188. Kono, H., et al., *Development of an intragastric enteral model in the mouse: studies of alcohol-induced liver disease using knockout technology.* J Hepatobiliary Pancreat Surg., 2000. **7**: p. 395-400

189. Oinonen, T., T. Koivisto, and K.O. Lindros, *No significant expression of CYP2E1 in rat liver stellate cells.* Biochem Pharmacol, 1998. **56**(8): p. 1075-8.

190. Yamada, T., et al., *Expression of cytochrome P450 isoforms in rat hepatic stellate cells.* Life Sci, 1997. **61**(2): p. 171-9.

191. Yamauchi, M., J.J. Potter, and E. Mezey, *Characteristics of alcohol dehydrogenase in fat-storing (Ito) cells of rat liver.* Gastroenterology, 1988. **94**: p. 163-9.

192. Greenwel, P., *Acetaldehyde-mediated collagen regulation in hepatic stellate cells.* Alcohol Clin Exp Res, 1999. **23**(5): p. 930-3.

193. Kenney, W.C., *Formation of Schiff base adduct between acetaldehyde and rat liver microsomal phosphatidylethanolamine.* Alcohol Clin Exp Res, 1984. **8**: p. 551-5.

194. Tuma, D.J., et al., *Covalent binding of acetaldehyde to proteins: participation of lysine residues.* Alcohol Clin Exp Res, 1987. **11**: p. 579-84.

195. Trudell, J.R., et al., *Binding of anti-acetaldehyde IgG antibodies to hepatocytes with an acetaldehyde-phosphatidylethanolamine adduct on their surface.* Alcohol Clin Exp Res, 1991. **15**: p. 295-9.

196. Mezey, E., et al., *Alcohol and dietary intake in the development of chronic pancreatitis and liver disease in alcoholism.* Am J Clin Nutr, 1988. **48**: p. 148-51.

197. Halsted, C.H., J.A. Vallanueva, and A.M. Devlin, *Folate deficiany, methinonine metabolism, and alcoholic liver disease.* Alcohol, 2002. **27**: p. 169-72.

198. Lu, S.C., *S-Adenosylmethionine.* Int J Biochem Cell Biol, 2000. **32**(4): p. 391-5.

199. Cantoni, G.L., S.H. Mudd, and V. Andreoli, *Affective disorders and S-adenosylmethionine: a new hypothesis.* Trends Neurosci., 1989. **12**: p. 319-24.

200. Mato, J.M., et al., *S-adenosylmethionine synthesis: molecular mechanisms and clinical implications.* Pharmacol Ther, 1997. **73**(3): p. 265-80.

201. Friedel, H.A., K.L. Goa, and P. Benfield, *S-adenosyl-L-methionine. A review of its pharmacological properties and therapeutic potential in liver dysfunction and affective disorders in relation to its physiological role in cell metabolism.* Drugs, 1989. **38**(3): p. 389-416.

202. Mudd, S.H. and J.R. Poole, *Labile methyl balances for normal humans of various dietary regimens.* Metabolism, 1975. **27**: p. 721-35.

203. Lu, S.C., *Regulation of hepatic glutathione synthesis.* Semin Liver Dis, 1998. **18**(4): p. 331-43.

204. Brown, K.E., et al., *Effect of vitamin E supplementation on hepatic fibrogenesis*

in chronic dietary iron overload. Am J Physiol Gastrointest Liver Physiol, 1997. **272**: p. G116-123.

205. Lieber, C.S., et al., *S-adenosyl-L-methionine attenuates alcohol-induced liver injury in the baboon.* Hepatology, 1990. **11**(2): p. 165-72.

206. Wang, X. and A.I. Cederbaum, *S-adenosyl-L-methionine attenuates hepatotoxicity induced by agonistic Jo2 Fas antibody following CYP2E1 induction in mice.* J Pharmacol Exp Ther, 2006. **317**(1): p. 44-52.

207. Nieto, N. and A.I. Cederbaum, *S-Adenosyl-L-Methionine represses the responsiveness of the alpha 2(I) collagen promoter to CCl4 in transgenic mice.* Supplement to Hepatology, 2003. **38**(4): p. 338A.

208. Song, Z., et al., *S-adenosylmethionine (SAMe) protects against acute alcohol induced hepatotoxicity in mice small star, filled.* J Nutr Biochem, 2003. **14**(10): p. 591-7.

209. Mato, J.M., et al., *S-adenosylmethionine in alcoholic liver cirrhosis: a randomized, placebo-controlled, double-blind, multicenter clinical trial.* J Hepatol, 1999. **30**(6): p. 1081-9.

210. Muriel, P., et al., *Protective effect of S-adenosyl-l-methionine on liver damage induced by biliary obstruction in rats: a histological, ultrastructural and biochemical approach.* J Hepatol, 1994. **21**(1): p. 95-102.

211. Rippe, R.A., Almounajed, G., Brenner, D.A., *Sp1 binding activity increases in activated Ito cells.* Hepatology, 1995. **22**(1): p. 241-51.

212. Rippe, R.A., G. Almounajed, and D.A. Brenner, *Sp1 binding activity increases in activated Ito cells.* Hepatology, 1995. **22**(1): p. 241-51.

213. Pfaffl, M.W., *A new mathematical model for relative quantification in real-time RT-PCR.* Nucleic Acids Res., 2001. **29**: p. e45.

214. Bradford, M.M., *A rapid and sensitive method for the quantitation of microgram quantities of protein utilizing the principle of protein-dye binding.* Anal Biochem, 1976. **72**: p. 248-254.

215. Galang, C.K., C.J. Der, and C.A. Hauser, *Oncogenic Ras can induce transcriptional activation through a variety of promoter elements, including tandem c-Ets-2 binding sites.* Oncogene, 1994. **9**(10): p. 2913-2921.

216. Iimuro, Y., et al., *NFκB prevents apoptosis and liver dysfunction during liver regeneration* J Clin Invest, 1998. **101**(4): p. 802-811.

217. Le Marchand, Y., et al., *A role for the microtubular system in the release of very low density lipoproteins by perfused mouse livers.* J Biol Chem, 1973. **248**(19): p. 6862-70.

218. Malawista, S.E. and P.T. Bodel, *Colchicine: a common mechanism for its anti-inflammatory and anti-mitotic effects.* Arthritis Rheum, 1968. **11**(2): p. 191-7.

219. Mourelle, M. and M.A. Meza, *Colchicine prevents D-galactosamine-induced hepatitis.* J Hepatol, 1989. **8**(2): p. 165-72.

220. Kershenobich, D., et al., *Colchicine in the treatment of cirrhosis of the liver.* N Engl J Med., 1988. **318**(26): p. 1709-13.

221. Zhang, F.K., J.Y. Zhang, and J.D. Jia, *Treatment of patients with alcoholic liver disease.* Hepatobiliary Pancreat Dis Int, 2005. **4**(1): p. 12-7.

222. Mathurin, P., et al., *Corticosteroids improve short-term survival in patients with severe alcoholic hepatitis (AH): individual data analysis of the last three randomized placebo controlled double blind trials of corticosteroids in severe AH.* J Hepatol, 2002. **36**(4): p. 480-7.

223. Rambaldi, A., G. Iaquinto, and C. Gluud, *Anabolic-androgenic steroids for alcoholic liver disease: a Cochrane review.* Am J Gastroenterol, 2002. **97**(7): p. 1674-81.

224. Luper, S., *A review of plants used in the treatment of liver disease: Part 1.* Altern Med Rev, 1998. **3**: p. 410-21.

225. Pascual, C., et al., *Effect of silymarin and silybinin on oxygen radicals.* Drug Develop Res, 2004. **29**(1): p. 73-77.

226. Mourelle, M., et al., *Prevention of CCL4-induced liver cirrhosis by silymarin.* Fundam Clin Pharmacol, 1989. **3**(3): p. 183-91.

227. Muriel, P., et al., *Resolution of liver fibrosis in chronic CCl4 administration in the rat after discontinuation of treatment: effect of silymarin, silibinin, colchicine and trimethylcolchicinic acid.* Basic Clin Pharmacol Toxicol, 2005. **96**(5): p. 375-80.

228. Pradhan, S.C. and C. Girish, *Hepatoprotective herbal drug, silymarin from experimental pharmacology to clinical medicine.* Indian J Med Res, 2006. **124**(5): p. 491-504.

229. Saller, R., R. Meier, and R. Brignoli, *The use of silymarin in the treatment of liver diseases.* Drugs, 2001. **61**(14): p. 2035-63.

230. Lucena, M.I., et al., *Effects of silymarin MZ-80 on oxidative stress in patients with alcoholic cirrhosis. Results of a randomized, double-blind, placebo-controlled clinical study.* Int J Clin Pharmacol Ther, 2002. **40**(1): p. 2-8.

231. Fremont, L., *Biological effects of resveratrol.* Life Sci, 2000. **66**(8): p. 663-673.

232. Chavez, E., et al., *Resveratrol prevents fibrosis, NF-kappaB activation and TGF-beta increases induced by chronic CCl4 treatment in rats.* J Appl Toxicol., 2008. **28**(1): p. 35-43.

233. Tsai, S.H., S.Y. Lin-Shiau, and J.K. Lin, *Suppression of nitric oxide synthase and the down-regulation of the activation of NFkappaB in macrophages by resveratrol.* Br J Pharmacol, 1999. **126**(3): p. 673-80.

234. Wasworth, T.L. and D.R. Koop, *Effects of the wine polyphenolics quercetin and resveratrol on pro-inflammatory cytokine expression in RAW 264.7 macrophages.* Biochem Pharmacol, 1999. **57**(8): p. 941-9.

235. Tsukamoto, H. and S.C. Lu, *Current concepts in the pathogenesis of alcoholic liver injury.* FASEB J, 2001. **15**(8): p. 1335-49.

236. Duce, A.M., et al., *S-adenosyl-L-methionine synthetase and phospholipid methyltransferase are inhibited in human cirrhosis.* Hepatology, 1998. **8**(1): p. 65-8.

237. Muriel, P. and V. Castro, *Effects of S-adenosyl-L-methionine and interferon-alpha2b on liver damage induced by bile duct ligation in rats.* J Appl Toxicol, 1998. **18**(2): p. 143-7.

238. Pascale, R.M., et al., *Chemoprevention of hepatocarcinogenesis: S-adenosyl-L-methionine.* Alcohol, 2002. **27**(3): p. 193-8.

239. Rambaldi, A. and C. Gluud, *S-adenosyl-L-methionine for alcoholic liver diseases.* Cochrane Database Syst Rev, 2006. **19**(2): p. CD002235.

240. Nieto, N. and A.I. Cederbaum, *S-adenosylmethionine blocks collagen I production by preventing transforming growth factor-beta induction of the COL1A2 promoter.* J Biol Chem, 2005. **280**(35): p. 30963-74.

241. Matsui, H. and N. Kawada, *Effect of S-adenosyl-L-methionine on the activation, proliferation and contraction of hepatic stellate cells.* Eur J Pharmacol, 2005. **509**(1): p. 31-6.

242. Finkelstein, J.D., *Methionine metabolism in mammals.* J Nutr Biochm, 1990. **1**(5): p. 228-37.

243. Jokelainen, K., L.A. Reinke, and A.A. Nanji, *Nf-kappab activation is associated with free radical generation and endotoxemia and precedes pathological liver injury in experimental alcoholic liver disease.* Cytokine, 2001. **16**(1): p. 36-9.

244. Li, N. and M. Karin, *Is NF-kappaB the sensor of oxidative stress?* Faseb J, 1999. **13**(10): p. 1137-43.

245. Veal, N., et al., *Inhibition of lipopolysaccharide-stimulated TNF-alpha promoter activity by S-adenosylmethionine and 5'-methylthioadenosine.* Am J Physiol Gastrointest Liver Physiol, 2004. **287**(2): p. G352-62.

246. Fernandez-Checa, J.C., A. Colell, and C. Garcia-Ruiz, *S-Adenosyl-L-methionine and mitochondrial reduced glutathione depletion in alcoholic liver disease.* Alcohol, 2002. **27**(3): p. 179-83.

247. Korus, M., et al., *p38 MAPK-mediated activation of NF-kappaB by the RhoGEF domain of Bcr.* Oncogene, 2002. **21**(30): p. 4601-12.

248. Kim, S.J., et al., *p38 kinase regulates nitric oxide-induced apoptosis of articular chondrocytes by accumulating p53 via NFkappa B-dependent transcription and stabilization by serine 15 phosphorylation.* J Biol Chem, 2002. **277**(36): p. 33501-8.

249. Kaur, J., R.C. Woodman, and P. Kubes, *P38 MAPK: critical molecule in thrombin-induced NF-kappa B-dependent leukocyte recruitment.* Am J Physiol Heart Circ Physiol, 2003. **284**(4): p. H1095-103.

250. Hsu, Y.C., et al., *Anti-fibrotic effects of tetrandrine on bile-duct ligated rats.* Can J Physiol Pharmacol, 2006. **84**(10): p. 967-76.

251. Son, G., et al., *Selective inactivation of NF-kappaB in the liver using NF-kappaB decoy suppresses CCl4-induced liver injury and fibrosis.* Am J Physiol Gastrointest Liver Physiol, 2007. **293**(3): p. G631-9.

252. Boya, P., et al., *Nuclear factor-kappa B in the liver of patients with chronic hepatitis C: decreased RelA expression is associated with enhanced fibrosis progression.* Hepatology, 2001. **34**(5): p. 1041-8.

253. Anan, A., et al., *Proteasome inhibition induces hepatic stellate cell apoptosis.* Hepatology, 2006. **43**(2): p. 335-44.

254. Esfandiari, F., et al., *Chronic ethanol feeding and folate deficiency activate hepatic endoplasmic reticulum stress pathway in micropigs.* Am J Physiol Gastrointest Liver Physiol, 2005. **289**(1): p. G54-63.

255. Jamsa, E., M. Simonen, and M. Markarow, *Selective retention of secretory proteins in the yeast endoplasmic reticulum by treatment of cells with a reducing agent.* Yeast, 1994. **10**(3): p. 355-70.

256. Hwang, C., A.J. Sinskey, and H.F. Lodish, *Oxidized redox state of glutathione in the endoplasmic reticulum* Science, 1992. **257**(5076): p. 1496-1502.

257. Papp, E., et al., *Changes of endoplasmic reticulum chaperone complexes, redox state, and impaired protein disulfide reductase activity in misfolding alpha1-antitrypsin transgenic mice.* FASEB J, 2006. **20**(7): p. 1018-20.

258. de la, M.H.P., et al., *Models of alcoholic liver disease in rodents: a critical evaluation.* Alcohol Clin Exp Res, 2001. **25**(5 Suppl ISBRA): p. 254S-261S.

259. Bode, C., V. Kugler, and J.C. Bode, *Endotoxemia in patients with alcoholic and non-alcoholic cirrhosis and in subjects with no evidence of chronic liver disease following acute alcohol excess.* J Hepatol, 1987. **4**(1): p. 8-14.

260. Bjarnason, I., T.J. Peters, and R.J. Wise, *The leaky gut of alcoholism: possible route of entry for toxic compounds.* Lancet, 1984. **1**(8370): p. 179-82.

261. Adachi, Y., et al., *Antibiotics prevent liver injury in rats following long-term exposure to ethanol.* Gastroenterology, 1995. **108**(1): p. 218-24.

262. Koteish, A., et al., *Chronic ethanol exposure potentiates lipopolysaccharide liver injury despite inhibiting Jun N-terminal kinase and caspase 3 activation.* J Biol Chem, 2002. **277**(15): p. 13037-44.

263. Lindros, K.O. and H.A. Jarvelainen, *A new oral low-carbohydrate alcohol liquid diet producing liver lesions: a preliminary account.* Alcohol Alcohol., 1998. **33**(4): p. 347-53.

264. Mathurin, P., et al., *Exacerbation of alcoholic liver injury by enteral endotoxin in rats.* Hepatology, 2000. **32**(5): p. 1008-17.

265. Garcia-Trevijano, E.R., et al., *Transforming growth factor beta1 induces the expression of alpha1(I) procollagen mRNA by a hydrogen peroxide-C/EBPbeta-dependent mechanism in rat hepatic stellate cells.* Hepatology, 1999. **29**(3): p. 960-70.

266. Fang, C., et al., *Zonated expression of cytokines in rat liver: effect of chronic ethanol and the cytochrome P450 2E1 inhibitor, chlormethiazole.* Hepatology, 1998. **27**(5): p. 1304-10.

267. Leonarduzzi, G., et al., *The lipid peroxidation end product 4-hydroxy-2,3-nonenal up-regulates transforming growth factor beta1 expression in the macrophage lineage: a link between oxidative injury and fibrosclerosis.* FASEB J, 1997. **11**(11): p. 851-7.

268. Tsukamoto, H., et al., *Roles of oxidative stress in activation of Kupffer and Ito cells in liver fibrogenesis.* J Gastroenterol Hepatol, 1995. **10**(Suppl 1): p. S50-3.

269. Karaa, A., W.S. Kamoun, and M.G. Clemens, *Chronic ethanol sensitizes the liver to endotoxin via effects on endothelial nitric oxide synthase regulation.* Shock, 2005. **24**(5): p. 447-54.

270. Donohue Jr., T.M., *Alcohol-induced steatosis in liver cells.* World J Gastroenterol, 2007. **37**(13): p. 4974-8.

271. Scott, M.J., et al., *Endotoxin uptake in mouse liver is blocked by endotoxin pretreatment through a suppressor of cytokine signaling-1-dependent mechanism.* Hepatology, 2009. **49**(5): p. 1695-708.

272. Borges, B.C., et al., *Expression of hypothalamic neuropeptides and the desensitization of pituitary-adrenal axis and hypophagia in the endotoxin tolerance.* Horm Behav, 2007. **52**(4): p. 508-19.

273. Morana, A., et al., *Synthesis and characterisation of a new class of stable S-adenosyl-L-methionine salts.* Int J Pharm, 2000. **194**(1): p. 61-8.

274. Desiderio, C., et al., *Evaluation of chemical and diastereoisomeric stability of S-adenosylmethionine in aqueous solution by capillary electrophoresis* J Pharm Biomed Anal, 2005. **38**(1): p. 449-56.

275. Gasso, M., et al., *Effects of S-adenosylmethionine on lipid peroxidation and liver fibrogenesis in carbon tetrachloride-induced cirrhosis.* J Hepatol, 1996. **25**(2): p. 200-5.

276. Tamai, H., et al., *Long-term ethanol feeding enhances susceptibility of the liver to orally administered lipopolysaccharides in rats.* Alcohol Clin Exp Res, 2002. **26**(8 Suppl): p. 75S-80S.

APPENDIX: ABSTRACTS AND MANUSCRIPTS PUBLISHED

PUBLICATIONS

1. Karaa A*, **Thompson KJ***, Clemens MG, McKillop IH, and Schrum LW. 2008. Shock 30(2):197-205. S-Adenosyl-L-Methionine Attenuates Oxidative Stress and Hepatic Stellate Cell Activation in a Fibrotic Alcohol/LPS Model. **Both authors contributed equally to this manuscript*

2. **Thompson KJ**, Tsukada, S, Rippe RA, and Schrum LW. S-adenosyl-L-methionine Decreases Type I collagen Expression Through Increased Polyubiquitination in Activated Hepatic Stellate Cells. In preparation.

ABSTRACTS

1. **Thompson KJ**, Xu H, Schrum LW. 2003. S-adenosyl-L-methionine inhibits acetaldehyde-induced collagen and α-smooth muscle actin expression in hepatic stellate cells. **Experimental Biology Meeting**, San Diego, CA.

2. **Thompson KJ**, Hedrick MN, Anguita J, Schrum LW. 2004. S-adenosyl-L-methionine increases NFκB: A potential mechanism for collagen inhibition in hepatic stellate cells. **Experimental Biology Meeting**, Washington, DC.

3. Schrum LW, **Thompson KJ**, Cross BW, Hedrick MN, and Anguita J. 2004. S-adenosyl-L-methionine Inhibits Collagen Accumulation by Hepatic Stellate Cells Through p38 MAPK and NFκB Activation. **Cells of the Hepatic Sinusoid Meeting**, Bilboa, Spain.

4. Karaa A, Kamoun WS, **Thompson KJ**, Schrum LW, Clemens MG. 2004. Chronic Alcohol consumption upregulates caveolin-1 and sensitizes the liver microcirculation to endotoxin. **Shock Society Meeting**, Nova Scotia, Canada.

5. Karaa A, **Thompson KJ**, Clemens MG and Schrum LW. 2006. S-Adenosyl-L-Methionine Attenuates Liver Injury and Fibrosis in an Alcohol-LPS Model. **International Symposium on Alcoholic Liver and Pancreatic Diseases and Cirrhosis**, Los Angeles, CA.

6. **Thompson KJ**, Tsukada S, Rippe RA and Schrum LW. 2006. S-adenosyl-L-methionine Decreases Type I Collagen Expression Through Ubiquitination in Activated Hepatic Stellate Cells. **International Symposium on Alcoholic Liver and Pancreatic Diseases and Cirrhosis**, Los Angeles, CA.

7. Karaa A, **Thompson KJ**, Clemens MG, Schrum LW. 2006. S-adenosyl-L-methionine Attenuates Liver Injury in an Alcohol-LPS Model. **Shock Society Meeting**, Broomfield, CO.